Technische Hochschule Ingolstadt

Faculty of Mechanical Engineering

B.Eng. Aerospace Engineering

Bachelor's Thesis

Conceptual Design and Aerodynamic Analysis of a Box Wing Configuration for the Extra EA 400-500

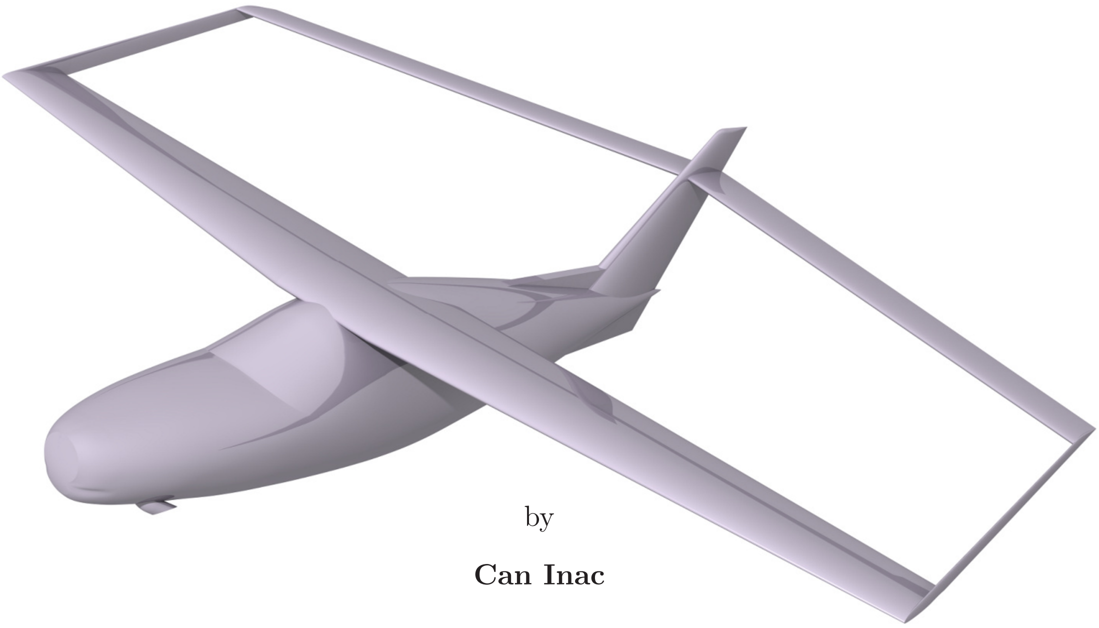

by

Can Inac

Issued on: 29.10.2021

Submitted on: 14.03.2022

First Examiner

Prof. Dr.-Ing. Erol Özger

Second Examiner

Prof. Dr.-Ing. Konrad Költzsch

ABSTRACT

It is the responsibility of every individual to maintain a low carbon footprint and protect our planet, thus the environment. The aviation sector is of no exception from this, even though of only being accountable for less than five percent of the global CO_2 emissions. As such, aircraft as much as engine manufacturers are continuously trying to reduce fuel consumption and increase the overall efficiency of their products by exploring and studying innovative solutions. Over the years, this has led to applications such as lightweighting with the usage of composite materials or aerodynamic advancements through for instance improved winglet designs. This thesis is conducted as a part of the overall aviation aim to further increase aircraft efficiency by exploring the conceptual design of a so-called box wing configuration. The study is performed on real data sets of the Extra EA 400-500 and consists of two aerodynamic studies, once for the original aircraft which is then complemented by the conceptual box wing configuration design of the EA 400-500. Results are promising in that it can be proven that the box wing design configured aircraft of this study achieved a mean lift coefficient increase of 3.78% and a mean reduction of the drag coefficient of 14.83%. These achievements did not only allow to effectively lower the fuel consumption, but were complemented by a solution fulfilling all stability requirements expected by an aircraft.

DEDICATION

DEĞERLİ ANNEM İÇİN

ACKNOWLEDGEMENT

This thesis marks the end of a long and tedious journey; with days in which no light was to be seen at the end of the tunnel; days in which I swore to turn my back on aviation and engineering once and for all – but as the great Tolstoy said: the two most powerful warriors are patience and time. And here I stay today: cheerful, happy and proud of that I did not give up; of what I achieved; of what is still awaiting me. I owe this achievement to many: friends, co-workers, my better half, as much as family members, but also the great support of dedicated and passioned fellow colleagues in the field of aviation; this thesis is based on dialogues and exchange of ideas with academics ranging from Germany, to the Netherlands and even all the way to India. The received support and candour of everyone in the aviation sector is unparalleled and shows the fellowship, which this industry is based on. Thus, this study of a conceptual box wing was not only conducted as part of my thesis, but shall be seen as an expression of thanks to all who deserve nothing but my absolute gratitude.

Special thanks are due to my first examiner, Prof. Dr.-Ing. Erol Özger, for believing in my vision about the future relevance of non-planar wings and my keen interest about box wings even beyond the scope of this study. I am equally thankful for the help of Mr. Spohr of SST Flugtechnik GmbH, who was so kind to provide me all required data of the unique Extra EA 400-500. Furthermore, I owe much of my knowledge to Ir. L.M.M. Boermans of the TU Delft, who was the aerofoil designer of the NLF-MOD22. Without his input and dedicated help, this study would have been far away from what I wanted to achieve.

This thesis – and more importantly, me succeeding in my studies – would not have been possible without my brother and my Ma. I dedicate every letter of this study, as much as each of my achievements, to her hard-working hands and her endless dedication. In a foreign country with little to no language skills and, alas, an uncountable number of challenging circumstances, she managed to raise my brother and me – always seeing education as the most valuable asset and fighting everything that could cause us to fail in succeeding. And with contentedness I can say that we succeed, and in doing so, she does too.

ACKNOWLEDGEMENT (TURKISH)

Bu tez uzun ve zor bir yolculuğun sonunu işaret ediyor; ışığın görünmediği günlerle dolu bir yol; uçak endüstriğine ve mühendisliğine sırtımı dönmeye yemin ettiğim günlerle dolu bir yol - ama büyük Tolstoy'un da dediği gibi: en güçlü iki savaşçı sabır ve zamandır. Ve bugün buradayım: neşeli, mutlu ve vazgeçmediğim için gururlu; geride bıraktığım günleri düşünerek; beni bekleyen günleri düşünerek. Bu başarıyı birçok insana borçluyum: arkadaşlarıma, iş arkadaşlarıma, hayatimin anlamına, aile üyelerime, aynı zamanda uçak alanındaki meslektaşlarımın büyük desteğine. Çünkü bu tez Almanya'dan Hollanda'ya ve hatta Hindistan'a kadar uzanan akademisyenlerle olan diyaloglara dayanmaktadır. Uçak sektöründeki herkesten aldığım destek ve samimiyet eşsizdir ve bu endüstrinin dostluk üzerine dayandığını göstermektedir. Bu nedenle, geliştirdiğim kanat tasarlaması sadece tezimin bir parçası olarak değil, aynı zamanda minnettar olduğum herkese bir teşekkür ifadesi olarak görülmelidir.

Özel olarak tezimde deştiğini hiçbir zaman eksik etmeyen Prof. Dr.-Ing. Erol Özger'e, *non-planar* kanatların gelecekteki önemine ve *box wing* hakkındaki vizyonuma inandığı için teşekkür ederim. SST Flugtechnik GmbH'dan Bay Spohr'un yardımı için de ayrıca minnettarım. Bana Extra EA 400-500'ün gerekli tüm verilerini sağlama nezaketini gösterdi. Ek olarak, bilgilerimin çoğunu NLF-MOD22'nin tasarımcısı olan TU Delft'den Ir. L.M.M. Boermans'a borçluyum. Onun özverili yardımı olmasaydı, bu çalışma ile başarmak istediklerimi başaramayabilirdim.

Bu tezle - ve daha da önemlisi, bütün üniversite hayatımda – başarılı olmam abim ve annem olmadan mümkün olmazdı. Tüm başarılarımı ve yazmış olduğum bu tezin her bir harfini annemin çalışkan ellerine ve bitmeyen özverisine adıyorum. Biz küçükken yabancı bir ülkede çok dil becerisi olmamasına ve sayısız zorlu günleri geçirmesine rağmen beni ve abimi yetiştirmeyi başardı – eğitimi her zaman her şeyden daha değerli olarak gördü ve başarısız olmamıza neden olabilecek her şeyle mücadele etti. O yüzden gururlu bir şekilde söyleyebilirim ki: Biz başarılıyız ve daha da önemlisi: bizim başarımızla o da başarılı.

DECLARATION

I hereby declare that this thesis is my own work, that I have not presented it elsewhere for examination purposes, and that I have not used any sources or aids other than those stated. I have marked verbatim and indirect quotations as such.

Place, Date

Can Inac

CONTENTS

LIST OF FIGURES

LIST OF TABLES

NOMENCLATURE

Abbreviations

AC	Aerodynamic Center
AOA	Angle of Attack
CATIA	CAD System by Dassault Systèmes
CFD	Computational Fluid Dynamics
CG	Centre of Gravity
DATCOM	USAF Data Compendium
EASA	European Union Aviation Safety Agency
EU	European Union
FL	Flight Level
GmbH	Company with Limited Liability (in Germany)
HAW	University of Applied Sciences (in Germany)
HFB	Hamburger Flugzeugbau
IAS	Indicated Airspeed
ICAO	International Civil Aviation Organisation
ISA	International Standard Atmosphere
L/D	Lift/Drag
LL	Limit Load
MAC	Mean Aerodynamic Chord
MEL	Minimum Equipment List
MLW	Maximum Landing Weight
MOD	Modification
MPL	Maximum Power Loading
MTOW	Maximum Take-Off Weight
NACA	National Advisory Committee for Aeronautics
NASA	National Aeronautics and Space Administration
NLF	Natural-Laminar Flow
NO	Normal Operations
NP	Neutral Point
OpenFOAM	CFD Tool: Open-source Field Operation And Manipulation

PS	Port Side	
RANS	Reynolds-Averaged Navier–Stokes Equations	
S/L	Sea Level	
SB	Starboard	
SI	International System of Unit	
SM	Static Margin	
SST	Menter's Shear Stress Transport	
STEP	File Type: Standard for the Exchange of Product Model Data	
TAS	True Airspeed	
TU	Technical University	
UAV	Unmanned Aircraft Vehicles	
VAT	Value Added Tax	
ZFW	Zero Fuel Weight	

Coefficients

C_D	Drag Coefficient	[−]
C_L	Lift Coefficient	[−]
C_m	Pitching Moment Coefficient	[−]
C_p	Pressure Coefficient	[−]
C_{D0}	Zero-Lift Drag Coefficient	[−]
$C_{f,W}$	Turbulent Flat Plate Skin-Friction Coefficient	[−]
$C_{l\beta}$	Roll Moment Coefficient	[$\frac{1}{rad}$]
$C_{n\beta}$	Yaw Moment Coefficient	[$\frac{1}{rad}$]

Greek Symbols

α	Angle of Attack	[deg/rad]
β	Sideslip Angle	[deg/rad]
χ	Mach-Factor	[−]
δ	Deflection of Control Surface	[deg/rad]
ϵ	Angle of Rearward Air Pressure Inclination	[deg/rad]
η	Static Pressure Ratio between Wing and Tail	[−]
Γ	Dihedral Angle	[deg/rad]
γ	Angle Between x_g and V_A	[deg/rad]
Λ	Sweep	[deg/rad]

λ	Taper Ratio	[–]
∇	Divergence of	[–]
ω	Downward Velocity (*Chapter 2.2.2*)	[$\frac{m}{s}$]
Φ	Roll Angle	[deg/rad]
ϕ	Tail Efficiency	[–]
Φ'	Trailing-Edge Angle	[deg/rad]
ψ	Yaw Angle	[deg/rad]
ρ	Air Density	[$\frac{kg}{m^3}$]
σ	Biplane: Gap-Span-Ratio (*Chapter 2.2.2*)	[–]
σ	Induced Sidewash Angle	[deg/rad]
τ	Control Surface Effectiveness	[–]

Latin Symbols

$\bar{c}$	Lenght of MAC	[m]
$\bar{q}$	Dynamic Pressure	[$\frac{kg}{ms^2}$]
$\overline{V}$	Volume Ratio	[–]
$\mathbf{U}$	Flow Velocity	[$\frac{m}{s}$]
A	Area	[m^2]
a	Curve Slope	[$\frac{1}{rad}$]
AR	Aspect Ratio	[–]
b	Span	[m]
b_f	Fuselage Width	[m]
c	Aerofoil Chord Length	[m]
$c(y)$	Chord Length Function	[m]
c_S	Speed of Sound	[$\frac{m}{s}$]
D	Drag	[N]
F	Force	[N]
Fi	Fineness Ratio	[–]
G	Gravitational Force	[N]
G	Height Between Wings on a Multiplane (*Chapter 2.2.2*)	[m]
i_b	Engine Installation Angle	[deg/rad]
i_T	Horizontal Tail Installation Angle	[deg/rad]
K	Variable Factor	[–]
k	Variable Factor	[–]

K_b	Control Surface Span Factor	[–]
L	Lift	[N]
L	Rolling Moment	[Nm]
l	Length	[m]
L'	Aerofoil Thickness Location Parameter	[–]
M	Moment	[Nm]
Ma	Mach Number	[–]
N	Yawing Moment	[Nm]
R	Sweep-Chord-Length-Reaction-Factor	[–]
r	Biplane: Ratio Upper to Lower Wing Length (*Chapter 2.2.2*)	[–]
r	Fuselage Depth	[m]
r	Yaw Rate	[$\frac{1}{rad}$]
Re	Reynolds Number	[–]
T	Thrust	[N]
t	Chord Thickness	[m]
V	Velocity of Flight	[$\frac{m}{s}$]
v	Remote Free Stream Velocity	[$\frac{m}{s}$]
V_T	Tail Volume Coefficient	[–]
w	Downward velocity produced by the wing (*Chapter 2.2.2*)	[$\frac{m}{s}$]
x	Coordinate on X-Axis	[m]
x_b	Body Axis	[–]
x_g	Geodetic Axis	[–]
Y	Side Force	[N]
y	Normal Coordinate	[m]
z	Vertical Component of Disturbance Velocity (*Chapter 2.2.2*)	[$\frac{m}{s}$]

Subscripts

1	Biplane: Upper Wing (*Chapter 2.2.2*)
11	Biplane: Upper Wing Self-Induced Drag (*Chapter 2.2.2*)
12	Biplane: Effect of Upper Wing on Lower Wing (*Chapter 2.2.2*)
2	Biplane: Lower Wing (*Chapter 2.2.2*)
21	Biplane: Effect of Lower Wing on Upper Wing (*Chapter 2.2.2*)
22	Biplane: Lower Wing Self-Induced Drag (*Chapter 2.2.2*)
A	Aspect Ratio

a	Aileron
B	Body (Fuselage)
b	Body (Fuselage)
b	Braced
BW	Box Wing
C	Chordwise
cor	Correction
CW	Cantilever Wing
des	Design
dg	Design Gross Weight
e	Elevator
e	Engine
f	Fuselage
fl	Flap
H	Horizontal Stabiliser
h	Distance Variable
hld	High Lift Device
i	Inner
L	Lift (3D)
l	Lift (2D)
loc	Local
M	Mach
N	Nose
NO	Normal Operations
no	Non-Optimum
o	Outer
R	Resultant
r	Rudder
S	Spanwise
sp	Spoiler
st	Stiffness
T	Tail
TE	Trailing Edge

tef	Trailing Edge Flap
TWW	Total Wing Weight
uc	Undercarriage
ult	Ultimate Load Case
V	Vertical Stabiliser
VS	Vertical Structure
W	Wing

Superscripts

$B(W)$	Body-Wing
H	Horizontal Stabiliser
T	Tail
V	Vertical Stabiliser
$V(BW)$	Vertical-Stabiliser-to-Body-Wing
$V(HB)$	Vertical-Stabiliser-to-Horizontal-Tail-Body
W	Wing
$W(B)$	Wing-Body

FOREWORD

This document follows the guidelines of the fifth edition of the Annex 5 to the Convention on International Civil Aviation titled *Units of Measurement to be Used in the Air and Ground Services* published by the International Civil Aviation Organisation (ICAO) within the Chicago Convention of 1944 in July 2010 [1]. As such, all SI units are given priority for any calculation whatsoever, with only exceptions made for information regarding the movement of an aircraft: longitudinal distance may be given in nautical miles; vertical distance for altitude, elevation, height and vertical speed may be given in feet; speed may be given in knots. Furthermore, the wing weight calculation, see (237), required the usage of British units. An overview of all exceptions is provided in Table 1.

Table 1: Non-SI Alternative Units

Quantity	Unit	Symbol	Conversion
Distance (longitudinal)	Nautical Miles	NM	$1\,\mathrm{NM} = 1{,}852\,\mathrm{m}$
Distance (vertical)$^{a)}$	Feet	ft	$1\,\mathrm{ft} = 0.3048\,\mathrm{m}$
Speed	Knot(s)	kt(s)	$1\,\mathrm{kt} = 0.541444\,\mathrm{m/s}$
Area	Square Feet	ft^2	$1\,\mathrm{ft}^2 = 0.092903\,\mathrm{m}^2$
Mass	Pound(s)	lb	$1\,\mathrm{lb} = 0.45359\,\mathrm{kg}$
Pressure	Pound Force per Square Feet	lbf/ft^2	$1\,\mathrm{lbf/ft}^2 = 47.88\,\frac{\mathrm{kg}}{\mathrm{ms}^2}$

a)altitude,elevation,height,verticalspeed

CHAPTER 1

INTRODUCTION

Aviation is an engineering art without equal. It is characterised by innovation, daring and fellowship - and as such, always a testimony to the achievements attainable for mankind. This can especially be seen in the never-ending efforts of established aircraft manufacturers to improve existing platforms, as much as the sheer number of aviation startups conquering the aviation market by utilizing new technologies. One such modern answer to the growing general aviation market was the Extra EA 400-500, shown in Figure 1.1, for which a non-planar wing was designed and analysed during this study.

1.1 Technical Information About the Extra EA 400-500

The Extra EA 400-500 (Sales designation: EXTRA 500) was developed by renowned Walter Extra's aircraft design and production organisation EXTRA Flugzeugproduktions- und Vertriebs-GmbH in Hünxe, Germany, and had its maiden flight on 26 April 2002. The aircraft is the turboprop version of the Extra EA 400 (Sales Designation: EXTRA 400), which was developed during the 90s in cooperation with Prof. Egbert Torenbeek and his team of the Delft University of Technology [2].

(a) Note the Complex Landing Gear

(b) Take-Off Roll

Figure 1.1: EXTRA 500 D-FBRS at Cannes. *Photos Courtesy of Samuel Parmentier.*

The EA 400-500 is equal to its predecessor, a six-seat, single engine light utility aircraft with a cantilever high wing, natural-laminar-flow (NLF) aerofoil section and T-tail. The carbon-fibre aircraft was designed with hostile conditions in mind and, together with a complex tiltable landing gear developed by Gomolzing Aircraft Services, allows landing on rough terrain such as grass runways [3]. The aircraft has a service life of 25 years/20,000 hours/30,000 cycles/22,500 pressurisation cycles and had a price of €1,249,500 (US$895,000) incl. VAT in 2008 when delivered with standard equipment [4]. Further technical as much as flight data can be seen in Table 1.1.

After a fatal accident of the EA 400 on its first customer flight after delivery, the German civil aviation authority, the *Luftfahrt-Bundesamt*, imposed a Type Rating on the EA 400 as much as EA 400-500 after a recommendation of the German Federal Bureau of Aircraft Accident Investigation, the *Bundesstelle für Flugunfalluntersuchung*, in their accident report 3X329-0/98 issued on June 1999 [5]. Only in 2015 was it achieved to change the Type Rating requirement to a Single Engine Piston Class Rating for the EA 400 and Single Engine Turbine Class Rating for the EA 400-500 [6][7]. The amendment was driven by the German SST Flugtechnik GmbH after receiving the Type Certificate from EXTRA Flugzeugproduktions- und Vertriebs-GmbH in November 2014 and becoming the responsible Type Certificate Holder, although the Type Design is owned by the Chinese Jiangsu A-Star Aviation Industry Co., Ltd. [6][8].

Table 1.1: Technical and Flight Data of the EA 400-500 [4][6][9][10]

Wing span	11.60 m	Empty weight	1,360 kg
Wing aspect ratio	9.3	MTOW	2,130 kg
Length overall	10.13 m	MLW	2,000 kg
Width of fuselage	1.46 m	MPL	5.96 kg/kW
Height overall	3.37 m	MTOW manoeuvring speed	156 kts IAS
Tailplane span	3.80 m	Cruise speed, 90%@FL150	220 kts IAS
Wheel track	2.20 m	Cruise speed, 75%@FL250	210 kts IAS
Wheelbase	2.65 m	Stalling speed	61 kts IAS
Wing area	14.3 m^2	Max rate of climb at S/L	1,700 ft/min
Horizontal tail area	2.81 m^2	Max range, with reserves	1,500 NM
Vertical tail area	2.41 m^2	Endurance @90%	4 h 6 min
Maximum operation altitude	25,000 ft	Endurance @75%	7 h 36 min

Over the years, only a total of twenty-nine EA 400 and seven EA 400-500 were produced, which resulted in the eventual sale of the Type Design. In 2015, the Vice President of Operations at Jiangsu A-Star Aviation Industry explained that the EA 400-500 would be their starting point in the Chinese general aviation market [11]. As of today, no Chinese EA 400-500 has been produced, however. The remaining produced aircraft are in direct competition with aircraft like the Socota TBM 850, Piper PA-46 and Pilatus PC-12.

1.2 Historial Overview of Non-Planar Wings

Blériot III: Louis Blériot, the famous French inventor, engineer and aviator, was not only the very first to cross the English Channel in an aircraft but began experimenting with non-planar wings as early as 1906, eventually resulting in the Blériot III [12]. The aircraft, as can be seen in Figure 1.2(a), had two equally sized elliptical tandem hollow ash wings covered with silk, creating a wing area of $60\,\mathrm{m}^2$ [13]. The back wing was equipped with a rudder, while the front wing included the elevators as much as two tractor propellers connected to a 24 hp, eight-cylinder Antoinette engine capable of 600 rpm [14]. The aircraft weighted 430 kg, of which approximately 110 kg resulted from the complex flexible shaft transmission. The aircraft was tested in May 1906 at Lake Enghien but did not manage to take-off and the trials were described as disastrous.

Custer CCW-5: In 1925, Willard Custer discovered that it was not only possible to lift an aircraft into the air by accelerating it relative to the air but also by accelerating the air relative to the aircraft [15]. 30 years later, this thought resulted in the CCW-5: the Custer Channel Wing aircraft based on the fuselage of the Baumann Brigadier, as can be seen in Figure 1.2(b). The pusher propellers were placed within the U-shaped wings consisting of a NACA 4418/4412 aerofoil with no high-lift devices [16]. This unusual configuration allowed the aircraft to fly as slow as 10 kts and take-off by using only a runway length of 28 m with a 680 kg load at 70% power [17]. However, strong vibrations caused by the high rotational propeller speed close to the wings as much as fuselage, and the fact that lift was only generated when the engines were not at idle resulted in difficult flight conditions and especially landing sequences [18][19].

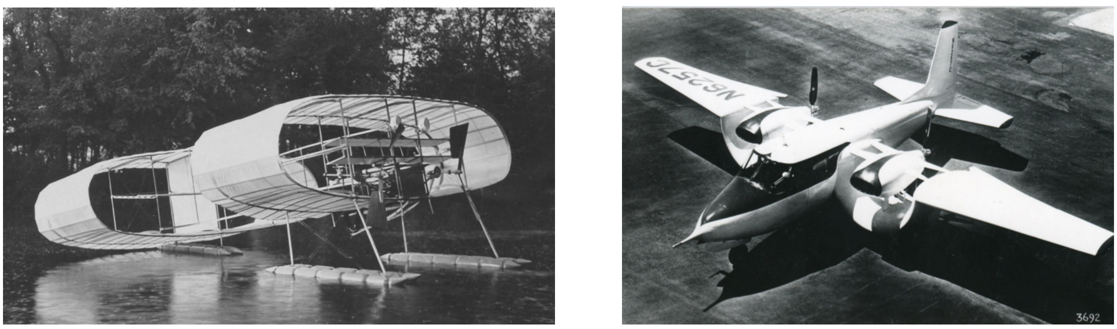

(a) Blériot III at Lake Enghien. *Public Domain Photo.*

(b) Custer CCW-5 (N6257C). *Photo Courtesy of Bibliothek für Zeitgeschichte, Stuttgart.*

Figure 1.2: Historical Aircraft With Non-Planar Wings: Blériot III and CCW-5

Narushevich OW-1: In 1988, a Belarusian company received the task to develop an easily manoeuvrable and light aircraft, that could withstand the strong side winds with which the An-2 often struggled [20]. During development, it was analysed that a closed oval wing, which was only connected via struts to the fuselage and thus providing clean wing aerodynamics, was the best solution for dealing with the strong winds in the open fields of the Russian land. Due to several technical as much as political circumstances, the first field tests were only conducted in 2004 with the aircraft being registered as EW-067LL and receiving the name OW-1 Ring Wing. The flight tests were successful and the flight characteristics quite promising: the aircraft had a take-off distance of only 150 m and showed no reactions to crosswinds of up to 25 kts. Even though the results were seen as intruding to conduct further studies, the aircraft received the registration EW-555AO, shown in Figure 1.3(a), and was stored indefinitely at the Belarus Aerospace Museum.

IDINTOS PrandtlPlane: More recent studies include a box-wing design co-funded by the Regional Government of Tuscany and developed by the Aerospace Division of the University of Pisa, Italy. The PrandtlPlane, shown in Figure 1.3(b), was completed in 2013 and is supposed to have intrinsic anti-stall behaviours while also providing highly aerodynamic efficiency, leading to lower fuel consumption [21]. Flight tests were only conducted with a 1/4 scaled model but showed that an induced drag reduction of 4% in comparison to a monoplane were possible [22].

(a) Narushevich Ring Wing OW-1 (EW-555AO). *Photo Courtesy of Evgeny Dovgospiny.*

(b) IDINTOS PrandtlPlane. *Photo Courtesy of Filippo Grassi.*

Figure 1.3: Historical Aircraft With Non-Planar Wings: OW-1 and PrandtlPlane

Over the years, many aircraft with non-planar wings have been developed, showing that advantages exist when considering specific application areas. However, more often than not, serious issues have halted the development and shown that more research and studies are required.

1.3 Problem Statement

The aviation sector was responsible for 3.8% of the total CO_2 emissions in the European Union (EU) in 2017, with forecasts of ICAO showing that international aviation emissions could triple by 2050 in comparison to 2015 [23]. This is in line with studies proclaiming that emissions will grow because even though the amount of fuel burned per passenger dropped by 24% between 2005 and 2017, air traffic in general has grown by 60% in the same period [24]. Therefore, the EU has set out the European Green Deal with the ultimate goal to reduce transport emissions by 90% until 2050 when compared to emission levels of the 90s [25]. A key element in the reduction of aviation emissions is the aerodynamic of aircraft, with studies showing that a 1% reduction of aerodynamic drag on aircraft such as the Airbus A340 during long-range flights will result in a saving of approximately 400,000 litres of fuel per year – the equivalent of nearly 5000 kg of noxious emissions [26]. This thesis therefore aims to study and analyse one unique solution for drag reduction applications in future aircraft and intents to contribute to the goal of the EU to reduce CO_2 emissions.

1.4 Thesis Outline

This study is divided into eight chapters, with the first chapter providing the reader a general impression of the Extra EA 400-500 aeroplane, an overview of notable non-planar wing design solutions throughout the history as much as the overall goal of this thesis and the contained study. Following in the second chapter is an analysis of the EA 400-500 wing and tailplane, definitions of used nomenclature as much as a theoretical approach explaining the origin of box wing configurations. It is briefly followed by short examples of said approach. The third chapter explains the methodology of this thesis, which the results provided in chapter four to seven will be based on. These results are subdivided into a fourth chapter analysing the Extra EA 400-500 with cantilever wing, after which the developed box wing configuration will be described and further examined in the fifth chapter. Following in the sixth chapter is proof, that the box wing configured Extra EA 400-500 is stable around all axes. Eventually, in the seventh chapter, a wing weight estimation will be presented to the reader. All results and the outcome of the study are summarised in chapter eight.

CHAPTER 2
STATE OF THE ART

With the growing possibilities of computational analysis in recent years, research and studies regarding non-planar wings have increased, paving the way for more practical applications. It was therefore of uttermost importance to understand not only the basics of the Extra EA 400-500, but also which kind of improvement could be achieved with the current state of research.

2.1 Studies on the Extra EA 400-500

Verification, thus the evaluation of results in order to ensure correctness, is a key element of every aircraft development, as is its relevance for academic studies [27]. The Extra EA 400 and EA 400-500 have only been of little interest in the aviation and academic world. Therefore, no significant studies have been conducted in the past making it difficult to verify results. Nevertheless, when broken down into more conclusive packages, this hurdle is overcome. Hence, the wing and horizontal tail aerofoil were reflected upon before analysing existing and provided data of the EA 400-500.

2.1.1 Wing Aerofoil: NLF-MOD22

The NLF-MOD22 natural laminar-flow wing aerofoil of the Extra EA 400-500 was designed and wind tunnel tested by Ir. L.M.M. Boermans during his time at the TU Delft together with his student P.B. Rutten [28]. The design was based on D.M. Somers' laminar aerofoil NLF(1)-0146 [29] and aimed to reduce the overall drag while maintaining its high lift capabilities. Due to an airworthiness requirement of a stall speed at MLW of 61 kts, a design requirement of a cruise lift coefficient of 0.4 at $Re = 6 \cdot 10^6$, as much as a high cruise speed, a small wing with a low profile drag and a single slotted flap was necessary [30]. However, the NLF(1)-0146 was not able to fulfil these requirements, as it did not provide a low enough drag at cruise and was limited due to its insufficient rear thickness for a slotted flap [28]. Hence, Boermans changed the lower surface pressure gradient in order to shift the transition backward up to 70% chord length. This resulted in a lower cruise drag and increased the thickness in the rear. The two aerofoils as much as their calculated characteristics are provided in Figure 2.1 and Figure 2.2 respectively.

Additionally, at 68% chord length, a zigzag tape tabulator of 0.5 mm thickness was added in order to eliminate a detrimental laminar separation bubble, which resulted in a reduction of aft-loading and decreased the pitching moment coefficient in cruise by approximately 30%. Eventually, this lowered the lift curve by $\Delta C_L = 0.1$, which made a slight decambering necessary. During wind tunnel tests [31], the design proved to be quite efficient in that a lower than estimated drag was achieved, which allowed an increase of the initially planned cruise speed.

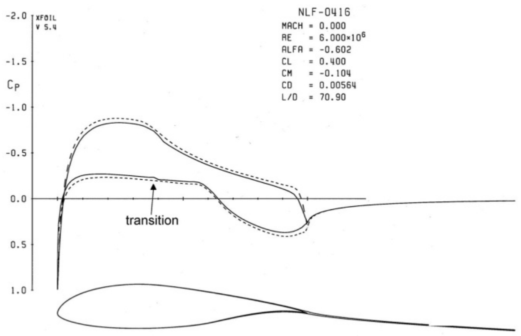

(a) C_p at $\alpha = 0$ for NLF(1)-0416

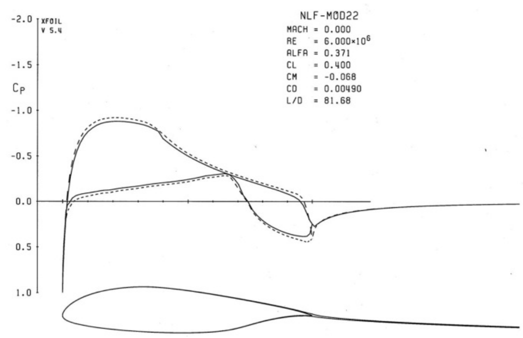

(b) C_p at $\alpha = 0$ for NLF-MOD22

Figure 2.1: Calculated Pressure Distribution C_p of Aerofoil NLF(1)-0146 and NLF-MOD22 [30]. *Photo Courtesy of Ir. L.M.M. Boermans.*

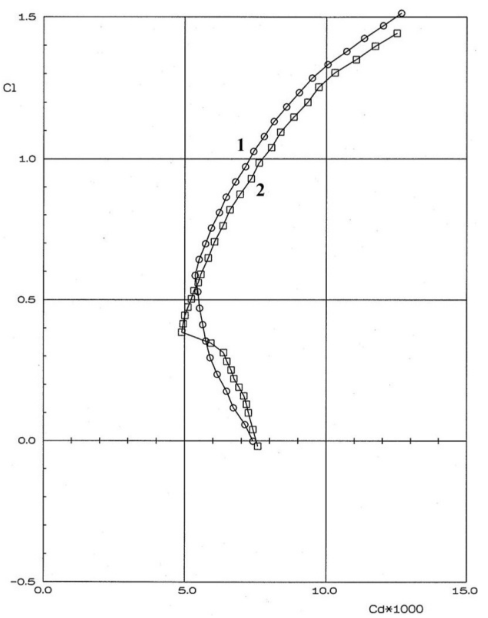

(a) C_L vs. C_D

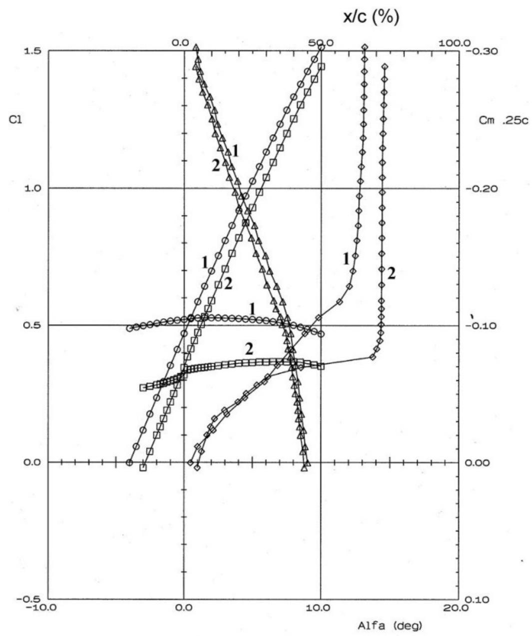

(b) C_L and C_m for $\alpha = -10$ to $\alpha = 20$

Figure 2.2: Comparison of Calculated Characteristics for **1:** NLF(1)-0416 and **2:** NLF-MOD22 at $Re = 6 \cdot 10^6$ [30]. *Photo Courtesy of Ir. L.M.M. Boermans.*

2.1.2 Horizontal Tail Aerofoil: NACA 0012

The Extra EA 400-500 has a T-tail configuration with both horizontal stabilisers spanning a total length of 3.80 m and a 1.13 m^2 total projected nested area for the elevators. The respective NACA 0012 aerofoil, as provided in its nomenclature, has a maximum thickness of 12% at 30% chord with no camber whatsoever [10]. Next to the EA 400 as much as EA 400-500, this specific aerofoil has seen usage in horizontal tails as early as 1938 with the Bonomi BS.28 Alcione sailplane, as well as modern aircraft such as the Cessna C170A and a modified version in the Lockheed P-3 Orion [16]. The exact aerofoil can be described by the following equation:

$$\begin{aligned} y_t = \pm\, 5t_c \Bigg[& 0.2969\sqrt{\left(\frac{x_c}{c}\right)} - 0.1260\left(\frac{x_c}{c}\right) \\ & - 0.3516\left(\frac{x_c}{c}\right)^2 + 0.2843\left(\frac{x_c}{c}\right)^3 - 0.1015\left(\frac{x_c}{c}\right)^4 \Bigg] \end{aligned} \tag{2}$$

where: c = Length of the chord

x_c = Position along the chord between 0 and c

t_c = Maximum thickness as a fraction of the chord

As noted by the plus-minus sign in (2), it becomes obvious that the provided aerofoil is symmetrical. Four-digit NACA aerofoils with no camber are known for providing good stall characteristics, posses a small centre of pressure movement, however have a low maximum lift coefficient as much as high drag and a high pitching moment [32]. The aerofoil is visualised in Figure 2.3(a) below.

The NACA 0012 aerofoil has been subject of many studies, most notable of Abbott and Doenhoff [33], Gregory and O'Reilly [34] as much as Ladson [35], which have all been verified by the NASA Langley Research Center [36]. The data sets have been merged by the author of his study into single plots shown in Figure 2.3, Figure 2.4 and Figure 2.5

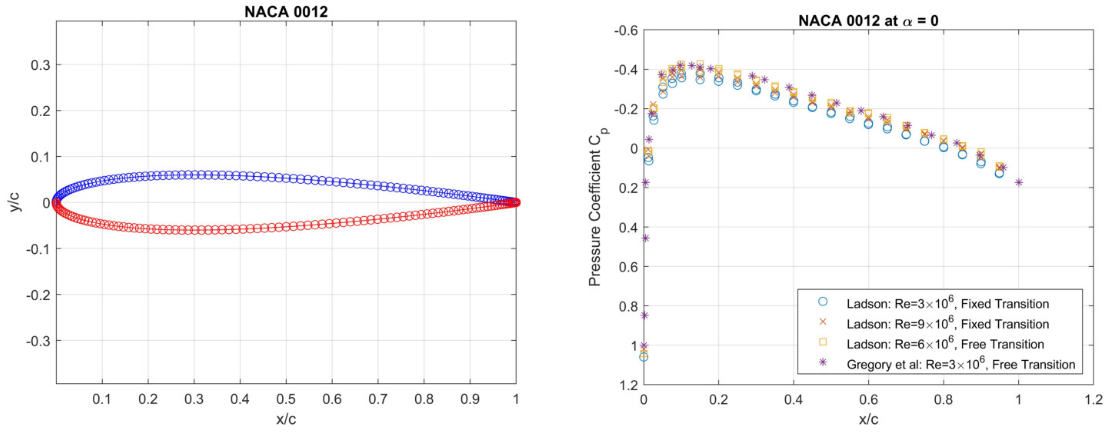

(a) Aerofoil Profile

(b) C_p at $\alpha = 0$

Figure 2.3: NACA 0012: Aerofoil and Pressure Coefficient C_p at $\alpha = 0$

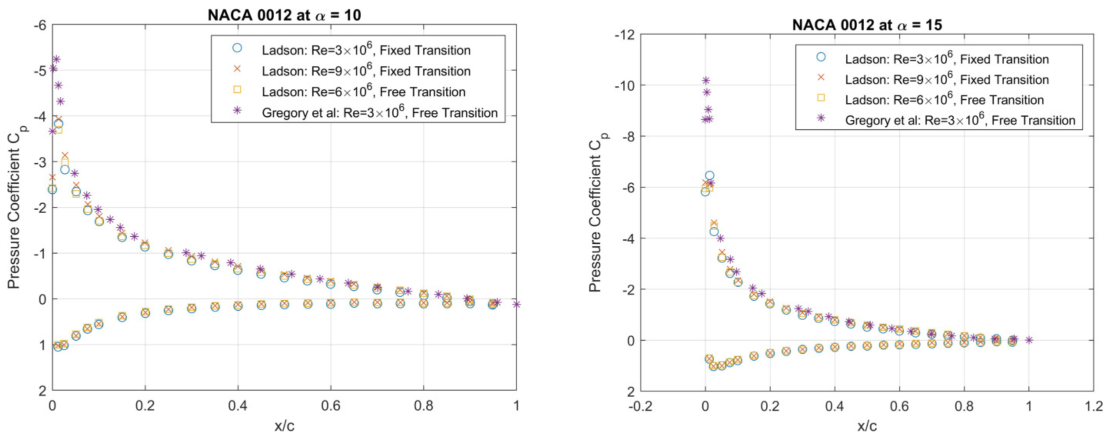

(a) C_p at $\alpha = 10$

(b) C_p at $\alpha = 15$

Figure 2.4: NACA 0012: Pressure Coefficient C_p at $\alpha = 10$ and $\alpha = 15$

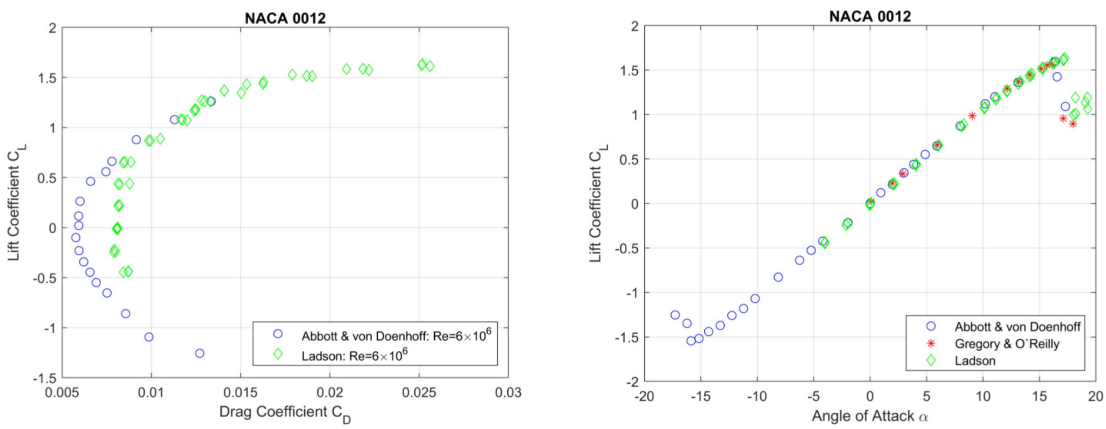

(a) C_L vs. C_D

(b) C_L vs. α

Figure 2.5: NACA 0012: C_L vs. C_D and C_L vs. α

2.2 Studies on Box Wing Configurations

Box wing configurations have seen a wide range of analysis in academic studies, ranging from one-seaters [37] up to large transport aircraft [38], as much as actual – although in a limited number – applications in unmanned aircraft vehicles (UAVs) like the RQ-6 [39] or scaled radio-controlled prototypes such as a tanker concept flown by Lockheed Martin in March 1997 [40]. In the aviation industry and likewise for the conceptual design of a box wing configuration for the Extra EA 400-500, such experiences built the fundament for future applications.

2.2.1 Classification of a Box Wing

Ludwig Prandtl, the German scientist with whom aviation would not be where it is today, published his landmark studies on aeroplanes with wings on more than one plane in 1924 and introduced their significant effect on induced drag to the world. Ever since, terms such as joined wing or box wing emerged and have been used wrongly as synonyms. This study follows the categorisation of wing configurations provided by Jansen and Perez [41], in which wings can be divided into four groups: conventional wings including cantilever wings; stagger wings such as tandem or bi-plane wings; wing-tip extensions such as the C-wing; and eventually so-called closed wings. Part of the closed wing configuration are ring wings, which have been introduced earlier such as in Figure 1.3(a). The latter also includes box wings and joined wings, which have been used interchangeably frequently and will therefore be defined in the following by their respective patents.

Joined Wing: "An aircraft having a fuselage and a pair of first airfoils in the form of wings extending outwardly from the vertical tail and a pair of second airfoils in the form of wings extending outwardly from the forward portion of the fuselage at a lower elevation than the first airfoils. The second wings extend rearwardly having a positive dihedral so that the tip ends of the second airfoil are located in close proximity to and may overlap the tip ends of the first wings. The pairs of wings along with the fuselage present a double triangle or diamond shape in both front elevational view and top plan view." [42]

Box Wing: "An aircraft wing system wherein a first pair of rearwardly swept wings is interconnected at the wing tips to a second pair of forwardly swept wings, the interconnection being accomplished by a pair of vertically swept fins, the two pair of wings being horizontally and vertically staggered relative to one another. Each pair of wings is also structurally attached to another aircraft component." [43]

As shown in Figure 2.6, the main difference between a box wing and joined wing is therefore the additional vertical structure between the main wing and horizontal stabiliser.

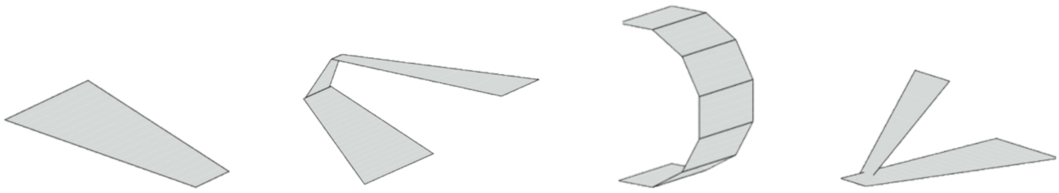

(a) Cantilever Wing (b) Box Wing (c) Ring Wing (d) Joined Wing

Figure 2.6: Comparison of a Cantilever Wing and Closed Wings Adapted From [41]

2.2.2 Prandtl's Best Wing System

According to Ludwig Prandtl's theory of induced drag on multiplanes [44][45], the induced drag of a wing system can be calculated when the lift distribution of every individual wing is known. Prandtl bases his work on Max Munk's Stagger Theorem [46], shown in Figure 2.7, of an unstaggered wing system describing that the total induced drag of any system is equal to a simpler system when compounding of the same front view in which "the centres of pressure of all constituent wing surfaces, while maintaining the same lift distribution, are shifted into one and the same plane, at right angles to the direction of flight" [45, p. 4].

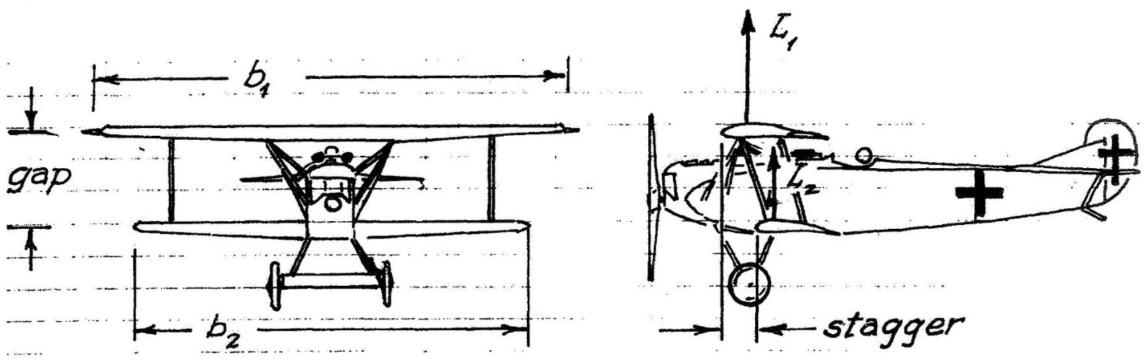

Figure 2.7: Stagger Theorem of Max Munk – *"The induced drag of a multiplane is independent of the streamwise location of its lifting element (the stagger) so long as its front view is unchanged (gap and span ratios), and so long as the lift distribution between the elements (L_1/L_2) is preserved."* [47, p. 323]

This idea is supplemented by the fact that the drag D_{12} induced by the first wing on the second wing equals the vice versa drag D_{21}. Prandtl further analysis that the drag D_{12} is produced by a downward air current towards the second wing. This leads to a rearward incline of the resulting air pressure on the second wing at an angle ϵ, which produces a new component of the drag: $L_2 sin(\epsilon)$, where L_2: Lift of the second wing. The effect of downwash and upwash is shown in Figure 2.8.

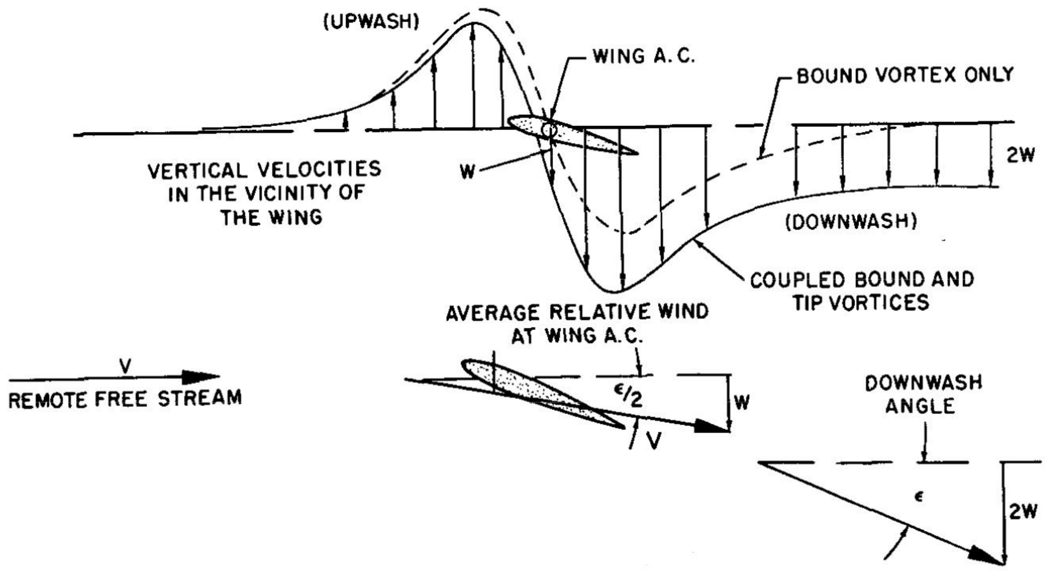

Figure 2.8: Downwash and Upwash in the Wing Vicinity [48]

When considering the velocity of flight v and the downward velocity produced by the first wing w_{12}, it can be concluded that $tan(\epsilon) = \left(\frac{w_{12}}{v}\right)$ with regard to $tan(\epsilon) \approx \epsilon$ and $sin(\epsilon) \approx \epsilon$, thus $tan(\epsilon) = sin(\epsilon)$, since only small angles are considered. Since w_{12} is not uniform along the span b, Prandtl writes that

$$D_{12} = \int \left(\frac{w_{12}}{v}\right) \mathrm{d}L_2 \tag{3}$$

and explains that based on previous work by Munk as much as Pohlhausen [49], the elliptical flow below and above a monoplane wing are equal to that of a plate moved at a right angle to its plane, visualised in Figure 2.9(a), and thus the value of z, the vertical velocity of said flow, see Figure 2.9(b), will be utilised so that the velocity w_{12} can be calculated as

$$w_{12} = \frac{2L_1}{\pi v {b_1}^2} z \tag{4}$$

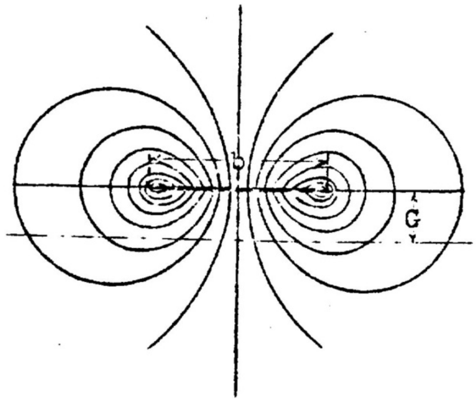

(a) Disturbance of Flow Around a Wing

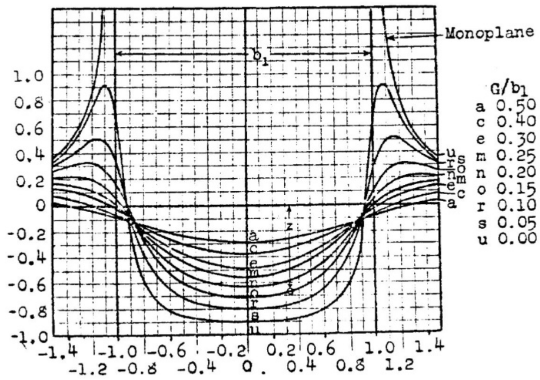

(b) Value of z for Velocity Calculation – *Vertical component of the disturbance velocity plotted against the lateral and the vertical distance from the wing.*

Figure 2.9: Disturbance Flow Around a Wing, and Vertical Component z [45]

Eventually, Prandtl explains that $\sigma = \frac{G}{\frac{b_1+b_2}{2}}$, with G being the gap of the biplane, and comes to the conclusion that

$$D_{12} = D_{21} = \frac{\sigma}{\pi\overline{q}}\frac{L_1}{b_1}\frac{L_2}{b_2} \tag{5}$$

Based on (5) and the assumption of $L_1 = L_2$, $b_1 = b_2$ and $G = 0$, the self-induced drag of one wing can be written as

$$D_{11} = \frac{{L_1}^2}{\pi\overline{q}{b_1}^2} \tag{6}$$

$$D_{22} = \frac{{L_2}^2}{\pi\overline{q}{b_2}^2} \tag{7}$$

For the unstaggered biplane, this therefore means that the induced drag of the upper wing D_1 and lower wing D_2 can be formulated as

$$D_1 = D_{11} + D_{12} = \frac{1}{\pi\overline{q}}\left(\frac{{L_1}^2}{{b_1}^2} + \sigma\frac{L_1 L_2}{b_1 b_2}\right) \tag{8}$$

$$D_2 = D_{22} + D_{21} = \frac{1}{\pi\overline{q}}\left(\frac{{L_2}^2}{{b_2}^2} + \sigma\frac{L_1 L_2}{b_1 b_2}\right) \tag{9}$$

Prandtl concludes that whether the biplane has a stagger or not, the induced drag is constant as can be seen when considering a positive stagger: The lower wing diminishes the drag of the upper wing by its upward air currents, while the drag of the lower wing is increased by the same amount due to the downward air current of the upper wing. Therefore (8) and (9) can be summed up to represent the total induced drag of a staggered and unstaggered biplane as

$$D = D_1 + D_2 = \frac{1}{\pi \bar{q}} \left(\frac{{L_1}^2}{{b_1}^2} + 2\sigma \frac{L_1 L_2}{b_1 b_2} + \frac{{L_1}^2}{{b_1}^2} \right) \tag{10}$$

In a following step, it is now possible to calculate how the lift of the biplane must be distributed in order to receive the minimum value of induced drag. Prandtl assumes that $L_1 = L(1-x)$ or $L_2 = Lx$ for that matter, and introduces $r = \frac{b_2}{b_1}$ in order to find the minimum of (10) with the help of

$$x = \frac{r - \sigma}{r + \frac{1}{r} - 2\sigma} \tag{11}$$

By inserting (11) in (10) and regarding the special case of $b_1 = b_2$, so that $r = 1$, the minimum value of the induced drag for an staggered and unstaggered biplane is received:

$$D_{min} = \frac{L^2}{\pi \bar{q} b^2} \frac{1+\sigma}{2} \tag{12}$$

Since $\sigma < 1$ in general and the term $\frac{L^2}{\pi \bar{q} b^2}$ being the induced drag of a monoplane with span b providing the same lift as the biplane, it can be seen that the induced drag of a biplane is always smaller than a monoplane of an equal span. With this knowledge in mind, Prandtl introduces the best wing system, shown in Figure 2.10, in which the ends of the wings of a biplane are laterally closed and the upper element is only subject to outward pressure, while the lower element being subject to inward pressure.

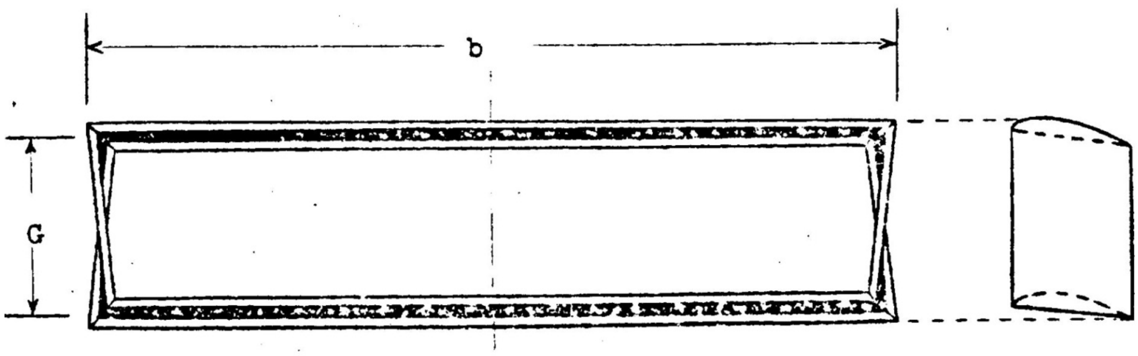

Figure 2.10: Ludwig Prandtl's Best Wing System [45]

By utilising "a method which cannot here be gone into in detail" [45, p. 16], the induced drag of said best wing system is to be calculated with

$$D_{BestWing} = D_{Monoplane} \frac{1 + 0.45\frac{G}{b}}{1.04 + 2.81\frac{G}{b}} \tag{13}$$

This best wing system builds the fundament for the box wing configuration and is, according to Prandtl, the wing system with the least induced drag of all wing systems when comparing equal spans and gaps. A simple example of an aircraft flying in ISA conditions (air density: $\rho = 0.0659\frac{kg}{m^3}$) at an altitude of 5,000 m (16,404 ft) with a constant velocity of v = 50 m/s (97 kts) and a load of 1000 kg shows the achievable reduction in induced drag. In a first step, the dynamic pressure is calculated to be $\overline{q} = \frac{\rho v^2}{2} = 82.38\frac{kg}{ms^2}$. Regarding a monoplane with a span b = 5 m, this would result in

$$D_{Monoplane} = \frac{L^2}{\pi \overline{q} b^2} = \frac{(9.81\frac{m}{s^2} \cdot 1000kg)^2}{3.14 \cdot 82.83\frac{kg}{ms^2} \cdot (5m)^2} = 14.9kN \tag{14}$$

With (12), the induced drag of a biplane with equal spans of b $= b_1 = b_2 =$ 5 m and G = 2 m can be calculated with $\sigma = \frac{G}{\frac{b_1+b_2}{2}} = 0.4$

$$D_{Biplane} = \frac{L^2}{\pi \overline{q} b^2} \frac{1+\sigma}{2} = \frac{(9.81\frac{m}{s^2} \cdot 1000kg)^2}{3.14 \cdot 82.38\frac{kg}{ms^2} \cdot (5m)^2} \frac{1+0.4}{2} = 10.4kN \tag{15}$$

By using (13), one can see that

$$D_{BestWing} = D_{Monoplane} \frac{1 + 0.45\frac{G}{b}}{1.04 + 2.81\frac{G}{b}} = 14.9kN \cdot 0.545 = 8.1kN \tag{16}$$

The theory of Prandtl's best wing system therefore shows that significant theoretical reductions in induced drag are possible when considering a box wing configuration instead of utilising monoplanes as is common today.

2.3 Examples of Box Wing Configurations

Most recent studies include a box wing configuration for a T-tail aircraft by Srinivasan [50], as shown in Figure 2.11. The study compared a mid and high box wing with a conventional low wing configuration and came to the conclusion that a drag reduction of up to 7.9% and a lift increase of 2%, both at higher angle of attacks, were possible. However, the study did not include a stability analysis, but is said to conduct further analysis in the future.

(a) Low Wing Configuration Design

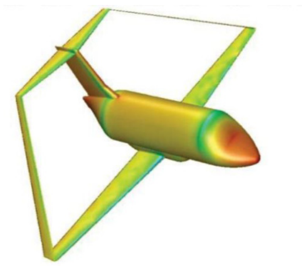

(b) Aerodynamic Analysis

Figure 2.11: Design Study of a Low Wing T-tail Aircraft by Srinivasan [50]

On the other hand, there have been studies proclaiming that a box wing configuration may actually result in an increase instead of a decrease of induced drag. One such example, based on the Airbus A320, is presented by Scholz of the HAW Hamburg [51]. The conceptual design box wing aircraft is shown in Figure 2.12. Here it was analysed that a box wing configuration's induced drag increased by up to 3.4% due to an required increase in the lift ratio between the first and second wing to greater than one. As described by Scholz, equal lift coefficients on both wings and a negative zero lift pitching moment resulted in an unstable aircraft. The higher induced drag in return was counteracted by decreasing the span efficiency factor of the same amount. However, when compared to the original aircraft of the study, this in return led to a 1% higher fuel burn, thus burning about 110 kg more during a normal mission profile compared to the A320.

(a) Side View

(b) Front View

Figure 2.12: Example Box Wing Configuration Study of the HAW Hamburg [52]

CHAPTER 3

METHODOLOGY

This thesis is divided into a design, as much as an aerodynamic analysis and flight mechanics study. All of which shall be introduced to the reader in the following.

3.1 Design and Analysis Process

In order to compare the cantilever and box wing configuration of the Extra EA 400-500, several process steps were conducted, as shown in Figure 3.1. Initially, the standard configuration aircraft was optimised with CATIA V5, meshed in OpenFOAM V7 and afterwards aerodynamically analysed within the same tool. After it was seen that the OpenFOAM settings were satisfactory, the box wing configuration was developed by using Datcom, see next subchapter, after which another aerodynamic analysis was conducted. Eventually, all calculated aerodynamic values were compared.

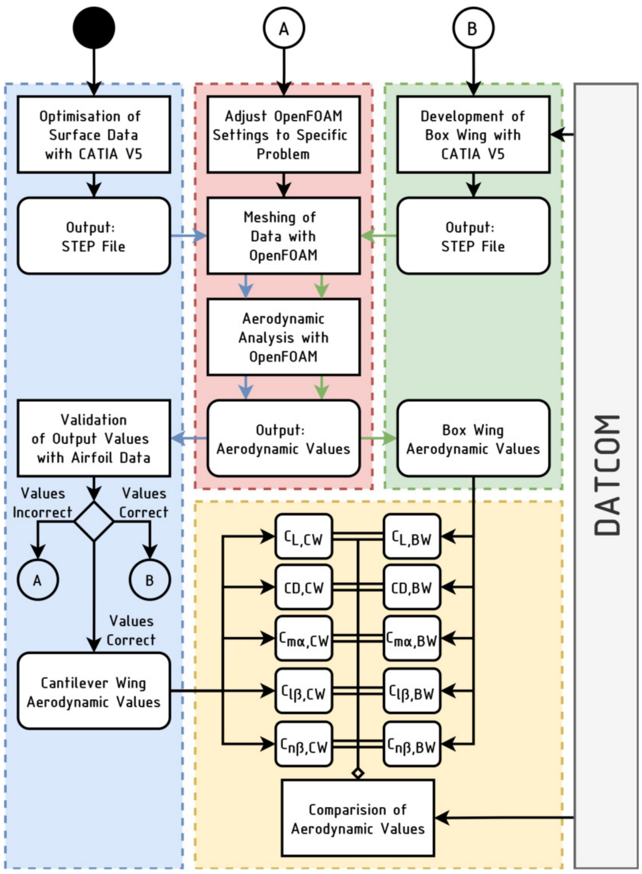

Figure 3.1: Design and Analysis Process of This Thesis

3.2 Stability and Control DATCOM

Datcom refers to the Data Compendium of the United States Air Force and its *Stability and Control DATCOM* handbook about the calculation of aerodynamic stability requirements for aircraft designs in early study phases [53][54]. This study presented here is based on the methods of the report of 1978, which is publicly available through the Defense Technical Information Center, and saw slight adjustments wherever deemed necessary for the development of a box wing configuration. The required formulas are provided to the reader in every respective chapter and all variables as much as values are explained in the light of the calculations.

3.3 Boundary Conditions for the CFD Analysis

In accordance with its Type Certificate, the Extra EA 400-500 has a maximum structural cruising speed $V_{NO} = 97\frac{m}{s}$ (188 kts). Taking into account the speed of sound in ISA conditions $c_S = 343\frac{m}{s}$, the Mach number used throughout this thesis resulted in $Ma = \frac{V_{NO}}{c_S} = \frac{97m/s}{343m/s} = 0.28 < 0.3$. With this assumption, the fluid was considered as incompressible, so that $\nabla \cdot \mathbf{U} = 0$. Additionally, the following boundary conditions were set for the case of this study in accordance with Puig [55]:

- Turbulent flow with SST k-w model
- Air considered as a Newtonian fluid
- Reynolds-averaged Navier–Stokes (RANS) equations turbulence model with wall function
- ISA sea level conditions
- No gravitational effects on the aircraft
- Exclusion of non-static elements such as the propeller or landing gear

CHAPTER 4

CANTILEVER WING CONFIGURATION

The cantilever wing configured Extra EA 400-500 was the fundament of this study. However, a number of steps were necessary before reaching the point of conducting an aerodynamic analysis of the aircraft. This included optimisation of the data set, meshing and eventually setting up of the OpenFoam case.

4.1 Review of Data

The current Type Certificate Holder of the Extra EA 400 and EA 400-500 is SST Flugtechnik GmbH in Memmingen, Germany. The author of this study approached the EASA approved Design Organisation to query whether it would be possible to use original data sets of the aircraft. The respective authorised officer of SST Flugtechnik affirmed the request, after which a Non-Disclosure Agreement was signed and the exchange of data started. The provided data included the following items:

- 3D-Model of the Extra EA 400-500 surfaces as a CATPart; see Figure 4.1
- Original three-view technical drawing of the Extra EA 400-500
- Original technical drawing of the front part of the lower ventral fin
- Original technical drawing of the aft part of the lower ventral fin

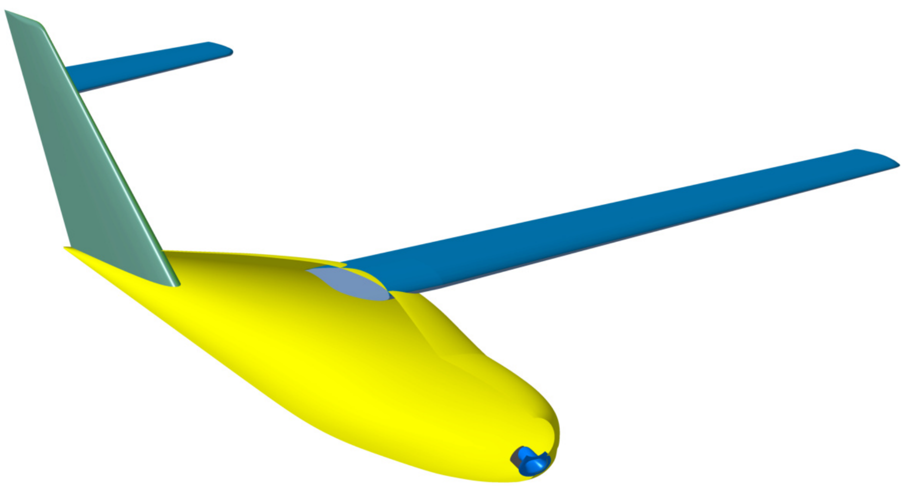

Figure 4.1: Provided 3D Model of the Extra EA 400-500

The 3D-Model consisted of a total of eleven surfaces, prominently with the left side of the aircraft available. Components such as the wing, horizontal stabiliser and the winglets were divided into an upper and lower half. Additionally, the vertical stabiliser consisted of a left and right component, while the left fuselage section, front air intake, as much as the engine exhaust outlet were provided as single surfaces.

4.2 Pre-processing

As can be seen in Figure 4.1, the provided data set was not in a state to conduct an aerodynamic analysis. It was therefore necessary to add and delete aircraft surfaces, create flight controls and eventually make assumptions about to what extent the aircraft for this study may differ from its real design.

4.2.1 Surface Optimisation

The provided data set did mostly only include the left-hand side (port side) of the aircraft and therefore needed to be mirrored. This was quickly done within CATIA, in which the right-hand (starboard) fuselage, wing and winglets, elevator, and exhaust pipe were duplicated by mirroring them along the XZ-axis. After this step, all intersecting elements between different components of the aircraft were analysed and excessive surfaces eliminated afterwards. This included surface intersections between the elevator and rudder, rudder and fuselage, fuselage and wing, as much as the exhaust pipe and fuselage. One such example can be seen in Figure 4.2, which shows the process of defining the intersection curve between the two components, before eliminating inner and outer surfaces to create one homogenous surface. This led to a reduction of the file size, although very marginal, but more importantly reduced the mesh complexity of the aircraft for the next steps.

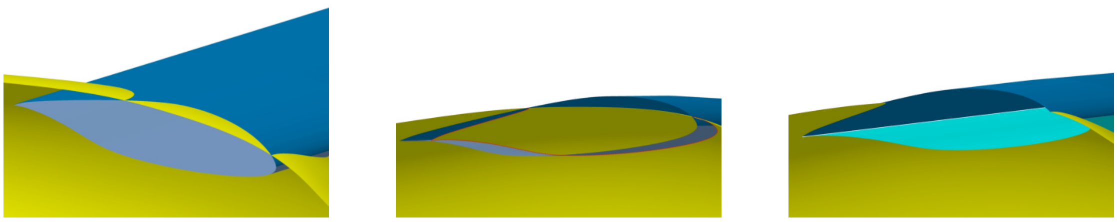

(a) Fuselage and Wing Before Cutting

(b) Intersection (red) Between Fuselage and Wing

(c) After Elimination of Excessive Surfaces

Figure 4.2: Elimination of Excessive Surfaces at Intersecting Elements

The Extra EA 400-500 has a single propeller in the nose section, which was decided to not be included in the conceptual design study. Therefore, the front of the aircraft differed from the original design, which made slight adjustments necessary. In order to not affect the aerodynamic analysis negatively in any way, the consultancy of an employee of OpenFoam Ltd. was sought before conducting next steps. After thorough analysis of various possibilities, it was decided unanimously to close the front section entirely and remove the air intake, as it would not impact the analysis of a box wing configuration significantly. The difference between the two states is visualised in Figure 4.3.

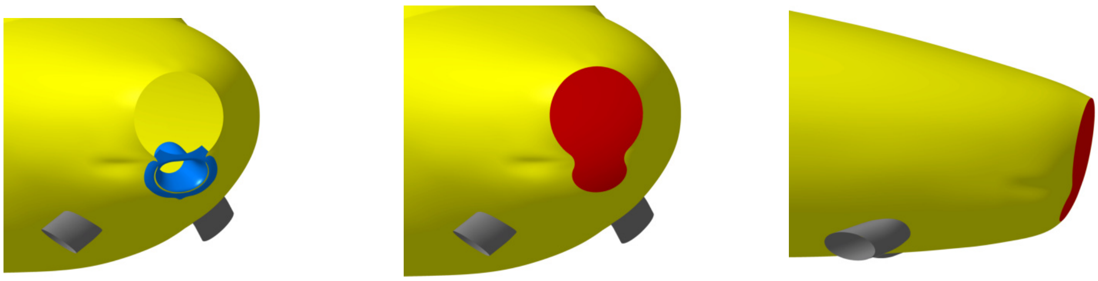

(a) Nose Section with Air Intake (blue)

(b) Isometric View of Closed Nose Section

(c) Side View of Closed Nose Section

Figure 4.3: Closure of Open Section at Propeller Opening

The data set provided by SST Flugtechnik showed small gaps of 1.5 mm and 3 mm between all divided surfaces such as the wing as much as vertical and horizontal stabiliser. In order to be able to create a working mesh, these gaps had to be closed. The process can be seen in Figure 4.4.

(a) Isometric View of Portside Winglet

(b) Gap Between Upper and Lower Surface (Light Blue)

(c) Closed Gap (Red)

Figure 4.4: Closure of Open Section at Wing Surfaces

The empennage of the Extra EA 400-500 is equipped with one ventral fin below and one dorsal fin in front of the vertical stabiliser, as shown in Figure 1.1. These fins were however not included in the provided data set and therefore needed to be added according to the original technical drawings provided by the Type Certificate Holder. The reconstructed fins are shown in Figure 4.5.

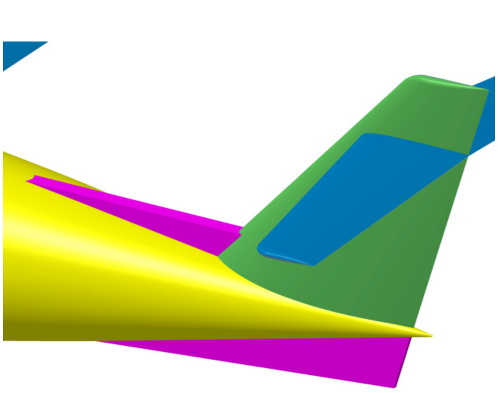

(a) The Ventral Fin Builds an Extension of the Vertical Stabiliser

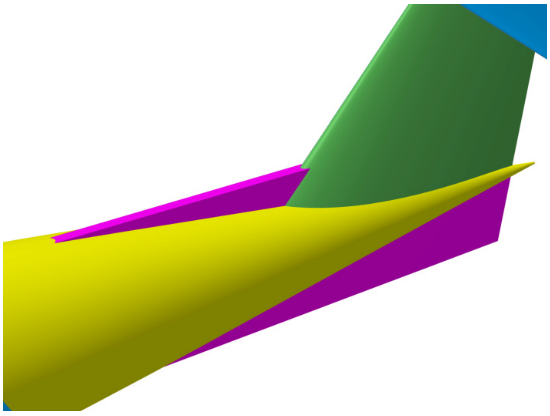

(b) The Dorsal Fin Supports the Vertical Stabiliser

Figure 4.5: Ventral and Dorsal Fin of the Extra EA 400-500

The result of this work was a representative version of the Extra EA 400-500, as is shown in Figure 4.6 below.

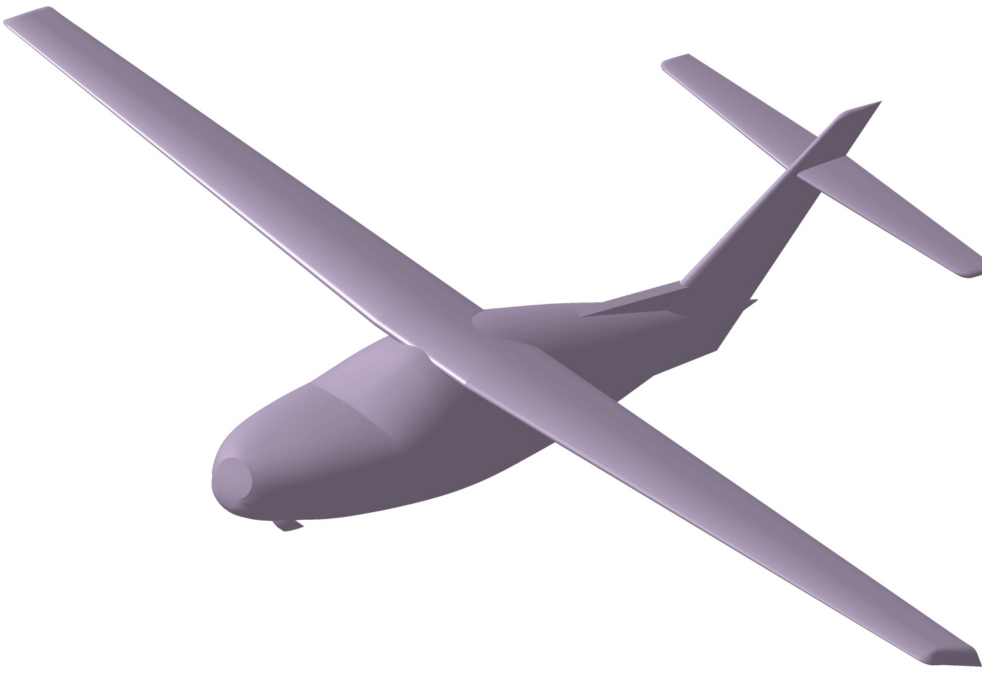

Figure 4.6: Improved 3D Model of the Extra EA 400-500

4.2.2 Creation of Control Surfaces

In order to fully analyse the behaviour of the Extra EA 400-500, missing control surfaces were required to be added to the 3D model. As they were not available in the provided data set, the ailerons, elevators as much as the rudder were designed based on technical drawings of the aircraft. As drawings with exact measurements of the control surfaces were not provided, an approximation based on a detailed three-view-drawing, similar but more detailed of which can be found in the Pilot's Operating Handbook of the EA 400-500 [56], was implemented. Figure 4.7 shows all control surfaces with their respective full positive and negative deflection: ailerons in green, elevators in red, and the rudder in blue. The ailerons had a deflection range between -19° and +27°, the elevators from -18° to +33°, while the rudder could deflect from -25° to +25°, on their respective axis [10].

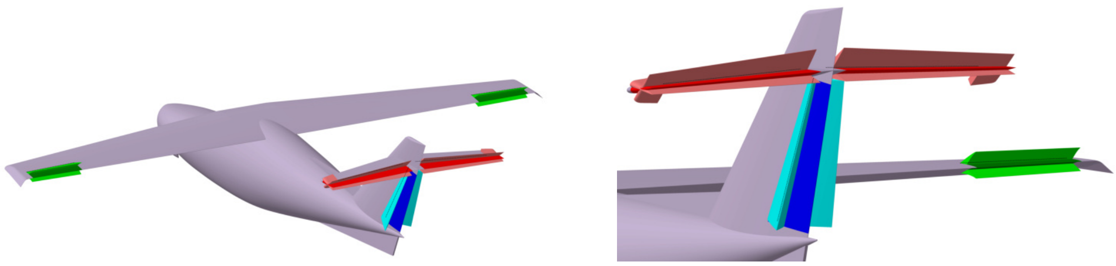

(a) Isometric View With Control Surfaces

(b) Close Up of Control Surfaces

Figure 4.7: Ailerons, Elevators and Rudder Added to the Extra EA 400-500

After designing of the control surfaces, a verification of the parts was conducted. This included the measurement of the total projected nested area of the ailerons, elevators and rudder. These values, shown in Table 4.1, were then compared to original values provided in the Maintenance Manual of the Extra EA 400-500 [10]. It was aimed to keep the difference of the original and replica area as minimal as possible, in order to minimise the effect it had on the aerodynamic analysis.

Table 4.1: Comparison of Total Projected Nested Areas of All Control Surfaces

Part	Original Area	Replica Area	Difference	Effect
Aileron	$0.309\,\mathrm{m}^2$	$0.317\,\mathrm{m}^2$	2.7 %	Minor
Elevator	$0.565\,\mathrm{m}^2$	$0.574\,\mathrm{m}^2$	1.5 %	Minor
Rudder	$0.633\,\mathrm{m}^2$	$0.629\,\mathrm{m}^2$	0.6 %	Minor

4.2.3 Assumptions, Boundary Conditions and Effects

For the purpose of this conceptual design study, several differences to the original Extra EA 400-500 have been made. The reasons varied from a limited number of resources up to the fact that elements would have not improved the study in any way. In some cases, technical drawings did exist, but were limited in their value, or did not exist at all. Reasons laid in the fact that the former Type Certificate Holder was not only the Design Organisation but also Production Organisation, which allowed the company to create less detailed drawings, as information was often internally shared without proper documentation [57]. Hence, often technical drawings did exist, however were deemed not sufficient to improve this study. Additionally, a number of assumptions and boundary conditions were determined by the author of this study. These results and their respective effects for a study on a conceptual level are shown in Table 4.2.

Table 4.2: Assumptions and Boundary Conditions for the Aerodynamic Analysis

Difference	Description	Effect
Propeller	An aerodynamic analysis including a propeller creates a complex and complicated case. This is not required for a conceptual design analysis, thus the propeller had not been included.	Medium
Landing Gear	The study was conducted with a retracted landing gear.	Nil
Landing Gear Doors	The EA 400-500 has a bulked-out landing gear door, when the gear is retracted. Since no technical drawings for these components were available, the doors had not been modelled. However, effects on the aerodynamic analysis were limited and close to zero.	Minor
Vertical Stabiliser	The Extra EA 400-500 has an asymmetric vertical stabiliser in order to cancel out the torque effect of the propeller. However, this effect and the torque values were not available. This would have resulted in an incorrect aerodynamic calculation, as the torque could not be compensated. Since most aircraft with propellers do not feature an asymmetric vertical stabiliser and can fly without any problem, the vertical stabiliser was made symmetrically for the purpose of this study.	Medium
NACA Ducts	The NACA ducts in the front section of the aircraft had not been modelled due to missing measurements and low impact on the aerodynamic analysis of the box wing configuration.	Minor
Flaps	The aerodynamic analysis was conducted in clean flight conditions, thus flaps were not extended.	Nil
Antennas	Antennas had not been modelled because of missing measurements and low impact on the aerodynamic analysis of the box wing configuration.	Minor
Trim Tabs	Trim tabs of the elevator and rudder had not been modelled because of missing measurements and because of the assumption that the aircraft was in a trimmed condition.	Nil

4.2.4 Generated Output Files

Afterwards, a total of eleven output files were generated for the purpose of this study. This included one case group with an angle of attack α of zero degrees, representing level flight, and several deflection cases with aileron deflection angles δ_a, elevator deflection angles δ_e, and rudder deflection angles δ_r as such:

- Case 1.0: $\alpha = 0$, $\delta_a = 0$, $\delta_e = 0$ and $\delta_r = 0$
- Case 1.1: $\alpha = 0$, $\delta_a = 0$, $\delta_e = 0$ and $\delta_r^+ = 25°$ (left)
- Case 1.2: $\alpha = 0$, $\delta_a = 0$, $\delta_e^+ = 33°$ (upward), and $\delta_r = 0$
- Case 1.3: $\alpha = 0$, $\delta_a =$, $\delta_e^- = -18°$ (downward) , and $\delta_r = 0$
- Case 1.4: $\alpha = 0$, $\delta_a^+ = 27°$ (left wing) $\wedge$ $\delta_a^- = -19°$ (right wing), $\delta_e = 0$ and $\delta_r = 0$

Equally, cases were created for different angle of attacks α with no deflections on any control elements:

- Case 2.0: $\alpha = 2°$, $\delta_a = 0$, $\delta_e = 0$ and $\delta_r = 0$
- Case 2.1: $\alpha = 5°$, $\delta_a = 0$, $\delta_e = 0$ and $\delta_r = 0$
- Case 2.2: $\alpha = 7°$, $\delta_a = 0$, $\delta_e = 0$ and $\delta_r = 0$
- Case 2.3: $\alpha = 10°$, $\delta_a = 0$, $\delta_e = 0$ and $\delta_r = 0$
- Case 2.4: $\alpha = 12°$, $\delta_a = 0$, $\delta_e = 0$ and $\delta_r = 0$
- Case 2.5: $\alpha = 15°$, $\delta_a = 0$, $\delta_e = 0$ and $\delta_r = 0$

The files were created with CATIA and exported as an IGS.-file.

4.3 Mesh Generation

For the purpose of a CFD analysis, the volume to be analysed is divided into a number of small cells [58]. All cells together create a so-called mesh, which is a representation of the actual object within the CFD analysis. These small discrete spaces are then analysed by mathematical equations describing the physics of the flow on a local scale [59]. The higher quality the mesh, the better results can therefore be achieved. During this study, blockMesh and snappyHexMesh were used, which is offered within OpenFoam itself [60] [61].

4.3.1 Background and Aircraft Mesh

During CFD analysis it was of importance to create a background mesh, in which the actual geometry was located in, of reasonable size. The background mesh built the computational domain and was required due to the fact that external aerodynamics were being analysed. This can be seen by the red dot within the yellow computational domain in Figure 4.8. The red dot is called the point-in-mesh and shows that the external aerodynamic are of matter since the dot is located within the computational area but outside the aircraft geometry. The background mesh was assigned a length of 80 m and equals nearly eight times the aircraft length. In this case, the section aft of the aircraft was defined to be five times the aircraft length to ensure enough room for low energy wake flows. While the front section before the aircraft was of 20 m and made sure that the flow could adjust to the aircraft geometry. Furthermore, the background mesh had a height of 25 m and width of 50 m, as shown in Figure 4.8 and Figure 4.9.

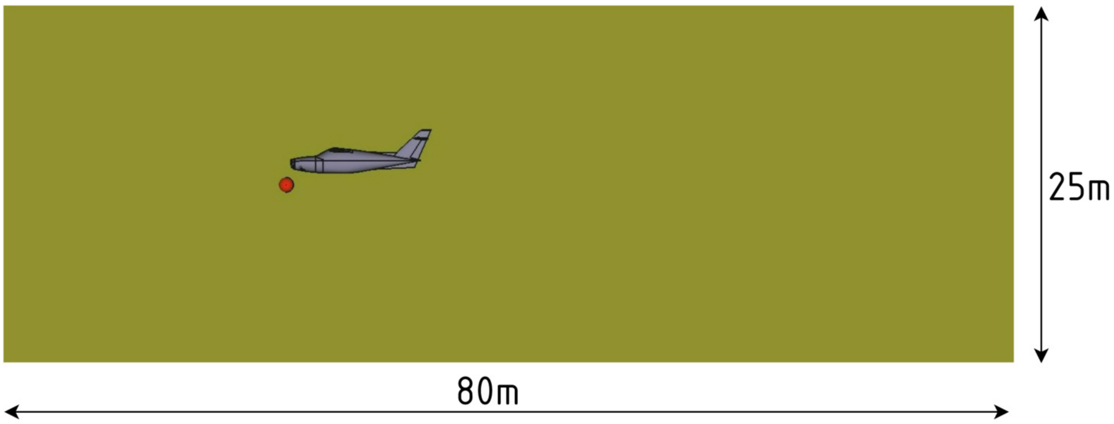

Figure 4.8: Side View of Background Mesh for the Cantilever Wing Configuration

(a) Top View

(b) Front View

Figure 4.9: Top and Front View of Background Mesh for the Cantilever Wing Configuration

The aircraft itself was meshed with the help of snappyHexMesh. The results are shown in Figure 4.10 as a surface geometry, and in Figure 4.11 as a wireframe including the computational area.

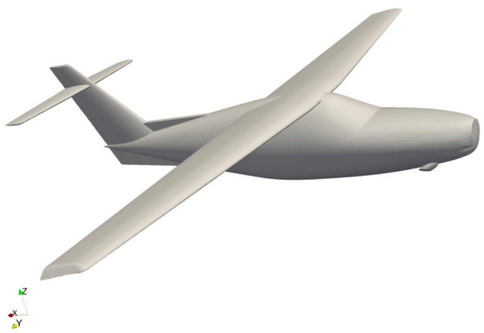

(a) Isometric Side View

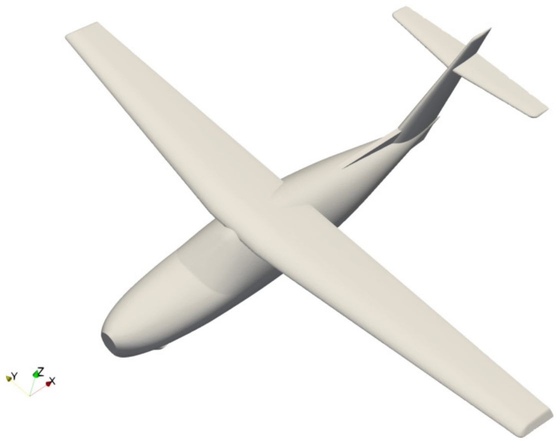

(b) Isometric Top View

Figure 4.10: Meshed Cantilever Wing Configuration as a Surface

(a) Aircraft with Background

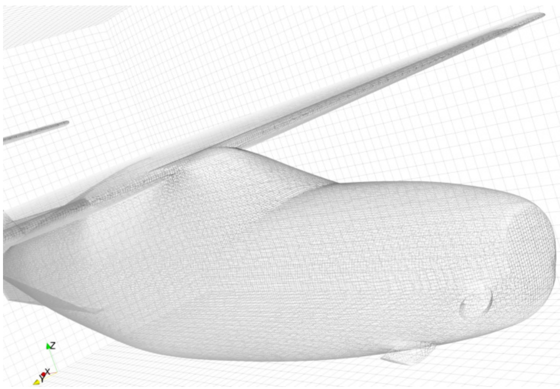

(b) Close Up of Wireframe

Figure 4.11: Meshed Cantilever Wing Configuration as a Wireframe

With the production of a working mesh, including the computational area as much as the outer surface of the cantilever wing Extra EA 400-500, it was possible to begin the actual CFD analysis of OpenFoam. It shall be noted to the reader that a grid independency study for the drag coefficient showed that the coefficient was constant for a mesh range between 550,000 and 770,000. The beforementioned geometries were all verified to be within said range. In this way, it was ensured that the solutions found during the analysis were not dependent on the grid size, but provided the actual flow behaviour.

4.4 Cantilever Wing Results of CFD Analysis

The CFD analysis was finished after several hundred iterations. Although the simulation was set to an initial iteration number of 1000, the analysis converged earlier. During the computational process, as shown in Figure 4.12, the calculations of greater angles took significantly longer, with $\alpha = 15°$ converging after 469 iterations.

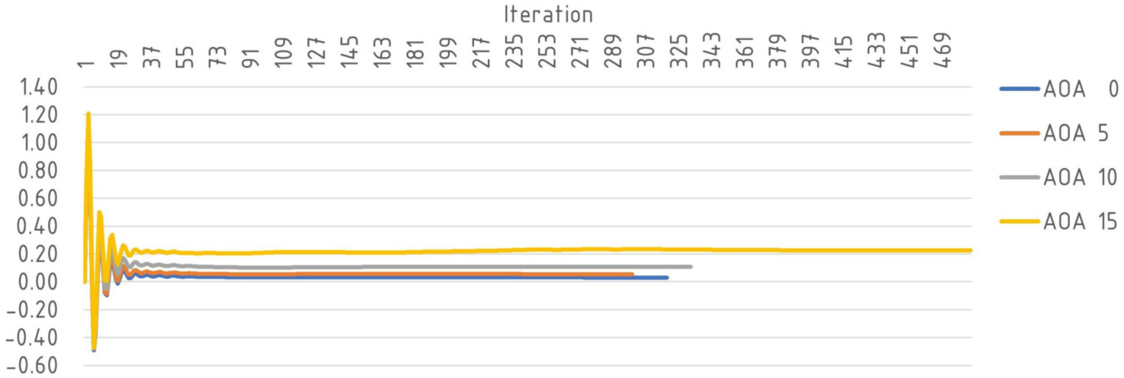

Figure 4.12: Iterations for the Cantilever Wing Configuration CFD Analysis

Figure 4.13 and Figure 4.14 shows the pressure distribution of the cantilever wing Extra EA 400-500 with AOAs ranging from zero up to fifteen degrees.

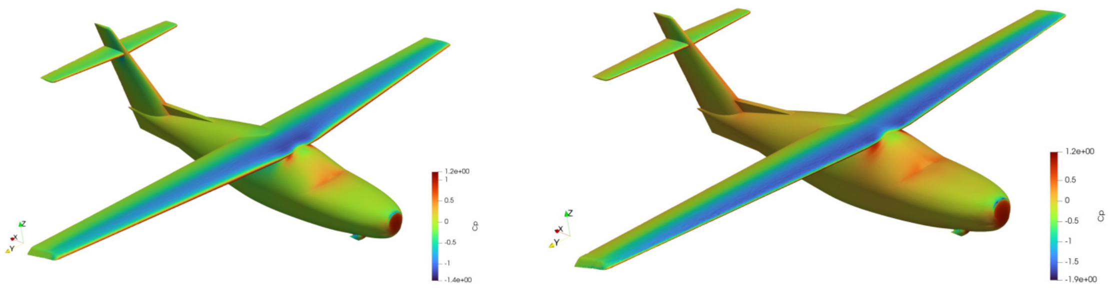

(a) AOA 0

(b) AOA 5

Figure 4.13: Results of the CFD Analysis for the Cantilever Wing with Low AOAs

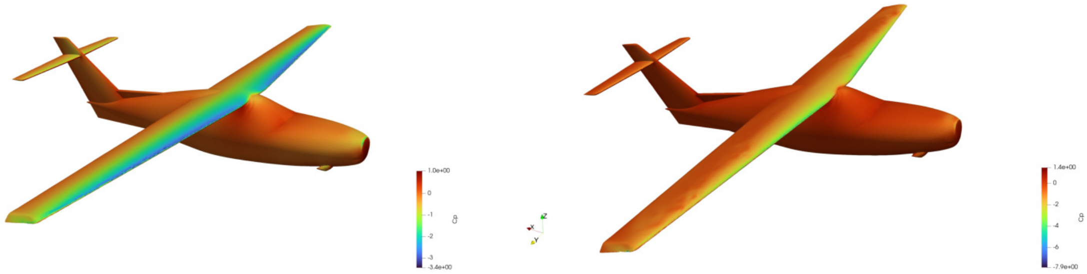

(a) AOA 10 (b) AOA 15

Figure 4.14: Results of the CFD Analysis for the Cantilever Wing with High AOAs

4.4.1 Lift and Drag Coefficient

The CFD analysis found that the cantilever wing configured Extra EA 400-500 showed typical behaviour for a high-wing T-tail aircraft. As seen in Figure 4.15(a), the highest lift coefficient C_L was found to be between an angle of attack of approximately 10° to 12°, whereafter a stalling of the wing was noticeable. This behaviour is typical for aircraft and the reader may be referred to Figure 2.5(b), where similar characteristics were shown for an isolated aerofoil. When evaluating the drag coefficient C_D, shown in Figure 4.15(b), it was found that the value increased at higher angle of attacks. This observation is supported by Figure 4.13 and Figure 4.14, in which the increase of the fuselage drag at higher AOA is clearly visible in the visualised pressure distribution.

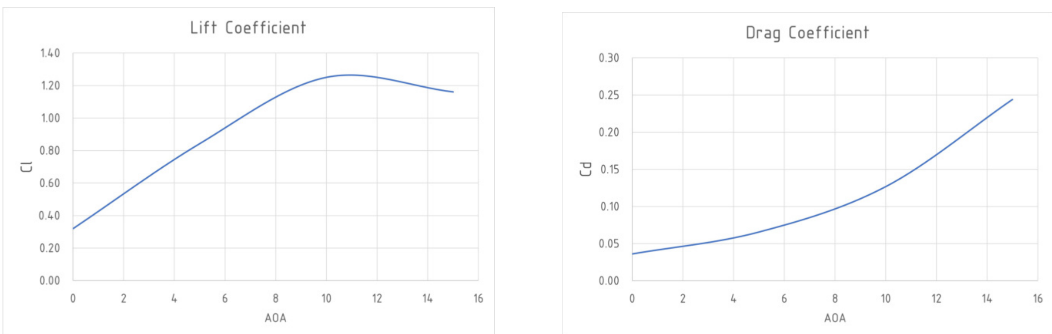

(a) Lift Coefficient $C_{L,CW}$ (b) Drag Coefficient $C_{D,CW}$

Figure 4.15: Drag and Lift Coefficient for Cantilever Wing Configuration

Both values resulted at a Lift/Drag-Ratio C_L/C_D, see Figure 4.16, between nearly nine for a zero degree AOA and about five for an AOA of 15°, reaching a maximum of approximately 13 at an AOA of 5°. The following Table 4.3 sums up the calculated values for AOAs between 0° and 15°.

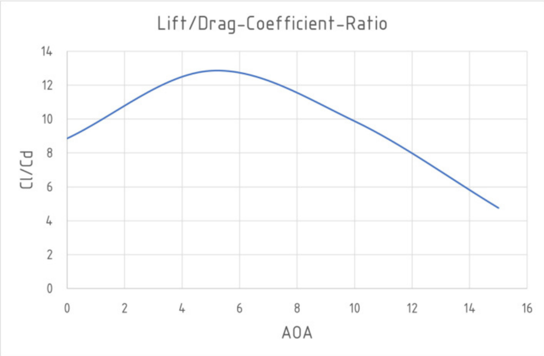

Figure 4.16: Lift/Drag-Ratio C_L/C_D for the Cantilever Wing Configuration

Table 4.3: C_L, C_D and C_L/C_D Values for the Cantilever Wing Configuration

AOA	C_L	C_D	C_L/C_D
0°	0.3194	0.0361	8.8476
1°	0.4412	0.0402	10.9751
2°	0.5416	0.0457	11.8512
3°	0.6476	0.0520	12.4538
4°	0.7556	0.0590	12.8067
5°	0.8620	0.0671	12.8464
6°	0.9632	0.0763	12.6238
7°	1.0556	0.0866	12.1893
8°	1.1356	0.0985	11.5289
9°	1.1996	0.1119	10.7202
10°	1.2440	0.1272	9.7798
11°	1.2652	0.1445	8.7557
12°	1.2596	0.1643	7.6664
13°	1.2136	0.1867	6.5002
14°	1.1736	0.2121	5.5332
15°	1.1611	0.2440	4.7586

CHAPTER 5

BOX WING CONFIGURATION

The aim of this study and the in the following presented new wing configuration was not only to develop a new design but be able to compare the two effectively. Therefore, a middle course was chosen to reach a satisfactory state between keeping and changing existing elements.

5.1 Development of the Box Wing Configuration

5.1.1 Main Wing

In a first step, it was required to slightly adjust the cantilever wing design by eliminating the wingtip devices. Since they were provided as single surfaces by the Type Certificate Holder, it was not necessary to estimate where to cut the winglets at. Therefore, the new end of the wings did indeed end at exactly the same distance of a real sans-winglet EA 400-500, when for instance operated at a sans-winglet MEL flight. This reduced the gross wing area from previously $14.3\,\mathrm{m}^2$ to a new wing area $A_{W,BW}$ of $13.5\,\mathrm{m}^2$. The results are shown in Figure 5.1.

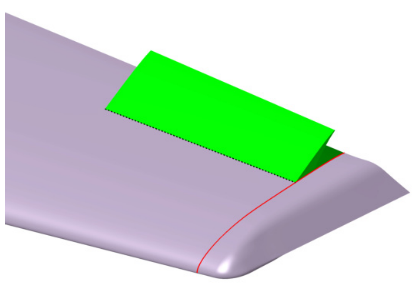

(a) The Wingtip Devices Start at the Red Line

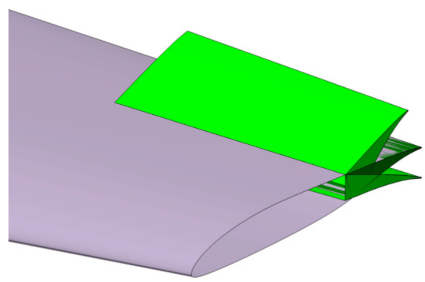

(b) Wing Without Wingtip Device

Figure 5.1: Adjustment to Wingtip of the Box Wing Configuration

Figure 5.1 above also shows, that the ailerons were located exactly at the end of the new wings. This led to difficulties in the design, as will be explained in a following subchapter.

5.1.2 Horizontal Stabiliser

The horizontal stabiliser had to be modified in order to allow a connection to the main wing. This was achieved by keeping the root of the stabiliser at its original state but changing the location of the stabiliser tip without changing the aerofoil geometry and size of said tip. The horizontal stabiliser therefore received a forward sweep $\Lambda_{H,BW}$ of -20° instead of the original $\Lambda_{H,CW} = 8°$. The stabiliser than had a length equal to the wings, thus 11 m in total, and a total area of $A_{H,BW}$ 8.8 m^2 including control elements surfaces. Figure 5.2 below shows the differences of the old and new horizontal stabiliser design.

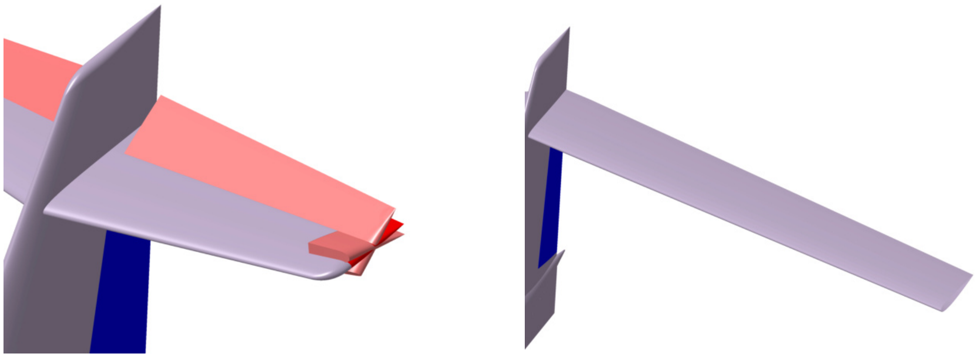

(a) Old Tailplane of the Cantilever Wing Design

(b) Extended Tailplane of the Box Wing Design

Figure 5.2: Adjustment to the Horizontal Stabiliser of the Box Wing Configuration

5.1.3 Vertical Connecting Structure

As a result of abovementioned adjustments to the wing and horizontal stabiliser, a stagger of $x_{AC,W\rightarrow AC,H} = 4.52m$ existed between the aerodynamic centre of the wing and the tailplane. The height difference between the two elements was measured to be $h_h = 0.80m$. It was therefore required to connect both open ends with a vertical connecting structure. During evaluation, it was determined that a symmetrical aerofoil would be best for such a structure, as it would not generate any asymmetric force inflight. However, this was only true when the structure had no vertical angle, which was ensured before, by adjusting the tailplane to exactly wings length. Additionally, to ensure commonality with at least one aerofoil of the EA 400-500, NACA 0012 was chosen as the vertical connecting structures' aerofoil. The structure had a backward sweep of 14.5°, tapered towards the tailplane, so that the aerofoil had a root chord length of 0.23 m and a tip chord length of 0.19 m. The aerofoil had a thickness of 0.03 m. The result is shown in Figure 5.3 and Figure 5.4.

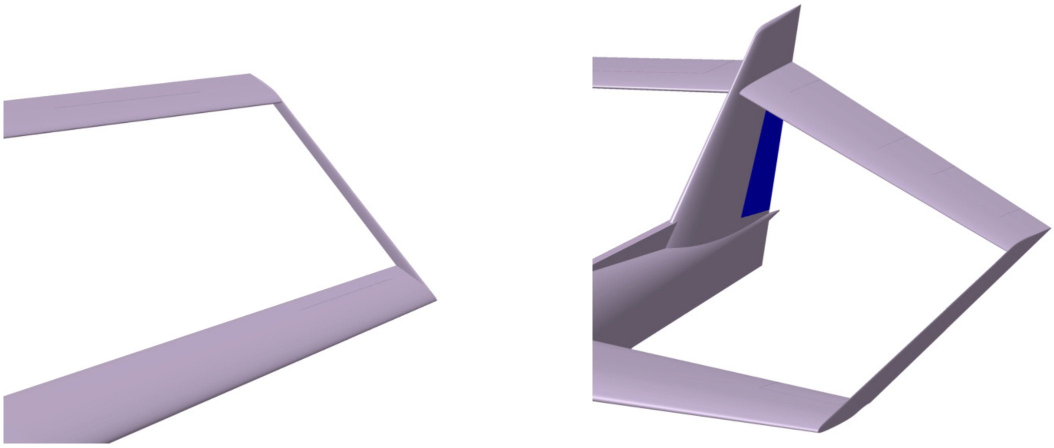

(a) Inner Surface (b) Outer Surface

Figure 5.3: Vertical Connecting Structure of the Box Wing Configuration

The design of the structure proved to be more difficult than anticipated as it was confined on the upper end by the upper surface of the tailplane while on the lower end by the lower surface of the wing. This required complex surfaces on both ends. As can be seen in Figure 5.4(a), the lower end of the vertical structure followed the lower aerofoil spline in order to ensure a flush ending. In contrast, it was decided to extend the vertical structure a bit further than the upper aerofoil spline of the tailplane. This ensured that no sharp ending could result in vortices being created at the tailplane wingtip. Therefore, a tangential ending of the vertical structure was chosen, which coincided with the aft aerofoil spline by ensuring adequate radii, as shown in Figure 5.4(b).

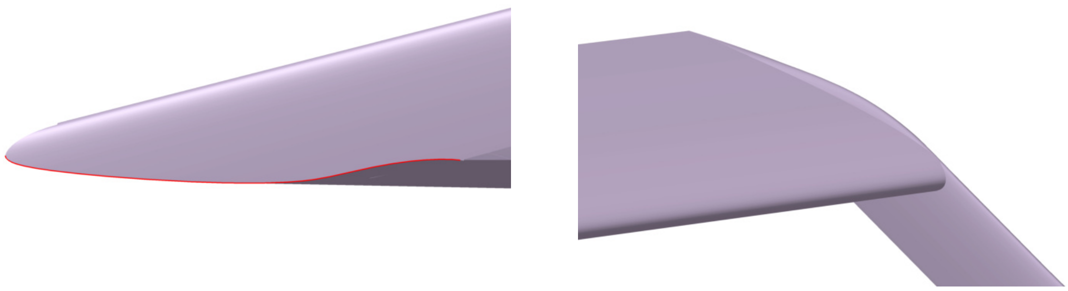

(a) Structure Adjusted to Aerofoil Spine (red) (b) Upper End of Structure

Figure 5.4: Adjustment to the Connecting Structure of the Box Wing Configuration

5.1.4 Control Surfaces

The change of wing design made some adjustments to the elevators and ailerons necessary. As the vertical stabiliser was not changed in any way, the rudder stayed as it was. However, as shown previously in Figure 5.1, the ailerons were exactly at the end of the wing. It needed to be ensured that sufficient space between the ailerons and the vertical structure was given. Additionally, it was analysed that the ailerons shall have some distance to the vertical structure in order to not be disrupted by any airflow discontinuities such as flow separation caused by the design of the structure and thus affecting the aileron effectiveness. As a result, the ailerons were moved 0.20 m towards the fuselage without change to any other geometry. The changes can be seen in Figure 5.5.

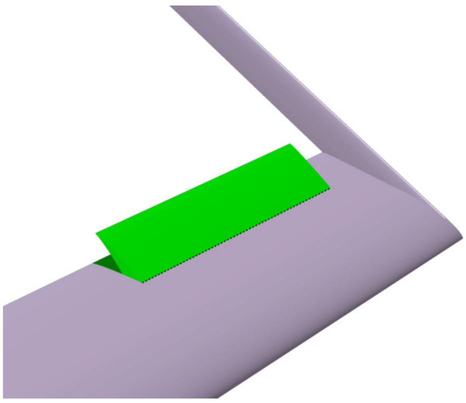

(a) Close-Up of the Aileron

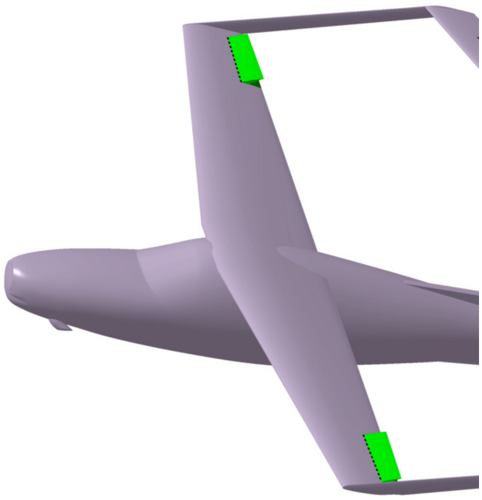

(b) Deflected Ailerons

Figure 5.5: Adjustment to Aileron Wing Location of the Box Wing Configuration

Due to the fact, that the tailplane was not only a small wing as previously but rather a big wing on its own, new control surfaces were required in order to ensure manoeuvrability. In a first step, new elevators were created for the box wing Extra EA 400-500. Usually, box wing configurations include ailerons of the length of the tailplane. After several iterations, a size of 0.48 m width and 2 m length was chosen. This resulted in an area of 0.96 m^2. These rather large elevators were limited in their deflection, but ensured that an elevator of smaller length than other solutions could be utilised. Furthermore, an additional set of ailerons were developed for the tailplane with a size of 0.33 m width and 1.5 m length, thus an area of 0.495 m^2. The tailplane elevators and ailerons are shown in Figure 5.6.

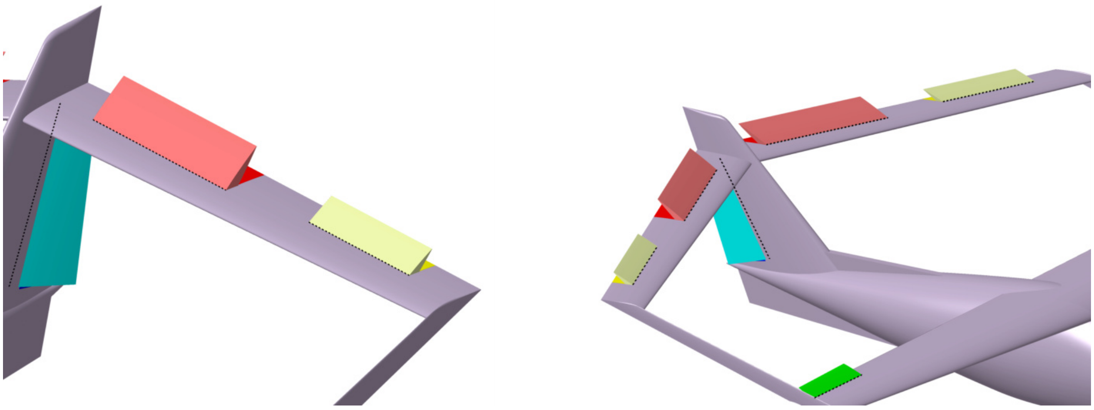

(a) Elevators (red) of the New Tailplane (b) Ailerons (yellow) of the New Tailplane

Figure 5.6: Elevators and New Ailerons of the Box Wing Configuration

5.1.5 Result of the Conceptual Design

Eventually, a box wing configuration for the Extra EA 400-500 was achieved. In the following, Figure 5.7, Figure 5.8, Figure 5.9, and Figure 5.10 show a general overview of the aircraft. A technical drawing can be found in Appendix B.

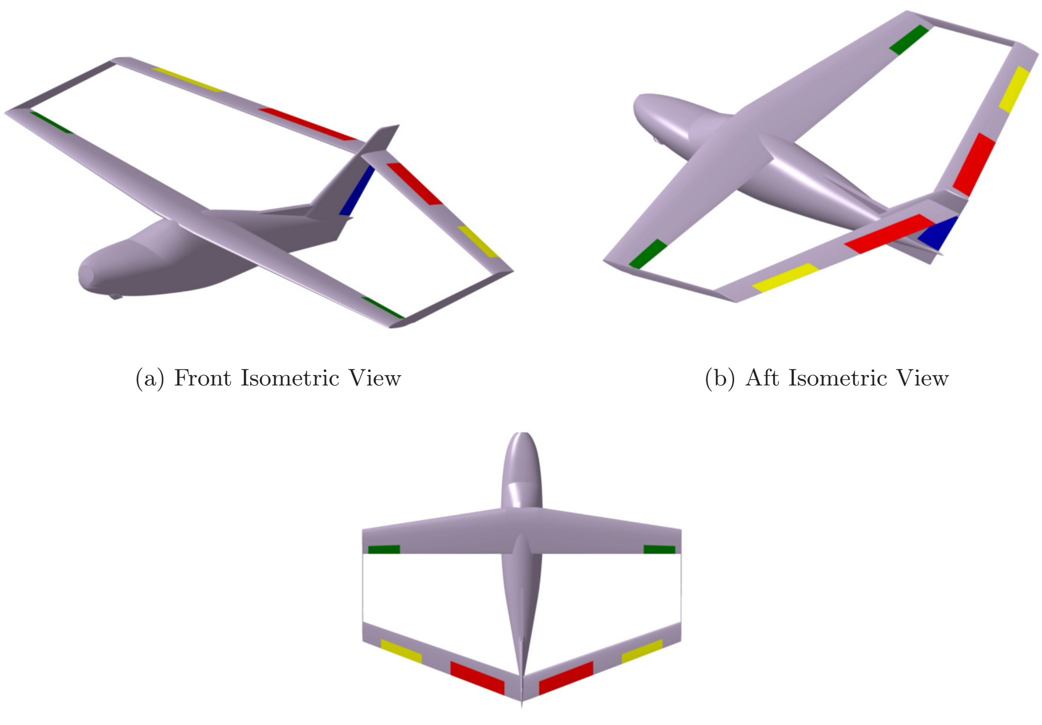

(a) Front Isometric View (b) Aft Isometric View

(c) Top View

Figure 5.7: Final Design of the Box Wing Configuration

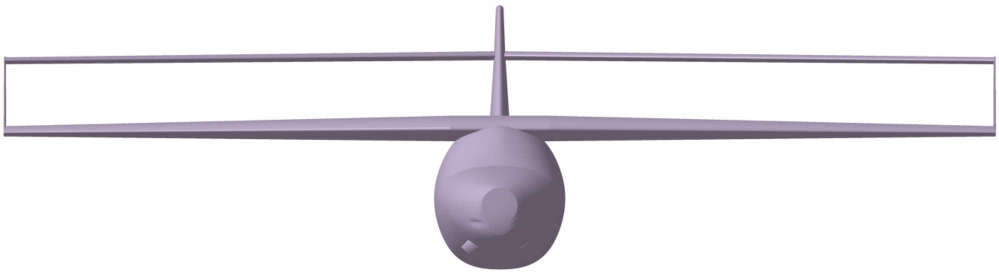

Figure 5.8: Front View of the Box Wing Configuration

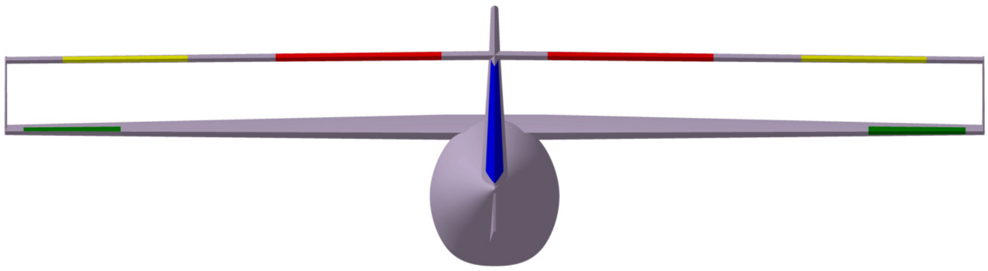

Figure 5.9: Back View of the Box Wing Configuration

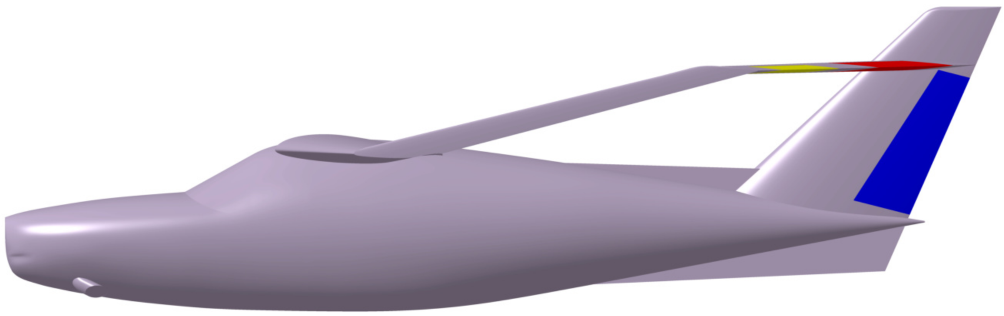

Figure 5.10: Side View of the Box Wing Configuration

5.2 Mesh Generation

Equally to the meshing process of the cantilever wing configuration, the Extra EA 400-500 with box wings had to be meshed in order to conduct a CFD analysis within OpenFoam. Special attention was paid to the fact that all settings were kept the same so that a correct comparison of both aircraft configuration were possible. The files exported from CATIA were again in an IGS.-file and with the same geometries as for the cantilever wing configuration.

5.2.1 Background and Aircraft Mesh

In the same manner as for the cantilever wing configuration, a computational domain was created. To ensure enough room for the flow to adapt to the geometry, the same background mesh as for the cantilever wing was created. As shown in Figure 4.8 and Figure 4.9, the computational domain was equally set to a height of 25 m, a width of 50 m and a length of 80 m. The background mesh including the box wing configured EA 400-500 is also shown in Figure 5.12(a). The result of the meshing process was the aircraft as shown with its surfaces in Figure 5.11 and as a wireframe in Figure 5.12(b). Once more, a grid study was conducted similarly to the cantilever wing configured analysis showing that a mesh range between 550,000 and 770,00 was sufficient for a stable calculation.

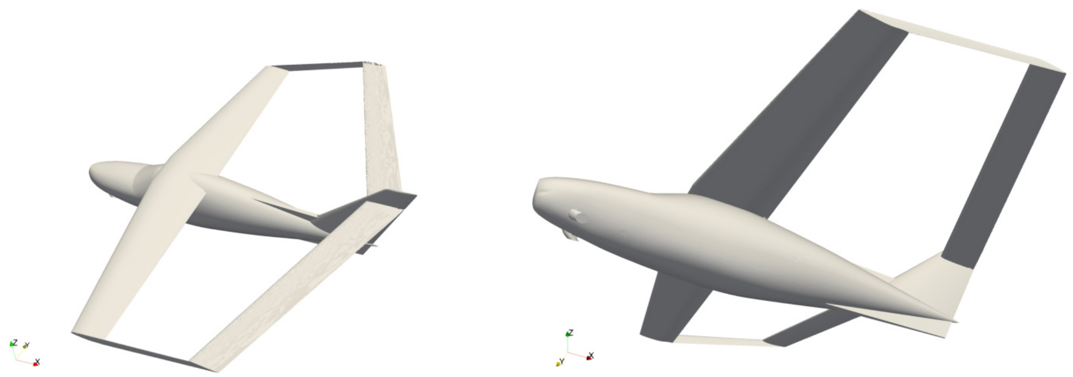

(a) Isometric Top View (b) Isometric Bottom View

Figure 5.11: Meshed Box Wing Configuration as a Surface

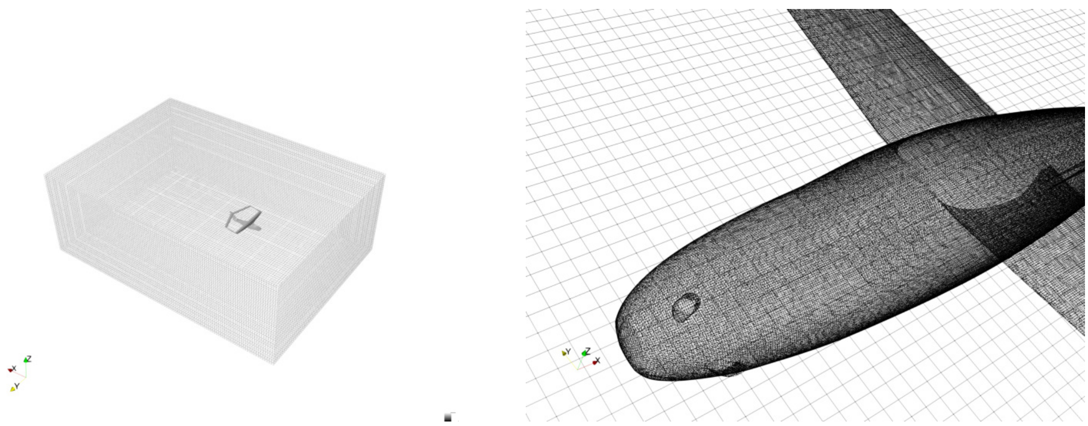

(a) Aircraft with Background (b) Close Up of Wireframe

Figure 5.12: Meshed Box Wing Configuration as a Wireframe

5.3 Box Wing Results of CFD Analysis

The calculation of all values relevant to the Extra EA 400-500 with box wings took approximately two times the calculation of the cantilever wing configuration. This can be seen, as shown in Figure 5.13, by the number of iterations reaching 617 before a conclusive solution was found.

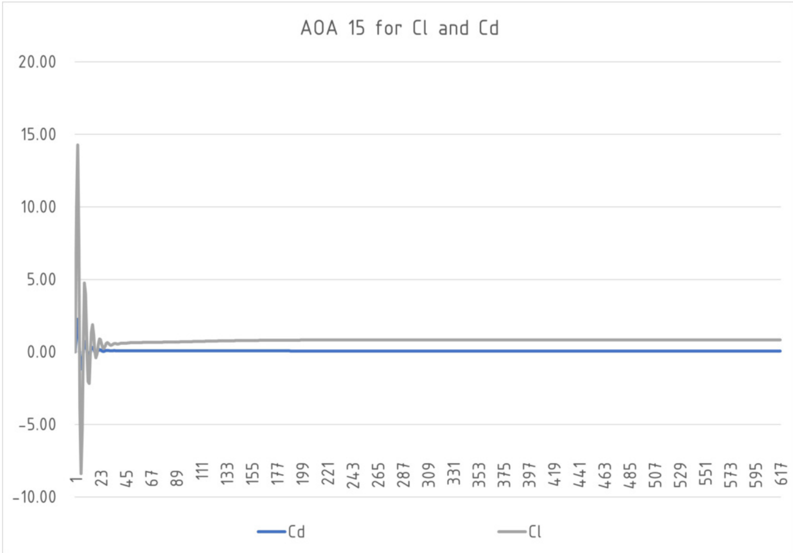

Figure 5.13: Iterations for the Box Wing Configuration CFD Analysis

Figure 5.14 below shows an excerpt of AOA angles: 5° and 15°. Of higher interest was the fifteen degree angle of attack, which showed differences to the cantilever wing configuration and will be further discussed in a later chapter.

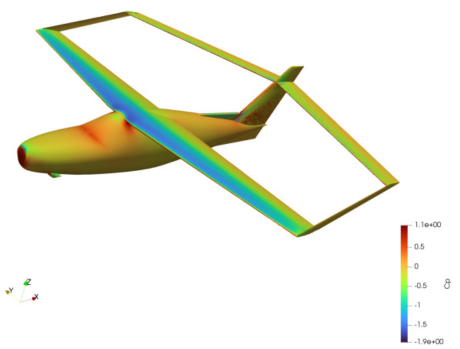

(a) AOA 5

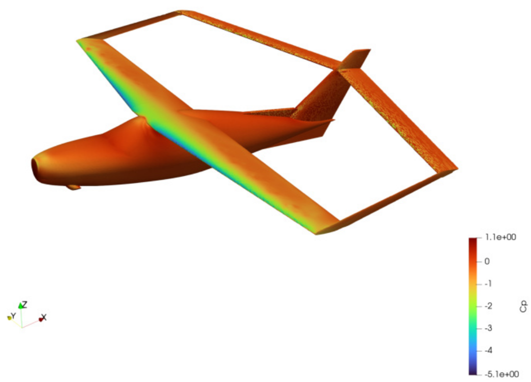

(b) AOA 15

Figure 5.14: Results of the CFD Analysis for the Box Wing

5.3.1 Lift and Drag Coefficients

The results for the lift and drag coefficient of the box wing configuration, C_L and C_D, were quite similar to the results of the cantilever wing Extra EA 400-500. This was to be expected considering the fact that the aircrafts remaining configuration was not changed, but only the horizontal stabiliser as much as the added vertical connecting structure. Therefore, it was observed that the box wing configurations lift and drag curve followed the same pattern but with slightly different values. The overall difference will be further discussed in the final chapter of this study, but it was seen that the box wing configuration had a higher lift coefficient for higher angle of attacks than the cantilever wing design and a lower drag coefficient, with the effect again increasing for higher angle of attacks. The increase of lift could mainly by explained due to the larger area of the horizontal stabiliser, while the difference in lift for greater AOAs could be explained by the forward sweep of the horizontal tail. The lift and drag coefficient, as much as their ratio, are shown in Figure 5.15 and Figure 5.16. In addition, Table 5.1 shows the values in more detail.

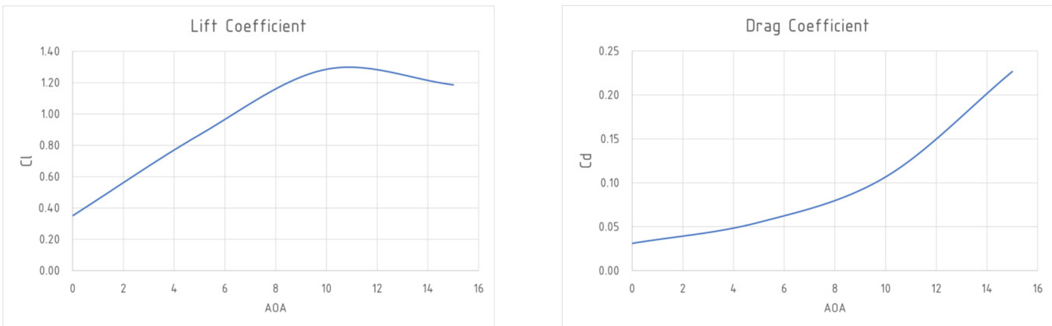

(a) Lift Coefficient $C_{L,BW}$ (b) Drag Coefficient $C_{D,BW}$

Figure 5.15: Drag and Lift Coefficient for the Box Wing Configuration

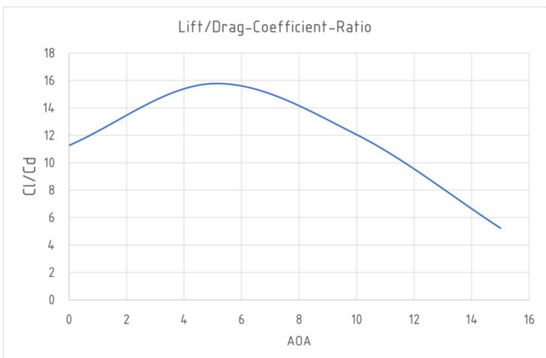

Figure 5.16: Lift/Drag-Ratio C_L/C_D for the Box Wing Configuration

Table 5.1: C_L, C_D and C_L/C_D Values for the Box Wing Configuration

AOA	C_L	C_D	C_L/C_D
0°	0.3501	0.0311	11.2572
1°	0.4649	0.0385	12.0753
2°	0.5820	0.0415	13.6915
3°	0.6563	0.0438	14.984
4°	0.7862	0.0499	15.7555
5°	0.8749	0.0547	15.994
6°	0.9694	0.0614	15.7915
7°	1.1295	0.0723	15.6375
8°	1.1645	0.08151	14.2865
9°	1.2283	0.0955	12.8617
10°	1.2877	0.1070	12.0345
11°	1.2919	0.1254	10.3022
12°	1.2831	0.1514	8.4749
13°	1.2548	0.1714	7.3208
14°	1.2390	0.2003	6.1857
15°	1.1859	0.2266	5.2334

CHAPTER 6

AERODYNAMIC ANALYSIS

Every aircraft flying in three-dimensional space, or in other words the air, has six degrees of freedom: surge forward or backward; heave up or down; sway left or right; pitch around the lateral axis; roll around the longitudinal axis; and yaw around the vertical axis. All possible movements are shown in Figure 6.1.

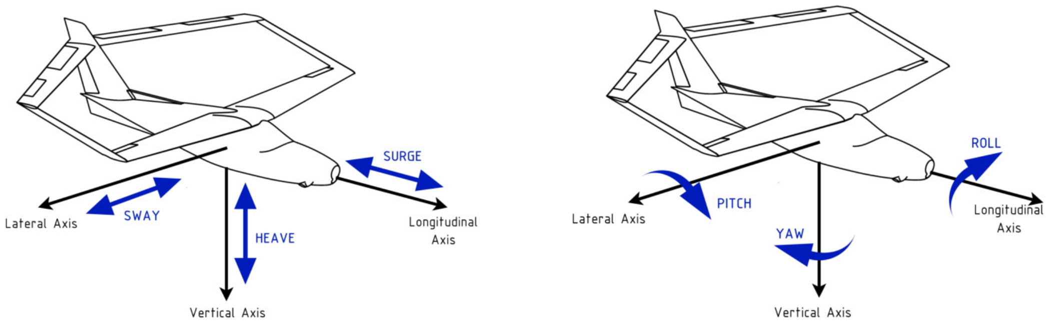

(a) Translational Motion (b) Rotational Motion

Figure 6.1: Six Degrees of Freedom for an Aircraft

In order to consider an aircraft as stable, it must fulfil several requirements regarding its motion around all axes: longitudinal stability around its lateral axis; lateral stability around its longitudinal axis; and directional stability around its vertical axis. The aim of every conceptual design should hence be to develop an aircraft, which shall be stable in every matter.

6.1 Longitudinal Motion

For an aircraft to maintain level flight with constant air speed, it is necessary for the whole system to have a balance of forces and moments. The required components for such a condition are visualised in Figure 6.2. Here, the drag D is by definition exactly opposite to the flight direction, shown by the speed vector V_A, while the lift L is perpendicular to V_A; gravitation G is vertically downward; and the thrust T is displaced by an engine installation angle i_b from the body axis x_b. Additionally, γ shows the inclination angle between V_A and the geodetic axis x_g, thus $\gamma = 0$ for level flight.

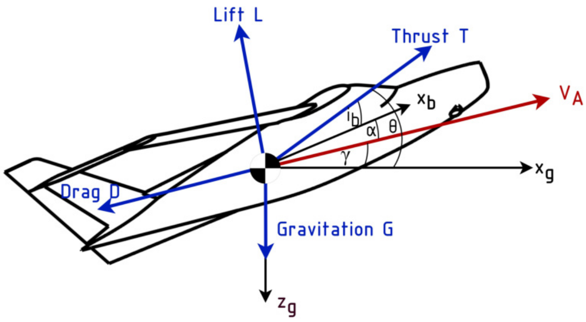

Figure 6.2: Longitudinal Forces During Flight – *Note: Angles Are Out of Proportion for Better Visualisation*

This allows for the following force equations as much as moment around the centre of gravity (CG):

$$-D + cos(\alpha + i_b)T - Gsin(\gamma) = 0 \tag{17}$$

$$-L + sin(\alpha + i_b)T + Gcos(\gamma) = 0 \tag{18}$$

$$M = 0 \tag{19}$$

When considering that i_b, α and γ are very small, one can assume that $sin(\gamma) \approx \gamma$ and $cos(\gamma) \approx 1$. Thus,

$$-D + T - G\gamma = 0 \tag{20}$$

$$-L + G = 0 \tag{21}$$

$$M = 0 \tag{22}$$

In summary, the abovementioned equations formulate that for level flight with $\gamma = 0$, thrust T has to counteract drag D, while the lift L must be of equal size to the gravitational force G. These forces and moments can be aerodynamically described by the following equations:

$$L = \frac{1}{2}\rho V_A^2 C_L A_W \tag{23}$$

$$D = \frac{1}{2}\rho V_A^2 C_D A_W \tag{24}$$

$$M = \frac{1}{2}\rho V_A^2 \bar{c}_W C_m A_W \tag{25}$$

where: A_W = Wing area

$\overline{c}_W$ = Length of wing Mean Aerodynamic Chord (MAC)

$\frac{1}{2}\rho V_A^2 = \overline{q}$ = Dynamic pressure

For the following calculations, this study will mainly focus on the aerodynamic coefficients C_L, C_D and C_m:

$$C_L = \frac{L}{\frac{1}{2}\rho V_A^2 A_W} \tag{26}$$

$$C_D = \frac{D}{\frac{1}{2}\rho V_A^2 A_W} \tag{27}$$

$$C_m = \frac{M}{\frac{1}{2}\rho V_A^2 \overline{c}_W A_W} \tag{28}$$

6.1.1 Longitudinal Stability

Longitudinal stability is defined as the stability of an aircraft along its lateral axis [62]. As shown in Figure 6.3, the aircraft needs to react to any longitudinal disturbance such as turbulences due to gust with a moment counteracting the undesired pitch moment. For this purpose, it is defined that an aircraft is in level flight, when the wings have an angle of attack α_0 which generates exactly enough lift to counteract the gravitational force. Under this circumstance, an equilibrium of moments exists, so that

$$C_m(\alpha_0) = 0 \tag{29}$$

In order for an aircraft to be longitudinal stable, therefore generate a counteracting moment when level flight is disturbed, the derivative $C_{m\alpha} = \frac{\partial C_m}{\partial \alpha}$ must be negative, hence $C_{m\alpha} < 0$. Additionally, one needs to take into account that $C_m(C_L = 0) > 0$ for an aircraft to be able to perform level flight and ensure static stability around the lateral axis.

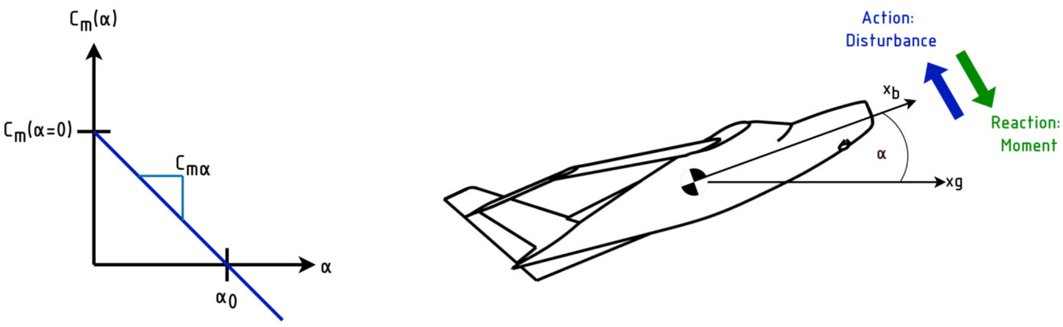

(a) Pitching Moment Coefficient (b) Additional Pitch Moment Due to Disturbances

Figure 6.3: Definition of Longitudinal Stability

The longitudinal stability is based on various interactions betweens forces acting on aircraft components, namely the wing and horizontal stabiliser. All relevant forces are shown in the following Figure 6.4, which visualises a wing and tail along the aircraft's box axis x_b as suggested by Fichter [63].

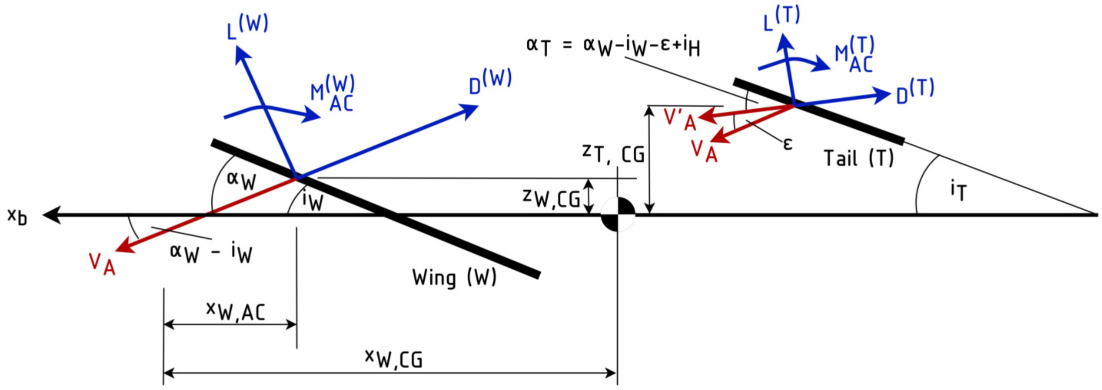

Figure 6.4: Forces Acting on Wing and Tail

With this schematic visualisation, it is now possible to find the moments along the aircraft's longitudinal axis:

$$\begin{aligned} M_{CG}^{(W)} =& L^{(W)} cos(\alpha_W - i_W)(x_{CG} - x_{AC}) + D^{(W)} sin(\alpha_W - i_W)(x_{CG} - x_{AC}) \\ & + L^{(W)} sin(\alpha_W - i_W) z_{CG} - D^{(W)} cos(\alpha_W - i_W) z_{CG} + M_{L,AC}^{(W)} \end{aligned} \tag{30}$$

Due to the size of forces as much as their lever arms, only the first and last terms are of significance. In addition, it is assumed that $\alpha_W - i_W$ are small, thus $cos(\alpha_W - i_W) = 1$. Additionally, the equation is divided by the static pressure $\overline{q}$ and mean aerodynamic chord

$\overline{c}$, to receive the respective coefficients. The equation is therefore simplified to

$$C_{m,CG}^{(W)} = C_L^{(W)} \left(\frac{x_{CG}}{\overline{c}_W} - \frac{x_{AC}}{\overline{c}_W} \right) + C_{m,AC}^{(W)} \tag{31}$$

Fichter defines that the lift is linearly dependent on the angle of attack, so that $C_L^{(W)} = C_{L0}^{(W)} + C_{L\alpha}^{(W)} \alpha_W$. Thus,

$$\begin{aligned} C_{m,CG}^{(W)} &= C_{m,AC}^{(W)} + C_{L0}^{(W)} \left(\frac{x_{CG}}{\overline{c}_W} - \frac{x_{AC}}{\overline{c}_W} \right) + C_{L\alpha}^{(W)} \left(\frac{x_{CG}}{\overline{c}_W} - \frac{x_{AC}}{\overline{c}_W} \right) \alpha_W \\ &= C_{m0}^{(W)} + C_{m\alpha}^{(W)} \alpha_W \end{aligned} \tag{32}$$

Since $C_{m,AC}^{(W)} < 0$ in general, static stability is not given without the help of a tail, or in other words: without a horizontal stabiliser. As can be seen in Figure 6.4, the tail is exposed to a lift $L^{(T)}$, drag $D^{(T)}$ and moment $M_{L,AC}^{(T)}$. The horizontal stabiliser has an installation angle i_T and is exposed to a downwash caused by the wings leading to an inclined flow by angle ϵ. The moment around the CG therefore can be described as

$$\begin{aligned} M_{L,CG}^{(T)} =& - x_T (L^{(T)} cos(\alpha_{xb} - \epsilon) + D^{(T)} sin(\alpha_{xb} - \epsilon)) \\ & - z_T (D^{(T)} cos(\alpha_{xb} - \epsilon) - L^{(T)} sin(\alpha_{xb} - \epsilon)) + M_{L,AC}^{(T)} \end{aligned} \tag{33}$$

where: $\alpha_{xb} - \epsilon =$ Angle between x_b-axis and V_A'

Similar to (30) and (31), the equation is again simplified and approximated, so that $M_{L,CG}^{(T)} = -x_T L^{(T)}$ as much as $L^{(T)} = \overline{q}_T A_H C_L^{(T)}$. Thus,

$$M_{L,CG}^{(T)} = -x_T \overline{q}_T A_H C_L^{(T)} \tag{34}$$

In the following step, the equation is divided by $\overline{q} A \overline{c}$. This results in the respective coefficient

$$C_{m,CG}^{(T)} = -\frac{-x_T A_H}{A_W \overline{c}_W} \frac{\overline{q}_T}{\overline{q}} C_L^{(T)} \tag{35}$$

Fichter defines $\eta = \frac{\overline{q}_T}{\overline{q}}$ as the ratio of static pressure between wing and tail, as much as the volume coefficient as $V_T = \frac{x_T A_H}{A_W \overline{c}_W}$. This leads to

$$C_{m,CG}^{(T)} = -\eta_T V_T C_L^{(T)} \tag{36}$$

In a last step, the lift coefficient of the tail can be described as a combination of α_T as much as the wing downwash including an effect caused by α_W, or in other words:

$$C_L^{(T)} = C_{L\alpha}^{(T)} \alpha_T = C_{L\alpha}^{(T)} (\alpha_W - i_W - \epsilon + i_T) \tag{37}$$

where: $\epsilon = \epsilon_0 + \frac{d\epsilon}{d\alpha} \alpha_W$

It is therefore possible to write

$$\begin{aligned} C_{m,CG}^{(T)} &= -\eta_T V_T C_{L\alpha}^{(T)} (i_T - i_W - \epsilon_0) - \eta_T V_T C_{L\alpha}^{(T)} \left(1 - \frac{d\epsilon}{d\alpha}\right) \alpha_W \\ &= -C_{m0}^{(T)} - C_{m\alpha}^{(T)} \alpha_W \end{aligned} \tag{38}$$

As mentioned earlier, longitudinal stability is not only affected by the wing but the tail equally: $C_{m\alpha} = C_{m\alpha}^{(W)} + C_{m\alpha}^{(T)}$, or in other words:

$$C_{m,CG} = C_{m0} + C_{m\alpha} \alpha_W \tag{39}$$

$$C_{m0} = C_{m,AC}^{(W)} + C_{L0}^{(W)} \left(\frac{x_{CG}}{\bar{c}_W} - \frac{x_{AC}}{\bar{c}_W}\right) + \eta_T V_T C_{L\alpha}^{(T)} (\epsilon_0 + i_W + i_T) \tag{40}$$

$$C_{m\alpha} = C_{L\alpha}^{(W)} \left(\frac{x_{CG}}{\bar{c}_W} - \frac{x_{AC}}{\bar{c}_W}\right) - \eta_T V_T C_{L\alpha}^{(T)} \left(1 - \frac{d\epsilon}{d\alpha}\right) \tag{41}$$

$C_{m\alpha}$ can also be defined by the location of the so-called neutral point (NP). The neutral point arrives from the thought that an additional lift is created when the angle of attack α increases. However, to maintain $C_{m\alpha} = 0$, it is necessary for this force to not affect the moment of the aircraft. This is only the case when the additional lift is located at a defined neutral point x_{NP}. It is therefore assumed that $C_{m\alpha} = 0$, see (29), and $x_{CG} = x_{NP}$. This results in

$$\frac{x_{NP}}{\bar{c}_W} = \frac{x_{AC}}{\bar{c}_W} + \eta_T V_T \frac{C_{L\alpha}^{(T)}}{C_{L\alpha}^{(W)}} \left(1 - \frac{d\epsilon}{d\alpha}\right) \tag{42}$$

$$\Longrightarrow \frac{x_{AC}}{\bar{c}_W} = \eta_T V_T \frac{C_{L\alpha}^{(T)}}{C_{L\alpha}^{(W)}} \left(1 - \frac{d\epsilon}{d\alpha}\right) - \frac{x_{NP}}{\bar{c}_W} \tag{43}$$

By inserting (43) into (41) follows

$$C_{m\alpha} = \left(\frac{x_{CG}}{\bar{c}} - \frac{x_{NP}}{\bar{c}}\right) C_{L\alpha}^{(W)} \tag{44}$$

To achieve longitudinal stability, $C_{m\alpha} < 0$, the following requirement must be given: $x_{NP} > x_{CG}$. Therefore, when the neutral point is behind the centre of gravity, a counteracting moment is created when a disturbance pitch is experienced and the nose will be lowered as a result.

For further calculations, the expression for $C_{m,CG}$ is realigned to

$$\begin{aligned} C_{m,CG} = & \underbrace{C_{m,AC}^{(W)} + C_{L0}^{(W)}\left(\frac{x_{CG}}{\bar{c}_W} - \frac{x_{AC}}{\bar{c}_W}\right) + C_{L\alpha}^{(W)}\left(\frac{x_{CG}}{\bar{c}_W} - \frac{x_{AC}}{\bar{c}_W}\right)}_{C_{m,CG}^{(W)}} \\ & \underbrace{+\eta_T V_T C_{L\alpha}^{(T)}(\epsilon_0 + i_W + i_T) - \eta_T V_T C_{L\alpha}^{(T)}\left(1 - \frac{d\epsilon}{d\alpha}\right)}_{C_{m,CG}^{(T)}} \end{aligned} \tag{45}$$

and $C_{m,CG}^{(B)}$ introduced to the equation as the effect of the fuselage body on the pitching moment around CG:

$$C_{m,CG} = \underbrace{C_{m,CG}^{(W)} + C_{m,CG}^{(B)}}_{C_{m,CG}^{(W(B))}} + C_{m,CG}^{(T)} \tag{46}$$

whereas $C_{m,CG}^{(W(B))}$ represents the wing-fuselage contribution in accordance with Datcom [53], especially for aircraft with relatively small wingspan-to-body-diameter ratios. The effects of the wing-body and the tail will be analysed in the following.

Wing-Fuselage Contribution

As noted above, when considering small wing-span-to-body diametres, it can be of advantage according to Datcom to evaluate the combined effect of the wing and fuselage. For this purpose, Datcom defines the estimated pitch moment coefficient of both elements as

$$C_{m,CG}^{(W(B))} = K_N + \left[K_{W(B)} + K_{B(W)}\right] C_{L\alpha,e} \frac{A_{W,exp}}{A_W} \tag{47}$$

where: A_{exp} = Exposed Wing Area (Outward of Fuselage Radius)

In the following, the nose lift K_N, wing-to-body lift $K_{W(B)}$ and body-to-wing lift $K_{B(W)}$ ratios will be calculated. While the two latter can be extracted from (49) and (50), the nose lift ratio is to be found as

$$K_N = \frac{2(k_2 - k_1)A_{B,max}}{A_W} \tag{48}$$

In this equation, $A_{B,max}$ is the maximum frontal area of the fuselage, A_W the wing area, whereas the factor of $(k_2 - k_1)$ depends on the fineness ratio of the aircraft and can be found with the help of Figure 6.5.

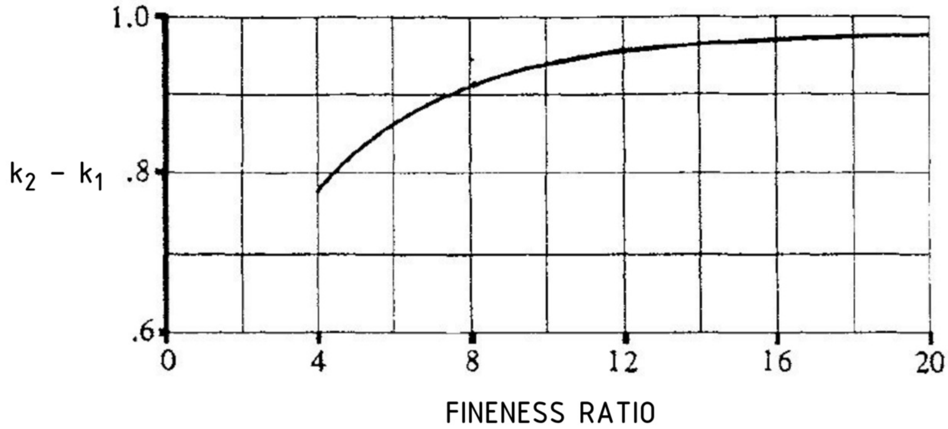

Figure 6.5: Fineness Ratio Diagram [53]

Factors $K_{B(W)}$ and $K_{W(B)}$ can be found with the help the following equations, where $b_{f,max}$ is the maximum width of the aircraft fuselage and b the total wing length.

$$K_{B(W)} = 0.1714\left(\frac{b_{f,max}}{b}\right)^2 + 0.8326\left(\frac{b_{f,max}}{b}\right) + 0.9974 \tag{49}$$

$$K_{W(B)} = 0.7810\left(\frac{b_{f,max}}{b}\right)^2 + 1.1976\left(\frac{b_{f,max}}{b}\right) + 0.0088 \tag{50}$$

According to Datcom, the wing lift-curve slope for conceptual designs can be evaluated to be

$$a_W = \frac{2\pi AR_W}{2 + \sqrt{\frac{AR_W^2 \chi^2}{k_W^2}\left(1 + \frac{tan^2(\Lambda_{c/2,W})}{\chi^2}\right) + 4}} \tag{51}$$

Where $\chi = \sqrt{1 - Ma^2}$, $\Lambda_{\frac{c}{2},W}$ is the midchord sweep, AR_W is the aspect ratio of $\frac{b^2}{A_W}$ and $k_W = \frac{a_{0,W}}{2\pi}$ is to be found with

$$a_{0,W} = \frac{1.05}{\sqrt{1 - Ma^2}}\left[\frac{a_0}{(a_0)_{theory}}\right]_W (a_0)_{theory,W} \tag{52}$$

where: a_0 = 2D sectional lift-curve slope

$(a_0)_{theory}$ = Theoretical 2D sectional lift-curve slope; See Figure 6.6(b)

$\frac{a_0}{(a_0)_{theory}}$ = Correction Factor; See Figure 6.6(a)

The Reynolds number of Figure 6.6 is with respect to the section chord. The trailing-edge included angle Φ'_{TE} is calculated by an angle between two lines passing $\frac{x}{c} = 0.9 \wedge 0.99$ on the lower and upper surfaces of the aerofoil [64]:

$$\tan\left(\frac{\Phi'_{TE}}{2}\right) = \frac{0.5y_{0.9} - 0.5y_{0.99}}{9} \tag{53}$$

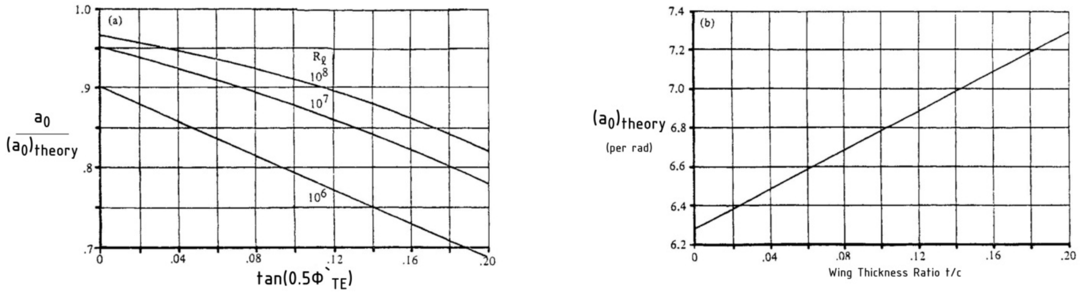

(a) Theoretical Sectional Lift-Curve Slope (b) Empirical Correction Factor

Figure 6.6: Sectional 2D Lift-Curve Slope of Wings [53]

Tail Contribution

According to Pamadi [64], the highly complex determination of the wing downwash onto the tail, see (37), can be substituted for early conceptual designs with the empirical relation presented by Datcom:

$$\frac{d\epsilon}{d\alpha} = 4.44\left[K_{AR}K_{\lambda}K_H \cos(\Lambda_{c/4,W})^{\frac{1}{2}}\right]^{1.19} \tag{54}$$

where: K_{AR} = Wing Aspect Ratio

K_{λ} = Wing Taper Ratio

K_H = Horizontal Tail Location Factor

$$K_{AR} = \frac{1}{AR_W} - \frac{1}{1 + AR_W^{1.7}} \tag{55}$$

$$K_{\lambda} = \frac{10 - 3\lambda_W}{7} \tag{56}$$

$$K_H = \frac{1 - \frac{h_H}{b}}{\sqrt[3]{\frac{2l_H}{b}}} \tag{57}$$

In equation (57), the term l_h is the parallel distance between the wing MAC quarter point and the horizontal stabiliser MAC quarter point. h_H is the distance of the tailplane MAC

measured from the wing root chord height. This eventually allows the formulation of $\epsilon = \frac{d\epsilon}{d\alpha}\alpha_W$.
Pamadi defines the tail lift as

$$L^{(T)} = q_T A_H C_L^{(T)} \tag{58}$$

and simplifies that

$$C_L^{(T)} = a_H \alpha_T = a_H(\alpha_W - i_W + i_T - \epsilon) \tag{59}$$

and further assumes that $C_L^{(T)} = a_W \alpha_W$, which leads to

$$\frac{dC_L^{(T)}}{dC_L} = \left(\frac{dC_L^{(T)}}{d\alpha_T}\right)\left(\frac{d\alpha_T}{d\alpha_W}\right)\left(\frac{d\alpha_W}{dC_L}\right) = \frac{a_T}{a_W}\left(1 - \frac{d\epsilon}{d\alpha}\right) \tag{60}$$

For further calculations, the tail lift-curve slope a_H is to be evaluated by utilising (51) and assuming that $C_{L\alpha} = a_H \cdot \alpha$ with the respective values adapted to the tailplane. Furthermore, the dynamic pressure ratio at the tailplane η_T needs to be taken into consideration, which describes the influence of the wing wake on the horizontal tail [64]. For this purpose, Datcom defines that

$$\eta_T = \frac{q_T}{q} = 1 - \frac{\Delta q}{q} = 1 - \frac{2.42\sqrt{C_{DO,W}}}{\frac{l_{H1}}{\bar{c}_W} + 0.3} \tag{61}$$

whereas the zero-lift drag coefficient can be calculated by

$$C_{DO,W} = C_{f,W}\left[1 + L'\left(\frac{t}{c}\right)_W + 100\left(\frac{t}{c}\right)_W^4\right] R_{LS,W} \frac{A_{W,wet}}{A_W} \tag{62}$$

where: l_{H1} = Distance between trailing edge of wing and AC of tailplane
$C_{f,W}$ = Turbulent Flat Plate Skin-Friction Coefficient; See Figure 6.7(a)
L' = Aerofoil Thickness Location Parameter
L' = 2.0 for aerofoil maximum thickness within 0.3c; else L' = 1.2
$R_{L,S}$ = Relation of sweep angle and specific chord location; See Figure 6.7(b)
A_{wet} = Wetted wing area; $A_{wet} = A$ for up to medium angles of attack

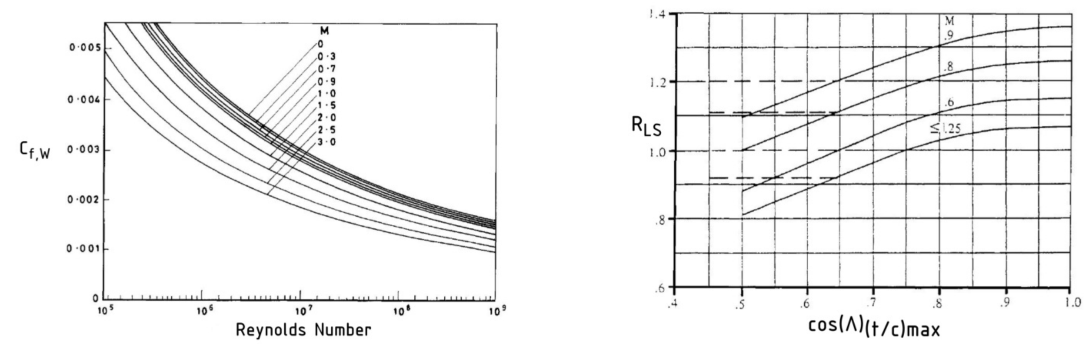

(a) Flat Plate Skin-Friction Coefficient

(b) Parameter R_{LS}

Figure 6.7: Parameters for Wing Zero-Lift Drag Coefficient [53]

Pamadi writes that

$$M^{(T)} = -L^{(T)} l_H \tag{63}$$

or in other words:

$$C_{m,CG}^{(T)} = -C_L^{(T)} \frac{q_T}{q} \frac{A_H l_H}{A_W \bar{c}_W} = -a_H(\alpha_W - i_W + i_T - \epsilon)\eta_T \frac{A_H l_H}{A_W \bar{c}_W} \tag{64}$$

Summary Directional Stability

This means that the pitching moment coefficient around CG can be calculated as

$$C_{m,CG} = K_N + \left[K_{W(B)} + K_{B(W)}\right] C_{L\alpha,e} \frac{A_{W,exp}}{A_W} - a_H(\alpha_W - i_W + i_T - \epsilon)\eta_T \frac{A_W l_H}{A_W \bar{c}_W} \tag{65}$$

6.1.2 Longitudinal Control: The Elevators

In order to change the pitch of an aircraft, elevators placed on the tailplane can be used. Their main function is to change the tail lift and hence the pitching moment equation of (46) by

$$C_{m,CG} = C_{m,CG}^{(W(B))} + C_{m,CG}^{(T)} = C_{m,CG}^{(W(B))} - a_H(\alpha_W - i_W + i_T - \epsilon + \tau_e \delta_e)\eta_T \frac{A_H l_H}{A_W \bar{c}_W} \tag{66}$$

with the elevator effectiveness defined as

$$\tau_e = \frac{d\alpha_T}{d\epsilon_e} \tag{67}$$

and estimated by the control surface span factor K_b from Figure 6.8(b), the ratio of the 2D-3D control effectiveness $\frac{(\alpha_\delta)_{C_L}}{(\alpha_\delta)_{C_l}}$ from Figure 6.8(a), $C_{l\delta} = \frac{\partial C_l}{\partial \delta_e}$ from Figure 6.9, and a_0 with respect to the required parameters from (52). Hence,

$$\tau_e = \frac{C_{l\delta}}{a_0}\left[\frac{(\alpha_\delta)_{C_L}}{(\alpha_\delta)_{C_l}}\right]K_b \tag{68}$$

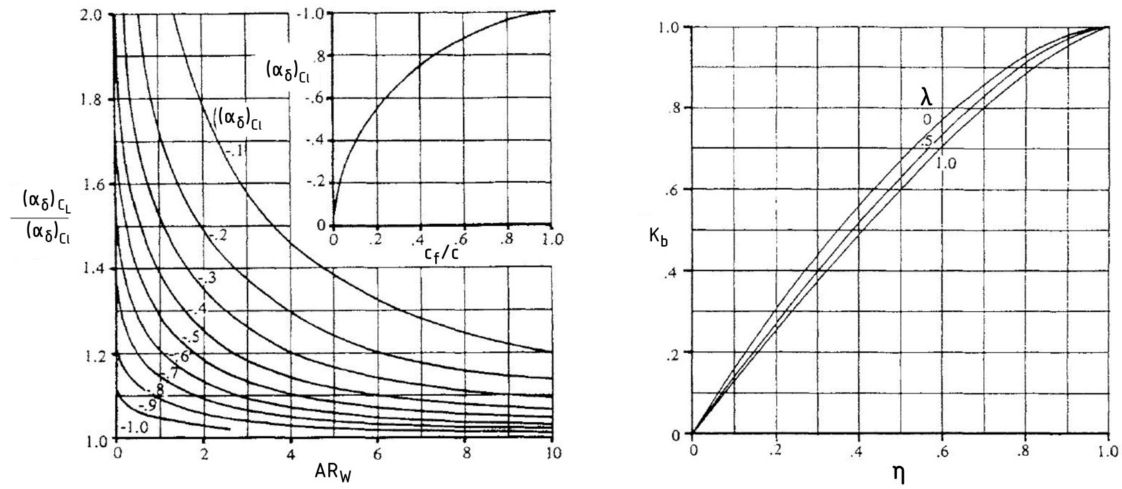

(a) Flap Chord Factor

(b) Flap Span Factor

Figure 6.8: Flap Factors for Elevator Evaluation [53]

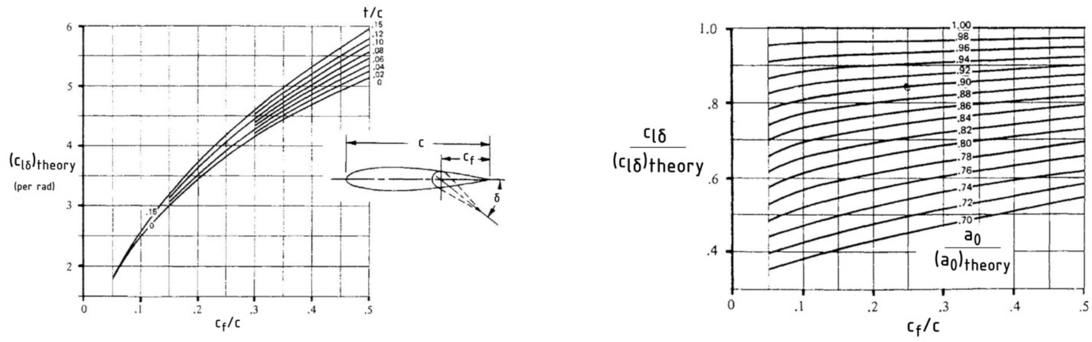

(a) Lift Effectiveness of Trailing-Edge Flaps

(b) Correction Factor For Lift Effectiveness

Figure 6.9: Factor for Lift Effectiveness of Trailing-Edge Flaps [53]

The elevator deflection under the constraint of $C_m = 0$ can be described as

$$\delta_e = \frac{C_{m,CG}^{(W(B))} - a_H(\alpha_W - i_W + i_T - \epsilon)\eta_T \frac{A_H l_H}{A_W \bar{c}_W}}{a_H \eta_T \frac{A_H l_H}{A_W \bar{c}_W}\tau_e} \tag{69}$$

This allows the formulation of

$$\frac{d\delta_e}{dC_L} = -\frac{\left(\frac{dC_m}{dC_L}\right)_{FIXED}}{c_{m\delta e}} = -\frac{x_{CG} - x_{NP}}{c_{m\delta e}} = -\frac{x_{CG} - x_{NP}}{-a_H \eta_T \frac{A_H l_H}{A_W \bar{c}_W} \tau_e} \tag{70}$$

According to Pamadi, a statically stable aircraft must fulfil the requirement that

$$\frac{d\delta_e}{dC_L} < 0 \tag{71}$$

6.1.3 Longitudinal Discussion of the Box Wing Configuration

To find out whether the Extra EA 400-500 with box wing configuration can be assumed to be longitudinal stable, the location of the neutral point was to be found. Furthermore, this study analysed the pitching moment coefficient of the aircraft as much as the effect of the elevators during flight.

Location of the Neutral Point: Longitudinal Stability

The centre of gravity (CG) of an empty cantilever wing Extra EA 400-500 lays 3.57 m behind reference datum, as stated in the Pilot's Operation Handbook [56, p. 6-21]. As measured in CATIA, the reference datum lays 0.31 m in front of the aircraft's most forward point, located at the upper portion of the nose section. This information was required in order to analyse the CG of the box wing configuration. A suitable solution was found by utilising the measure inertia function of CATIA and assuming that the connecting structure as much as the tailplane are to be made of a homogenous material. This allowed to calculate a correction factor ratio between CATIA's assumed CG and the real CG: $\frac{CG_{real}}{CG_{catia}} = 0.74$. Thus, it was verified that the cantilever wing CG lied at $CG_{CW,real} = 0.74 \cdot CG_{CW,catia} = 0.74 \cdot 4.853m = 3.60m$ behind reference datum. In the same manner, the box wing CG with respect to reference datum was calculated to be

$$x_{CG} = CG_{BW,real} = 0.74 \cdot CG_{BW,catia} = 0.74 \cdot 5.343m = 3.95m \tag{72}$$

To further analyse whether the box wing aircraft was longitudinal stable or not, the distance between the aircraft's aerodynamic centre (AC) to the neutral point was calculated. For this purpose, the following conceptual design stage equation [65] was used:

$$\Delta x_{AC \to NP} = \sqrt[4]{\frac{A_W}{b}} \cdot 0.25 \cdot \Delta x_{AC,W \to AC,H} \cdot \frac{A_H}{A_W} \cdot \phi_T \tag{73}$$

where: $\Delta x_{AC \rightarrow NP}$ = Distance between AC and NP
A_W = Wing Area [$13.5m^2$]
b = Wing span [$11.0m$]
$\Delta x_{AC,W \rightarrow AC,H}$ = Distance between AC of wing and stabiliser
A_H = Horizontal stabiliser area [$8.44m^2$]
ϕ_T = Tail Efficiency [T-tail: 0.85]

The location of the aerodynamic centre of the wing was found with the fact, that the wing "MAC is 1322 mm; 0% is at 3200 mm aft reference datum"[56, p. 6-21]. Assuming that the aerodynamic centre of the wing is located at $0.25\bar{c}$, the distance of the AC from reference datum was calculated to be $x_{AC,W} = 0.25\bar{c}_W + 3.20m = 0.25 \cdot 1.322m + 3.20m = 3.53m$. Equally, the AC of the NACA 0012 profile is located at $0.25\bar{c}_H$ [66]. With a MAC of 0.8 m and the horizontal stabiliser leading edge at that position being 7.85 m aft of reference datum, the distance of the AC was calculated at $x_{AC,H} = 0.25\bar{c}_H + 7.85m = 0.25 \cdot 0.8m + 7.85m = 8.05m$ With the help of the above calculated values and (73), the location of the neutral point measured from AC was

$$\Delta x_{AC \rightarrow NP} = \sqrt[4]{\frac{13.5m^2}{11.0m}} \cdot 0.25 \cdot (8.05m - 3.53m) \cdot \frac{8.44m^2}{13.5m^2} \cdot 0.85 = 0.63m \tag{74}$$

The solution showed, that the neutral point of the box wing configuration laid 0.63 m behind the AC, thus at $x_{NP} = 4.16m$ aft reference datum. This meant, that (44) was fulfilled because of $x_{NP} > x_{CG}$ so that $C_{m\alpha} < 0$ and longitudinal stability was given. The static margin was found to be

$$SM = \frac{x_{NP} - x_{CG}}{\bar{c}} = \frac{4.16m - 3.95m}{1.32m} = 0.16 \tag{75}$$

Pitching Moment Coefficient

As noted earlier, see (65), the pitching moment coefficient for a conceptual design can be calculated as a combination of the wing-body contribution and the tail contribution. This required several factors and ratios to be calculated, such as the nose-lift factor K_N, see (76). With the help of CATIA, the fineness ratio was found by dividing the aircraft length to the maximum aircraft fuselage diametre: $Fi = \frac{9.56m}{1.42m} = 6.7$. Thus, by referring to Figure 6.5, it was evaluated that $(k_2 - k_1) = 0.88$. Additionally, $A_{B,max} = 1.94m^2$. With these information, the nose lift factor was calculated as

$$K_N = \frac{2(k_2 - k_1)A_{B,max}}{A_W} = \frac{2 \cdot 0.88 \cdot 1.94m^2}{13.5m^2} = 0.25 \tag{76}$$

The remaining two factors for $K_{B(W)}$ and $K_{W(B)}$ were calculated by utilising (49) and (50), respectively. The maximum fuselage width equals the already used width of 1.42 m.

$$K_{B(W)} = 0.1714\left(\frac{1.42m}{11.0m}\right)^2 + 0.8326\left(\frac{1.42m}{11.0m}\right) + 0.9974 = 1.11 \tag{77}$$

$$K_{W(B)} = 0.7810\left(\frac{1.42m}{11.0m}\right)^2 + 1.1976\left(\frac{1.42m}{11.0m}\right) + 0.0088 = 0.17 \tag{78}$$

By following the descriptions presented throughout (51) to (53), the wing lift-curve slope were found in the following matter:

$$\chi = \sqrt{1 - Ma^2} = \sqrt{1 - 0.28^2} = 0.96 \tag{79}$$

The trailing edge angle $\Phi'_{TE,W}$ was geometrically determined. The angle itself is visualised in Figure 6.10 and measured to be $\Phi'_{TE,W} = 15.85°$, thus $\tan\left(\frac{\Phi'_{TE,W}}{2}\right) = 0.14$.

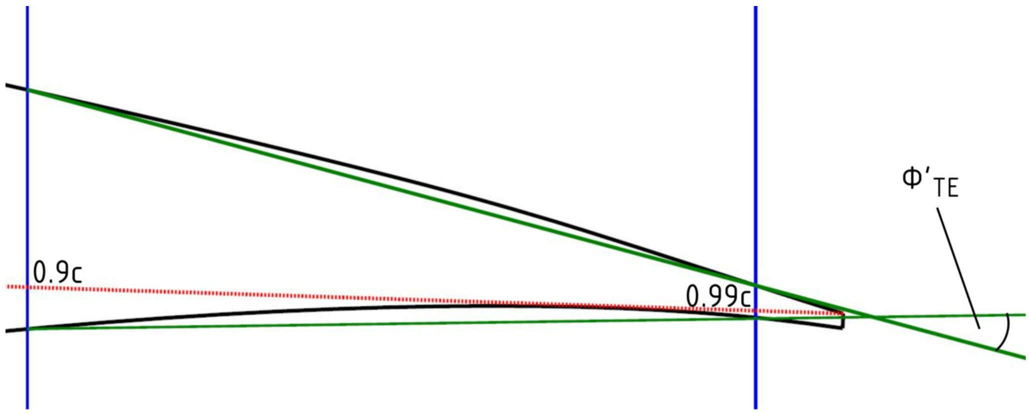

Figure 6.10: Wing Trailing-Edge of NLF-MOD22 for Angle Calculation

Furthermore, the Reynolds number was expressed with respect to the MAC and V_{NO} in ISA conditions at sea level as $Re = \frac{\bar{c}_W V_{NO}}{\nu} = \frac{1.32m \cdot 97\frac{m}{s}}{1.461 \cdot 10^{-5}\frac{m^2}{s}} = 8.76 \cdot 10^8$. The wing thickness ratio for the NFL-MOD22 aerofoil on the Extra EA 400-500 was calculated as $\left(\frac{t}{c}\right)_W = \frac{0.26m}{1.32m} = 0.2$. Using now Figure 6.6, the following values were found: $\left(\frac{a_0}{(a_0)_{theory}}\right)_W = 0.89$ and $(a_0)_{theory,W} = 7.25\frac{1}{rad}$. This allowed the calculation of the wing lift-curve slope with the help of the midchord sweep $\Lambda_{\frac{c}{2},W} = 4.4°$, the aspect ratio $AR_W = 8.96$, and

$$a_{0,W} = \frac{1.05}{\sqrt{1-0.28^2}} \cdot 0.89 \cdot 7.25 \frac{1}{rad} = 7.06 \frac{1}{rad} \tag{80}$$

$$k_W = \frac{a_{0,W}}{2\pi} = \frac{7.06\frac{1}{rad}}{2\pi} = 1.12 \frac{1}{rad} \tag{81}$$

so that

$$a_W = \frac{2\pi \cdot 8.96}{2 + \sqrt{\frac{8.96^2 \cdot 0.96^2}{\left(1.12\frac{1}{rad}\right)^2}\left(1 + \frac{tan^2(4.4°)}{\left(1.12\frac{1}{rad}\right)^2}\right) + 4}} = 5.66 \frac{1}{rad} \tag{82}$$

The wing fuselage contribution was thus summed up by using (47) and assuming, in accordance with Pamadi, $C_{L\alpha,e} = a_W \alpha$, as much as $A_{exp} = A_W$ for high wing configurations, so that

$$C_{m,CG}^{(W(B))} = 0.25 + (0.17 + 1.11) \cdot 5.66 \frac{1}{rad} \cdot \alpha \cdot \frac{13.5m^2}{13.5m^2} = 0.25 + 7.25 \frac{1}{rad} \cdot \alpha \tag{83}$$

Additionally, the tail contribution to the pitching moment coefficient had to be calculated with the help of (54) and by finding the respective wing aspect and wing taper ratio, as much as the tailplane location factor. For this calculation, the wing taper ratio was found to be $\lambda_W = \frac{c_{tip}}{c_{root}} = \frac{0.85m}{1.61m} = 0.53$, while $l_H = 4.52m$ and $h_H = 0.8m$. Hence,

$$K_{AR} = \frac{1}{8.96} - \frac{1}{1 + 8.96^{1.7}} = 0.088 \tag{84}$$

$$K_\lambda = \frac{10 - 3 \cdot 0.53}{7} = 1.20 \tag{85}$$

$$K_H = \frac{1 - \frac{0.8m}{11m}}{\sqrt[3]{\frac{2 \cdot 4.52m}{11m}}} = 0.99 \tag{86}$$

With a quarter wing sweep angle of $\Lambda_{\frac{c}{4},W} = -19.84°$ followed

$$\frac{d\epsilon}{d\alpha} = 4.44\left[0.088 \cdot 1.20 \cdot 0.99 \cdot \cos(-19.84°)^{\frac{1}{2}}\right]^{1.19} = 0.29 \frac{1}{rad} \tag{87}$$

$$\epsilon = \frac{d\epsilon}{d\alpha}\alpha = 0.29\alpha \tag{88}$$

To find the dynamic pressure ratio at the tailplane η_T, see (61), the zero-lift drag coefficient, see (62), was required. With the help of Figure 6.7, the values $c_{f,W} = 0.002$ and $R_{LS,W} =$

1.1 (with a sweep angle of 5.7° at $0.35\bar{c}_W$) were determined. This led to:

$$C_{DO,W} = 0.002\left[1 + 1.2 \cdot 0.2 + 100 \cdot 0.2^4\right] \cdot 1.1 \cdot \frac{13.5m^2}{13.5m^2} = 3.1 \cdot 10^{-3} \tag{89}$$

The distance between the wing trailing edge and AC of the horizontal stabiliser was $l_{H1} = 3.53m$, so that

$$\eta_T = \frac{q_T}{q} = 1 - \frac{\Delta q}{q} = 1 - \frac{2.42\sqrt{3.1 \cdot 10^{-3}}}{\frac{3.53m}{1.32m} + 0.3} = 0.95 \tag{90}$$

Furthermore, a_H was calculated with respect to the horizontal stabiliser parameters by using (51). The following parameters differed from the calculation shown between (80) and (82): $\Phi'_{TE,H} = 4.12°$, so that $\left(\frac{a_0}{(a_0)_{theory}}\right)_H = 0.95$ and the maximum horizontal stabiliser thickness ratio $\left(\frac{t}{c}\right)_H = 0.12$ so that $(a_0)_{theory,H} = 6.87\frac{1}{rad}$. Furthermore, $AR_H = \frac{(11.0m)^2}{8.8m^2} = 13.75$ and $\Lambda_{\frac{c}{2},H} = -20.0°$. Therefore,

$$a_{0,H} = \frac{1.05}{\sqrt{1 - 0.28^2}} \cdot 0.95 \cdot 6.87rad = 7.14\frac{1}{rad} \tag{91}$$

$$k_H = \frac{a_{0,H}}{2\pi} = \frac{7.14\frac{1}{rad}}{2\pi} = 1.14\frac{1}{rad} \tag{92}$$

so that

$$a_H = \frac{2\pi \cdot 13.75}{2 + \sqrt{\frac{13.75^2 \cdot 0.96^2}{\left(1.14\frac{1}{rad}\right)^2}\left(1 + \frac{tan^2(-20.0°)}{\left(1.14\frac{1}{rad}\right)^2}\right) + 4}} = 6.0\frac{1}{rad} \tag{93}$$

Finally, the following conclusion was made by extracting the values for $i_W = 1.9°$ and $i_T = 0°$ from CATIA:

$$\begin{aligned} C_{m,CG}^{(T)} &= -C_L^{(T)}\frac{q_T}{q}\frac{A_H l_H}{A_W \bar{c}_W} = -a_H(\alpha - i_W + i_T - \epsilon)\eta_T\frac{A_H l_H}{A_W \bar{c}_W} \\ &= -6.0\frac{1}{rad}(\alpha - 0.033rad - 0.29 \cdot \alpha) \cdot 0.95 \cdot \frac{8.8m^2 \cdot 4.52m}{13.5m^2 \cdot 1.32m} \\ &= -12.72\frac{1}{rad} \cdot (0.71 \cdot \alpha - 0.033rad) \end{aligned} \tag{94}$$

Than, the following expression for the overall pitching moment coefficient was formulated:

$$C_{m,CG} = C_{m,CG}^{(W(B))} + C_{m,CG}^{(T)} = 0.25 + 7.19\frac{1}{rad} \cdot \alpha - 12.72\frac{1}{rad} \cdot (0.71 \cdot \alpha - 0.033rad) \tag{95}$$

Table 6.1 shows the values of the coefficient with varying angles from $\alpha = -5°$ to 15°. Attention needed to be paid to the fact that the angle α of the pitching moment coefficient had to be in radiant. Figure 6.11 shows the results of the analysis for the pitching moment coefficient.

Table 6.1: $C_{m,CG}$ Values for the Box Wing Configuration

α	$-5°$	$-2°$	$0°$	$2°$	$5°$	$7°$	$10°$	$12°$	$15°$
$C_{m,CG}^{(W(B))}$	-0.377	-0.001	0.250	0.501	0.877	1.128	1.505	1.756	2.132
$C_{m,CG}^{(T)}$	1.197	0.731	0.420	0.109	-0.357	-0.668	-1.134	-1.445	-1.911
$C_{m,CG}$	0.819	0.730	0.670	0.610	0.520	0.460	0.370	0.312	0.221

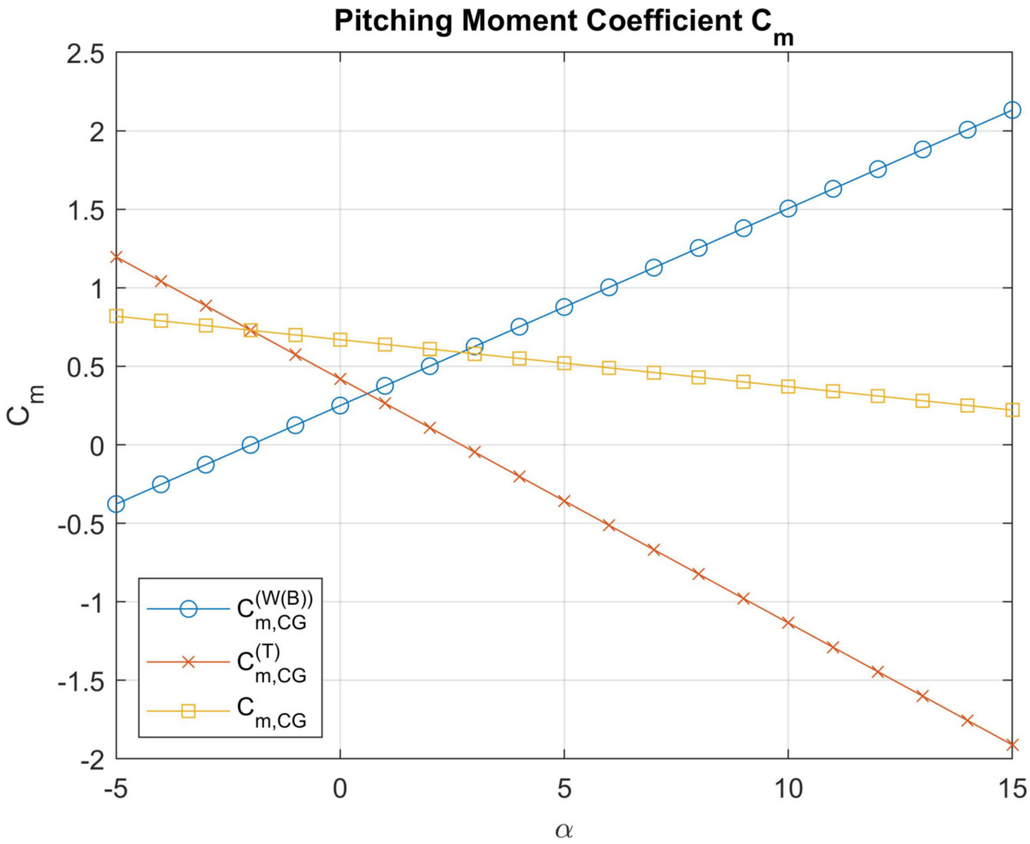

Figure 6.11: Pitching Moment Coefficient C_m for the Box Wing Configuration

The results showed that longitudinal stability was given by the fact that $C_{m\alpha} = \frac{\partial C_m}{\partial \alpha} < 0$

Longitudinal Control

The calculation of the elevators were based on (68), as much as Figure 6.8 and Figure 6.9. For this purpose, the chord length of the elevator and tailplane ratio was calculated to be $\left(\frac{c_f}{\bar{c}}\right)_H = 0.54$, so that $(\alpha_\delta)_{C_l,H} = -0.83\frac{1}{rad}$. Together with the horizontal tailplane area, it was found that $\left(\frac{(\alpha_\delta)_{C_L}}{(\alpha_\delta)_{C_l}}\right)_H = 1.02$. Additionally, the factor $K_{b,H}$ was found by subtracting the outer flap span factor from the inner flap span factor, where $\eta = \frac{2y}{b_H}$ and $\lambda_H = 0.78$, thus

$$K_{b,H} = K_b(\eta_o) - K_b(\eta_i) = K_b(0.431) - K_b(0.093) = 0.55 - 0.15 = 0.4 \tag{96}$$

Figure 6.9 showed that for values of the box wing configuration, the following parameter could be estimated: $(c_{l\delta})_{theory,H} = 0.58\frac{1}{rad}$ and $\left(\frac{c_{l\delta}}{(c_{l\delta})_{theory}}\right)_H = 0.95$. This led to $c_{l\delta,H} = 0.551\frac{1}{rad}$ and therefore the change in tail AOA per elevator unit deflection was calcuated as

$$\tau_e = \frac{0.551\frac{1}{rad}}{7.14\frac{1}{rad}} \cdot 1.02 \cdot 0.4 = 0.0315 \tag{97}$$

According to Pamadi, a statically stable aircraft must fulfill $\frac{d\delta_e}{dC_L} < 0$, which was proven by the following equation:

$$\frac{d\delta_e}{dC_L} = -\frac{3.95m - 4.16m}{-6.0\frac{1}{rad} \cdot 0.95 \cdot \frac{8.8m^2 \cdot 4.52m}{13.5m^2 \cdot 1.32m} \cdot 0.0315} = -0.524 < 0 \tag{98}$$

where the elevator power control was

$$C_{m\delta e} = -6.0\frac{1}{rad} \cdot 0.95 \cdot \frac{8.8m^2 \cdot 4.52m}{13.5m^2 \cdot 1.32m} \cdot 0.0315 = -0.40\frac{1}{rad} \tag{99}$$

6.1.4 Comparison to the Cantilever Wing Configuration

To compare both aircraft wing configurations, the same process as shown above was conducted for the cantilever wing Extra EA 400-500. The reader may be referred to Appendix A, in which all required results are listed. In summary, between the two designs, the main wings were only of little difference. This was mainly due to the slightly larger wing area of the cantilever wing and thus a greater wing span. However, the addition of both values was only due to the winglets and not the wing itself. The greatest difference with effect on the pitch moment was due to the larger horizontal stabiliser. Most notable was the horizontal tail volume coefficient. This value is often between 0.5 and 1.0 [67]. And while this coefficient was indeed 0.88 for the cantilever wing, the box wing had a coefficient of 2.23. This unusual number, see (94), was achieved because of a stabiliser area three times the area of the original horizontal tail and even though the distance between the AC of the wing and horizontal stabiliser was reduced due to a forward sweep. The effect of this result can especially be seen in the decrease of pitch moment coefficient over alpha, thus

$C_{m\alpha}$. The graphs in Figure 6.12, show that the cantilever wing had a higher decrease in comparison to the cantilever wing configuration. The following Table 6.2 shows the difference between both configurations. However, it shall be noted that Datcom calculations can vary from reality for higher AOAs.

Table 6.2: $C_{m,CG}$ Values for the Box Wing and Cantilever Wing Configuration

α	$-5°$	$-2°$	$0°$	$2°$	$5°$	$7°$	$10°$	$12°$	$15°$
$C_{m,CW}$	0.608	0.550	0.511	0.471	0.413	0.374	0.315	0.276	0.217
$C_{m,BW}$	0.819	0.730	0.670	0.610	0.520	0.460	0.370	0.312	0.221
$\lvert\Delta C_{m,CG}\rvert$	0.211	0.180	0.159	0.139	0.107	0.086	0.055	0.036	0.004

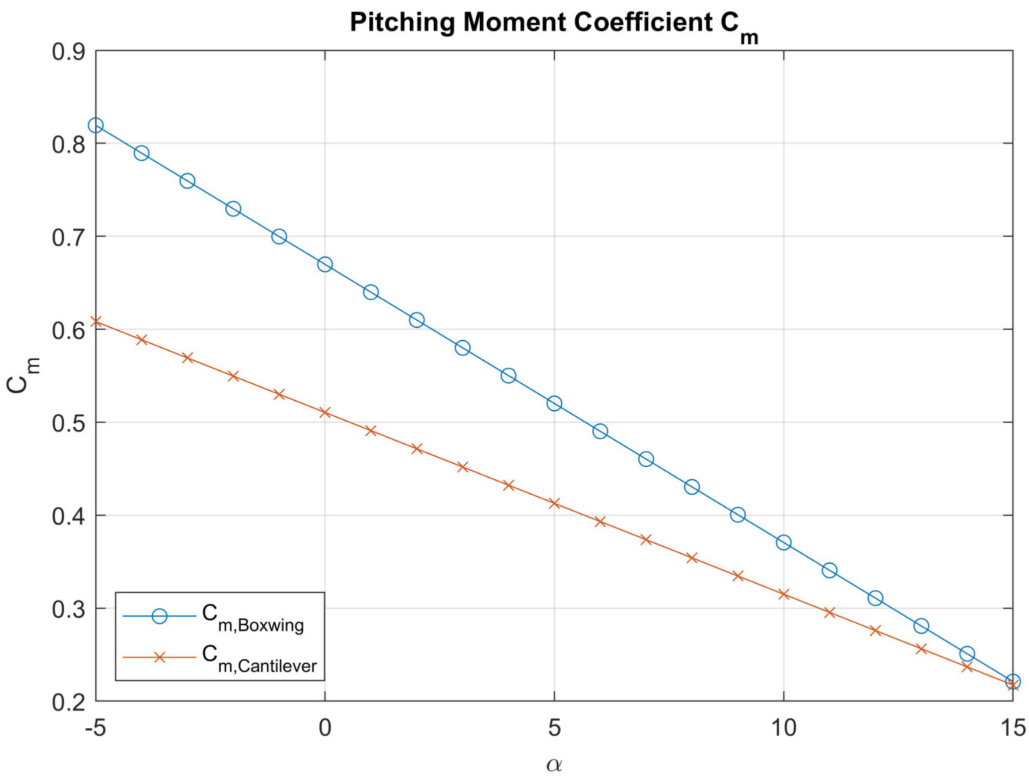

Figure 6.12: Comparison of C_m for the Box Wing and Cantilever Configuration

When considering $C_{m\alpha}$ once more by developing the derivative of (95), it was seen that $C_{m\alpha,BW} = -1.17 > C_{m\alpha,CW} = -0.56$. This shows, that the behaviour of the aircraft regarding pitching could be improved when using a box wing configuration due to its greater horizontal tail area. Additionally, as noted earlier, the elevators were adapted to the box wing configuration for this study. The elevator area for the new design was nearly

1.7 times greater than the original area and it was seen that the elevator power control increased as well. For both designs, the elevator contributed to an overall statically stable aircraft by fulfilling $\frac{d\delta_e}{dC_L} < 0$. All results for longitudinal control are shown in Table 6.3.

Table 6.3: Longitudinal Control Values for the Box Wing and Cantilever Configuration

Parameter	Cantilever	Box Wing
τ_e	0.067	0.0315
$\frac{d\delta_e}{dC_L}$	$-0.271\frac{1}{rad}$	$-0.40\frac{1}{rad}$
$C_{m\delta e}$	-0.859	-0.524

6.2 Directional Motion

Every aircraft must be able to counteract any disturbance such as gusts, winds or even rudder deflections of little magnitude affecting it along its vertical axis and resulting in a so-called sideslip. This motion consists of a sideslip velocity v, yaw angle ψ and yaw rate r, and effectively allows an aircraft to change its orientation in space, although its heading with regards to the Earth remains the same [64]. This is visualised in Figure 6.13, where an aircraft in level flight is disturbed by a starboard side gust V_w and reacts with a resulting velocity V_R.

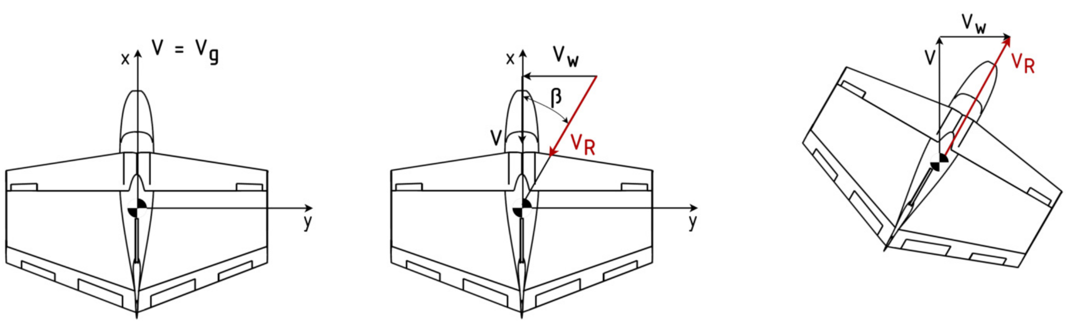

(a) Moments Before Side Gust (b) Side Gust V_w and Resultant (c) Sideslip of Zero

Figure 6.13: Sideslip Velocities Due to Side Gust

Eventually, see Figure 6.13(c), the aircraft has realigned itself with respect to the disturbance and has changed its orientation although its velocity V remains the same. In this case, the sideslip angle β between the sideslip velocity vector v and its longitudinal axis x_b is zero, as the aircraft is aligned with gust V_w. In general, the angle of sideslip is

$$sin(\beta) = \frac{v}{V} \tag{100}$$

where: β^+ = Aircraft sideslips to starboard

β^- = Aircraft sideslips to port side

Furthermore, the aircraft has a kinematic angle of yaw ψ, which shows the change in heading of the aircraft with respect to the Earth and is measured between the aircraft's symmetry plane in steady flight and symmetry plane after disturbance. Pamadi notes that β and ψ are in principle independent. However, $-\beta = \psi$, when the yawed aircraft continuous with an unchanged direction of motion. This case is shown in Figure 6.14.

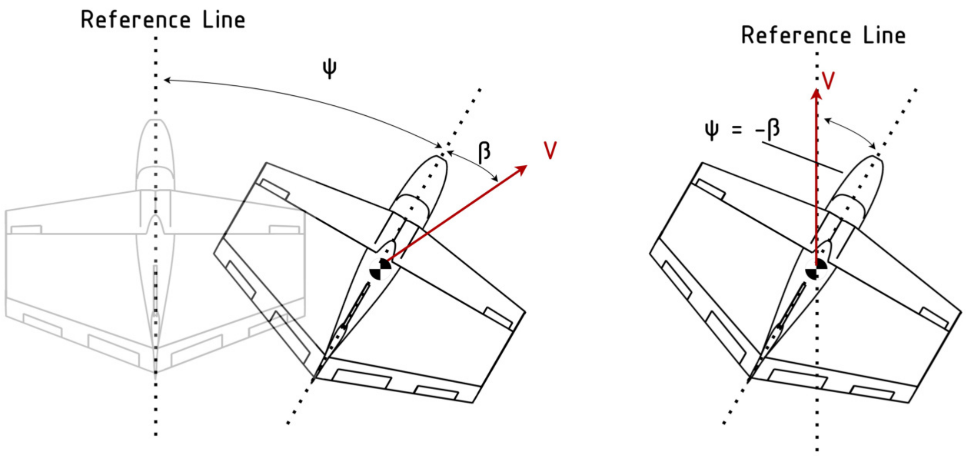

Figure 6.14: Sideslip Angles Due to Side Gust

6.2.1 Directional Stability

In order to define directional stability, the following equations are formulated:

$$C_n = \frac{N}{\bar{q} A_W b} \tag{101}$$

$$C_{n\beta} = \frac{\partial C_n}{\partial \beta} \tag{102}$$

where: N = Yawing Moment

Under these conditions, an aircraft is considered directional stable if

$$N_\beta > 0 \tag{103}$$

$$C_{n\beta} > 0 \tag{104}$$

For the purpose of analysing the directional stability, the overall effects of the wing, fuselage and the tail section need to be taken into consideration. The wing has only an effect on the directional stability if the dihedral and leading-edge sweep are of greater magnitude. Together, these two aspects built the wing contribution to the stability:

$$(C_{n\beta})_W = (C_{n\beta})_{\Gamma,W} + (C_{n\beta})_{\Lambda,W} \tag{105}$$

For further studies, the wing dihedral angle is defined as Γ and describes the upward or downward angle of the wings. Additionally, the sideslip velocity $v = V_0\beta$ is divided into a spanwise and normal component:

$$v = \begin{cases} \text{spanwise component: } V_0\beta cos(\Gamma_W) \simeq V_0\beta \\ \text{normal component: } V_0\beta sin(\Gamma_W) \simeq V_0\beta\Gamma_W \end{cases} \tag{106}$$

Pamadi notes that $V_0\beta$ does not affect the lift distribution on the wing, so that only the normal velocity with regards to the wing is considered:

$$V_N = V_0(sin(\alpha) \pm \beta sin(\Gamma_W)) \tag{107}$$

When assuming that α, β and Γ_W are small, this equation can be further simplified. As shown in the case for a positive sideslip:

$$V_N = \begin{cases} \text{Starboard Wing: } V_0(\alpha + \beta\Gamma_W) \\ \text{Port Side Wing: } V_0(\alpha - \beta\Gamma_W) \end{cases} \tag{108}$$

Under the same circumstances, the velocity of a chordwise element V_C, the local angle of attack α_{loc}, and local dynamic pressure $\overline{q}_{loc}$ are assumed to be:

$$V_C = V_0 cos(\alpha) = V_0 \tag{109}$$

$$\alpha_{loc} = \frac{V_N}{V_C} = \alpha \pm \beta\Gamma_W \tag{110}$$

$$\overline{q}_{loc} = \frac{1}{2}\rho(V_N^2 + V_C^2) \simeq \frac{1}{2}\rho V_0^2 \tag{111}$$

The result is that an increase in the lift coefficient as much as a decrease in drag coefficients of the starboard wing is observed for a positive sideslip, while the port side wing is affected by an opposite reaction. Due to this fact, a rolling moment is commenced, which will be studied in a later chapter of this study, leading to a yawing moment. The analysis for the purpose of a conceptual design of said yawing moment will be based on the strip theory. The strip theory is a well-known method [68][69] for valid solutions in low subsonic speeds, although neglecting downwash variations along the length of the wing. For this matter, a wing strip RT of width dy on the starboard wing, in accordance with Figure 6.15, is defined.

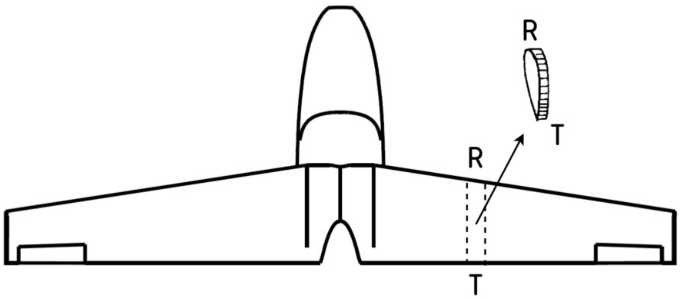

Figure 6.15: Element RT of Strip Theory for Sideslip Calculation

The strip theory denotes the force F along RT for small angles as

$$\begin{aligned} dF &= dLsin(\alpha_{loc} - \alpha) - dDcos(\alpha_{loc} - \alpha) \\ &= dL(\alpha_{loc} - \alpha) - dD \\ &= dL\beta\Gamma_W - dD \\ &= \frac{1}{2}\rho V_0^2 c(y)dy(C_{L,loc,SB}\beta\Gamma_W - C_{D,loc,SB}) \end{aligned} \tag{112}$$

where: $\alpha_{loc} - \alpha = \beta\Gamma_W$

$c(y)$ = local chord

and the sectional lift and drag coefficients as

$$C_L = a_{0,W}\alpha_{loc} \tag{113}$$

$$C_D = C_{D0,loc} + C_{D\alpha,loc}\alpha \tag{114}$$

where: $a_{0,W}$ = Sectional 2D Lift-Curve Slope

$C_{D0,loc}$ = Sectional Zero-Lift Drag Coefficient

$C_{D\alpha,loc}$ = Increase of $C_{D,loc}$ per unit increase of AOA

This allows to calculate the force on the wing section as follows:

$$dF = \frac{1}{2}\rho V_0^2 c(y)d(y)\big[C_{L,loc,SB}\beta\Gamma - C_{D0,loc} - C_{D\alpha,loc}(\alpha + \beta\Gamma)\big] \tag{115}$$

With regards to the strip theory, the yawing moment of RT can be summed up to be represented by

$$dN = -ydF = \frac{1}{2}\rho V_0^2 c(y)yd(y)\big[-C_{L,loc,SB}\beta\Gamma_W + C_{D0,loc} + C_{D\alpha,loc}(\alpha + \beta\Gamma_W)\big] \tag{116}$$

Hence, the starboard (SB) wing creates a yawing moment of

$$N_{SB} = \frac{1}{2}\rho V_0^2\big[-C_{L,loc,SB}\beta\Gamma_W + C_{D0,loc} + C_{D\alpha,loc}(\alpha + \beta\Gamma_W)\big] + \int_0^{\frac{b}{2}} c(y)ydy \tag{117}$$

while the port side (PS) wing is the cause of

$$N_{PS} = \frac{1}{2}\rho V_0^2\big[-C_{L,loc,SB}\beta\Gamma_W - C_{D0,loc} - C_{D\alpha,loc}(\alpha - \beta\Gamma_W)\big] + \int_0^{\frac{b}{2}} c(y)ydy \tag{118}$$

In order to receive the total yawing moment N, it is necessary to build the sum of all yawing moments:

$$\begin{aligned} N = N_{SB} + N_{PS} &= \frac{1}{2}\rho V_0^2\big[-\beta\Gamma_W(C_{L,SB} + C_{L,PS}) + 2C_{D\alpha,loc}\beta\Gamma_W\big]\int_0^{\frac{b}{2}} c(y)ydy \\ &= -\rho V_0^2\beta\Gamma_W \int_0^{\frac{b}{2}}(C_L - C_{D\alpha,L})c(y)ydy \end{aligned} \tag{119}$$

where: $C_{L,SB} = a_{0,W}(\alpha + \beta\Gamma_W)$

$C_{L,PS} = a_{0,W}(\alpha - \beta\Gamma_W)$

$C_{L,SB} + C_{L,PS} = 2a_{0,W}\alpha = 2C_L$

This equation leads to its coefficient form of

$$(C_n)_{\Gamma_W} = -\frac{2\beta\Gamma_W}{Ab}\int_0^{\frac{b}{2}}(C_L - C_{D\alpha,L})c(y)ydy \tag{120}$$

$$(C_{n\beta})_{\Gamma_W} = -\frac{2\Gamma_W}{Ab}\int_0^{\frac{b}{2}}(C_L - C_{D\alpha,L})c(y)ydy \tag{121}$$

As noted earlier, equal to analysis by Pamadi, the strip theory ignores effects caused by induced drag, so that an error might appear under special circumstances. For this case, Seckel [70] suggest his empirical formula of

$$(C_{n\beta})_{\Gamma,W} = -0.075\Gamma_W C_L \tag{122}$$

Effect of Sweep

The wing sweep, thus the forward or backward angle of a wing, has a positive effect on directional stability if back-sweep exists. When considering a swept-back angle of Λ, the spanwise, chordwise and normal velocities with respect to small angles are for the starboard and port side wing:

$$V_S = \begin{cases} \text{SB: } V_0(sin(\Lambda_W)cos(\alpha) - \beta cos(\Lambda_W)) = V_0 cos(\Lambda_W)(tan(\Lambda)_W - \beta) \\ \text{PS: } V_0(sin(\Lambda_W)cos(\alpha) + \beta cos(\Lambda_W)) = V_0 cos(\Lambda_W)(tan(\Lambda_W) + \beta) \end{cases} \tag{123}$$

$$V_C = \begin{cases} \text{SB Wing: } V_0(cos(\Lambda_W)cos(\alpha) - \beta sin(\Lambda_W)) = V_0 cos(1 + \beta tan(\Lambda_W)) \\ \text{PS Wing: } V_0(cos(\Lambda_W)cos(\alpha) + \beta sin(\Lambda_W)) = V_0 cos(1 - \beta tan(\Lambda_W)) \end{cases} \tag{124}$$

$$V_N = V_0\alpha \tag{125}$$

As noted by Pamadi, the local angle of attack is expressed by

$$\alpha_{loc} = tan(\alpha_{loc}) = \frac{V_N}{V_C} = \begin{cases} \text{Starboard Wing: } \alpha\sec(\Lambda_W)(1 - \beta\tan(\Lambda_W)) \\ \text{Port Side Wing: } \alpha\sec(\Lambda_W)(1 + \beta\tan(\Lambda_W)) \end{cases} \tag{126}$$

Further, the local AOA during level flight with $\beta = 0$ is formulated as

$$\alpha_S = \alpha sec(\Lambda_W) \tag{127}$$

thus,

$$\alpha_S - \alpha_{loc} = \begin{cases} \text{Starboard Wing: } \alpha sec(\Lambda_W)\beta tan(\Lambda_W) \\ \text{Port Side Wing: } -\alpha sec(\Lambda_W)\beta tan(\Lambda_W) \end{cases} \tag{128}$$

The local dynamic pressure is defined as

$$\overline{q}_{loc} = \frac{1}{2}\rho(V_C^2 + V_N^2) = \begin{cases} \text{Starboard Wing: } \frac{1}{2}\rho V_0^2 cos^2(\Lambda_W)(1 + \beta tan(\Lambda_W))^2 \\ \text{Port Side Wing: } \frac{1}{2}\rho V_0^2 cos^2(\Lambda_W)(1 - \beta tan(\Lambda_W))^2 \end{cases} \tag{129}$$

The strip theory is again used to find the yawing moment of both wings. For this purpose, a strip RT on the starboard wing with width dy_h is defined, where y_h is the spanwise coordinate and $c(y_h)$ represents the local chord normal to the leading edge. Therefore, the force along x_b for small angles is

$$\begin{aligned} dF &= -dLsin(\alpha_S - \alpha_{loc}) - dDcos(\alpha_S - \alpha_{loc}) = -dL(\alpha_S - \alpha_{loc}) - dD \\ &= -dL\alpha sec(\Lambda_W)\beta tan(\Lambda_W) - dD \\ &= -\frac{1}{2}\rho V_0^2 cos^2(\Lambda_W)(1 + \beta tan(\Lambda_W))^2 \Big[C_{loc,SB}\alpha sec(\Lambda_W)\beta tan(\Lambda_W) + C_{D0,loc} \\ &+ C_{D\alpha,loc}\left(\frac{\alpha sec(\Lambda_W)}{1 + \beta tan(\Lambda_W)}\right)\Big]c(y_h)dy_h \end{aligned} \tag{130}$$

By introducing $a_{0,W} = a_{0,W}(y)$ as the local lift-curve slope and

$$C_{loc,SB} = \frac{a_{0,W}\alpha sec(\Lambda_W)}{1 + \beta tan(\Lambda_W)} \tag{131}$$

it is possible to further refine the force equation to

$$\begin{aligned} dF = &- \frac{1}{2}\rho V_0^2 cos^2(\Lambda_W)(1 + \beta tan(\Lambda_W))\big[a_0\alpha^2 sec^2(\Lambda_W)\beta tan(\Lambda) \\ &+ C_{D0,loc}(1 + \beta tan(\Lambda_W)) + C_{D\alpha,loc}\alpha sec(\Lambda_W)\big]c(y_h)dy_h \end{aligned} \tag{132}$$

Thus, the yawing moment due to the starboard wing is expressed by

$$\begin{aligned} N_{SB} = &- ydF = \frac{1}{2}\rho V_0^2 cos^2(\Lambda_W)(1 + \beta tan(\Lambda_W))\big[a_{0,W}\alpha^2 sec^2(\Lambda_W)\beta tan(\Lambda_W) \\ &+ C_{D0,loc}(1 + \beta tan(\Lambda_W)) + C_{D\alpha,loc}\alpha sec(\Lambda_W)\big] \int_0^{\frac{bsec(\Lambda_W)}{2}} c(y_h)y_h dy_h \end{aligned} \tag{133}$$

while the yawing moment due to the port side wing is expressed by

$$\begin{aligned} N_{PS} = &\frac{1}{2}\rho V_0^2 cos^2(\Lambda_W)(1 - \beta tan(\Lambda_W))[a_{0,W}\alpha^2 sec^2(\Lambda_W)\beta tan(\Lambda_W) \\ &- C_{D0,loc}(1 - \beta tan(\Lambda_W)) - C_{D\alpha,loc}\alpha sec(\Lambda_W)] \int_0^{\frac{bsec(\Lambda_W)}{2}} c(y_h)y_h dy_h \end{aligned} \tag{134}$$

Logically, the total yawing moment due to the wing sweep is $N = N_{SB} + N_{PS}$ and therefore

$$\begin{aligned} N =& \rho V_0^2 \beta sin(\Lambda_W) cos(\Lambda_W) \int_0^{\frac{bsec(\Lambda)_W}{2}} (a_{0,W} \alpha^2 sec^2(\Lambda_W) \\ &+ 2C_{D0,loc} + C_{D\alpha,loc} \alpha sec(\Lambda_W)) c(y_h) y_h dy_h \end{aligned} \tag{135}$$

The coefficient form is given by

$$\begin{aligned} (C_n)_{\Lambda,W} =& \left(\frac{2\beta sin(\Lambda_W)}{A_W b}\right) \int_0^{\frac{bsec(\Lambda_W)}{2}} \Big[a_{0,W} \alpha^2 sec^2(\Lambda_W) + 2C_{D0,loc}(cos\Lambda_W) \\ &+ C_{D\alpha,loc} \alpha \Big] c(y_h) y_h dy_h \end{aligned} \tag{136}$$

as much as

$$\begin{aligned} (C_{n\beta})_{\Lambda,W} =& \left(\frac{2 sin(\Lambda_W)}{A_W b}\right) \int_0^{\frac{bsec(\Lambda_W)}{2}} \Big[C_{L,loc} \alpha + 2C_{D0,loc} cos(\Lambda_W) \\ &+ C_{D\alpha,loc} \alpha \Big] c(y_h) y_h dy_h \end{aligned} \tag{137}$$

where: $C_{L,loc} = a_{0,W} \alpha sec(\Lambda_W)$ if $\beta = 0$

It shall be noted that a backward sweep wing can be considered as a stabilising component for directional stability, as the overall integral is positive, so that $(C_{n\beta})_W > 0$. This effect is even more prominent for high angle of attacks. However, the derived equation ignores the induced drag as a result of the strip theory and can therefore be supplemented by the following empirical equation of Datcom [53]:

$$\begin{aligned} (C_{n\beta})_{\Lambda,W} =& C_L^2 \Bigg[\frac{1}{4\pi AR_W} - \frac{tan(\Lambda_{\frac{c}{4},W})}{\pi AR_W (AR_W + 4cos(\Lambda_{\frac{c}{4},W}))} \\ &\cdot \left(cos(\Lambda_{\frac{c}{4},W}) - \frac{AR_W}{2} - \frac{AR_W^2}{8cos(\Lambda_{\frac{c}{4},W})} - 6\overline{x}_a \frac{sin(\Lambda_{\frac{c}{4},W})}{AR_W} \right) \Bigg] \end{aligned} \tag{138}$$

where: $\Lambda_{\frac{c}{4},W}$ = Quarter Chord Wing Sweep
AR_W = Wing Aspect Ratio
$\overline{x}_a$ = Distance between CG and AC of MAC

Fuselage

In general, it can be said that the fuselage has a negative effect on the directional stability, the result of which is directly correlated to the wing geometry as much as the wing placement [64]. For the purpose of this design study, $(C_{n\beta})_{B(W)}$ is calculated by Datcom's empirical equation of

$$(C_{n\beta})_{B(W)} = -K_N K_{Rl} \frac{A_{B,S}}{A_W} \frac{l_f}{b} \frac{1}{deg} \tag{139}$$

where: K_N = Wing-Body Interference Factor; see Figure 6.16

K_{Rl} = Fuselage Reynolds Number Factor; see Figure 6.17

l_f = Length of aircraft

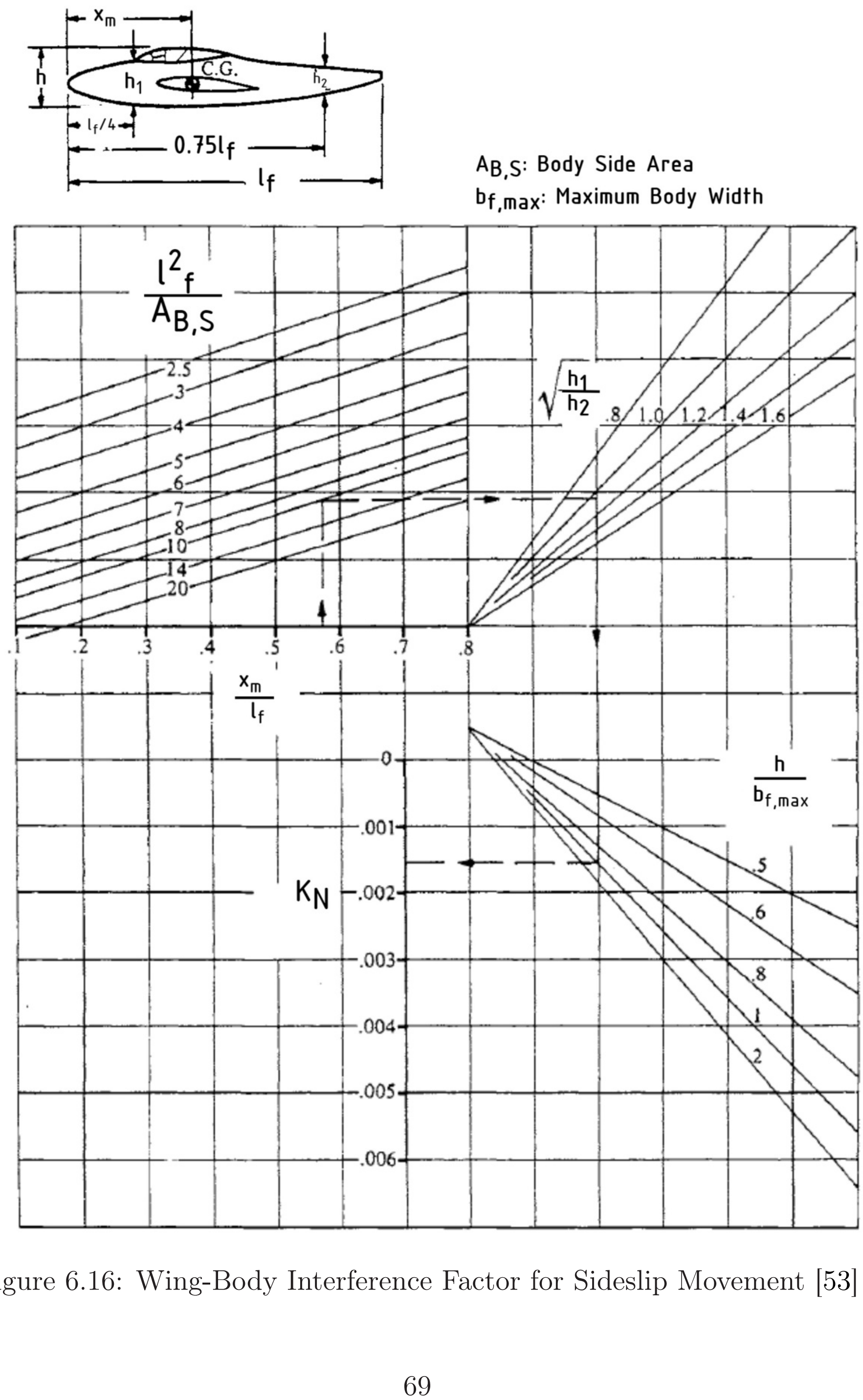

Figure 6.16: Wing-Body Interference Factor for Sideslip Movement [53]

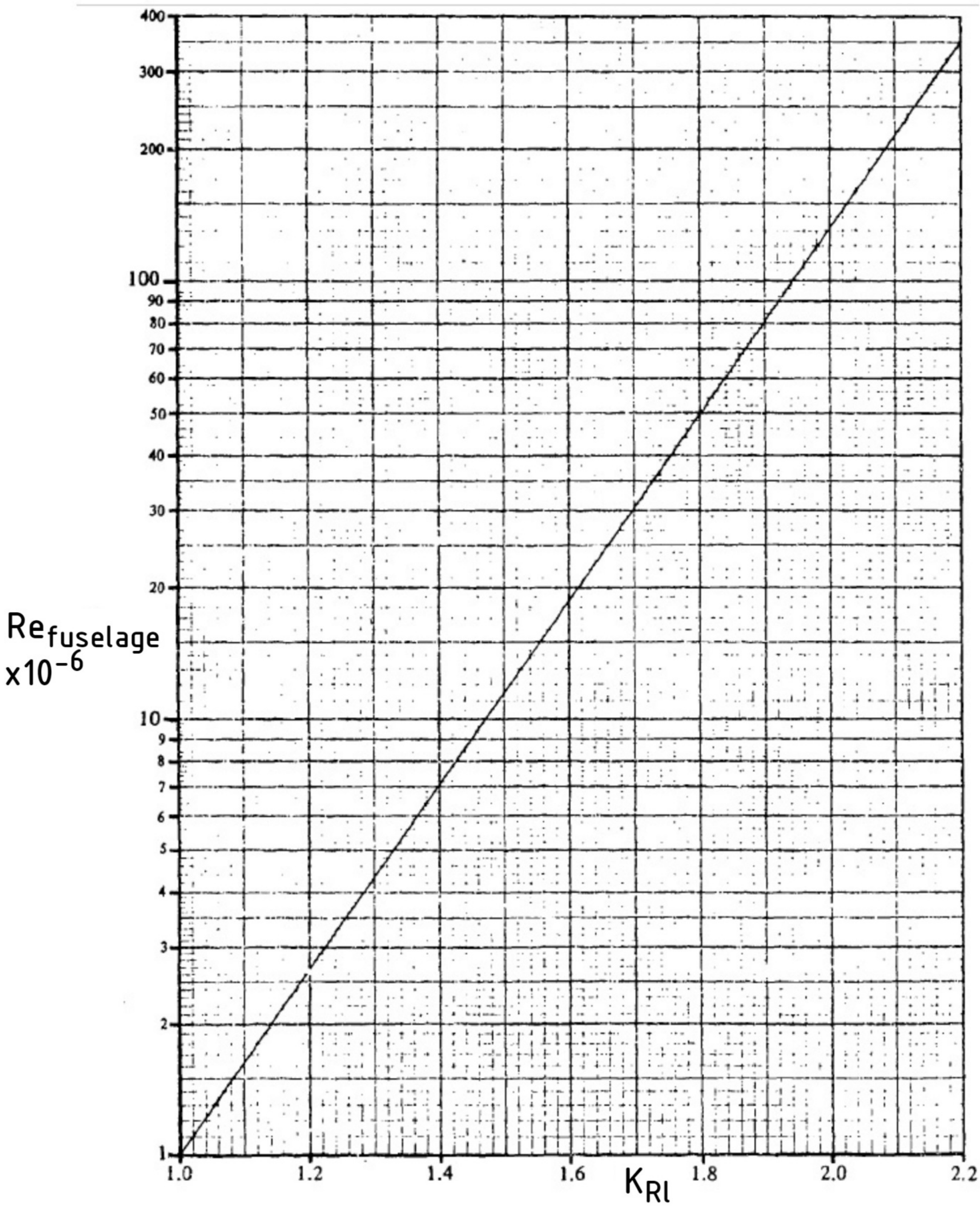

Figure 6.17: Empirical Factor for Fuselage Reynolds Number [53]

Tail section

The tail section can be divided into its vertical stabiliser and horizontal stabiliser, the latter of which shall be considered as a wing with dihedral and sweep with only little to no effect on the directional stability due to its small size. This statement is however only correct for normal aircraft configurations, and is therefore only true for the cantilever wing but not box wing configuration of this design study. The box wing configuration will hence be further analysed regarding its horizontal stabiliser, while both aircraft's vertical stabiliser will be part of this study as well. For this case, several aspects such as the stabilisers moment arm from CG, its area and aspect ratio, the sweep as much as the empennage geometry and fuselage sidewash have to be taken into consideration [64]. As such, the first step is to identify the rudder-fixed side force Y_V produced by the vertical stabiliser. Datcom suggest the following expression, its respective coefficient form and derivative:

$$Y_V = -k\bar{q}_V a_V(\beta + \sigma)A_V \tag{140}$$

$$C_{Y,V} = \frac{Y_V}{\bar{q}A} = -ka_V(\beta+\sigma)\left(\frac{A_V}{A_W}\right)\eta_V \tag{141}$$

$$C_{Y\beta,V} = \frac{\partial C_{y,V}}{\partial \beta} = -ka_V\left(1+\frac{\partial\sigma}{\partial\beta}\right)\left(\frac{A_V}{A_W}\right)\eta_V \tag{142}$$

Figure 6.18 shows the empirical parameter k depending on the height of the tail, therefore the vertical tail span b_V extending up to the fuselage centerline, as much as the average fuselage radius r_1 beneath the vertical stabiliser. Additionally, the vertical tail area A_V measured up to the fuselage centerline, the induced sidewash angle σ, and the vertical stabiliser dynamic pressure ratio η_V are required. According to Datcom, the effect of σ, β and η_V are empirically related by

$$\left(1+\frac{\partial\sigma}{\partial\beta}\right)\eta_V = 0.724 + \frac{3.06\frac{A_V}{A_W}}{1+\cos(\Lambda_{\frac{c}{4},W})} + \frac{0.4z_W}{d_{f,max}} + 0.009AR_W \tag{143}$$

where: z_W = Distance between Wing Root Quarter Chord Point to Fuselage Centerline

$d_{f,max}$ = Maximum Fuselage Depth

AR_W = Wing Aspect Ratio

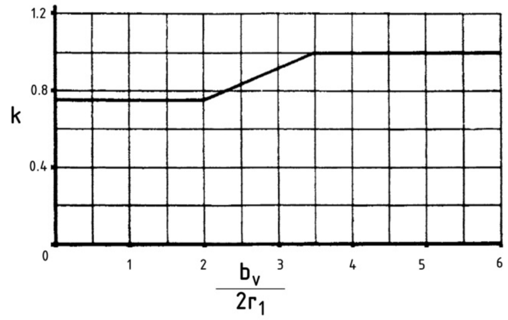

Figure 6.18: k-Factor for Vertical Stabiliser [53]

The factor a_V represents the lift-curve slope of the vertical stabiliser in the presence of the fuselage [64]. According to Datcom, a_V can be calculated in the same manner as (51), however, the effective vertical tail aspect ratio $AR_{V,eff}$ is required, which is an expression of

$$AR_{V,eff} = \left(\frac{AR_{V(B)}}{AR_V}\right) AR_V \left[1 + K_H\left(\frac{AR_{V(HB)}}{AR_{V(B)}} - 1\right)\right] \tag{144}$$

where: $AR_{V(B)}$ = Vertical Tail Aspect Ratio (with respect to the fuselage body)
AR_V = Vertical Tail Aspect Ratio, isolated
$AR_{V(HB)}$ = Vertical Tail Aspect Ratio (with respect to stabiliser and body)

The respective factors $\frac{AR_{V(B)}}{AR_V}$, $\frac{AR_{V(HB)}}{AR_{V(B)}}$ and K_H are shown in Figure 6.19 and Figure 6.20 and are calculated with the help of: the vertical tail taper ratio λ_V; the vertical tail aspect ratio including the span and area; and the vertical tail span b_V with all mentioned elements measured from the fuselage centerline. Additionally, the average depth at vertical tail of the fuselage $2r_1$ is required. Further components are provided in Figure 6.20.

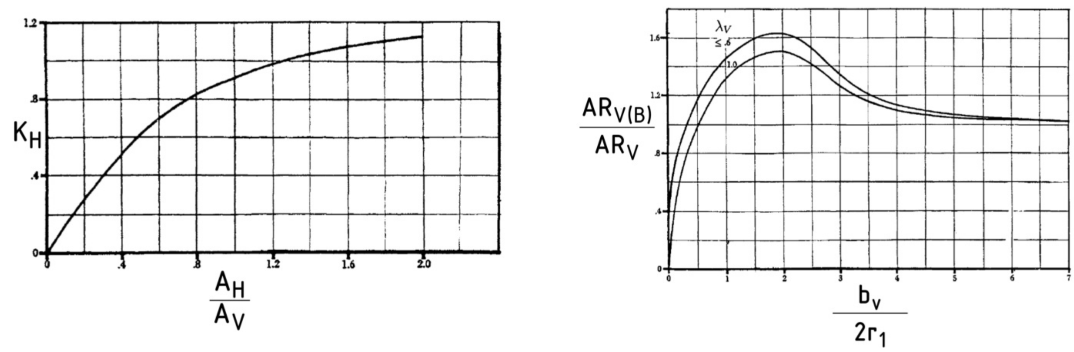

(a) K_H-Factor

(b) Vertical Tail AR-Factors

Figure 6.19: Vertical Tail Calculation Factors [53]

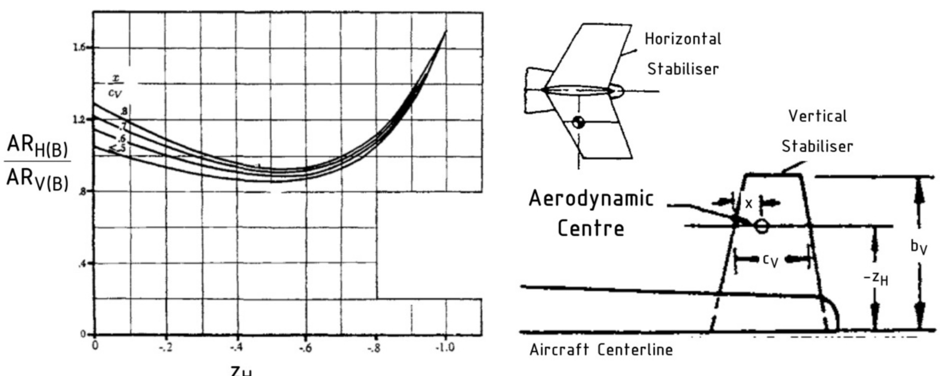

Figure 6.20: AR-Factor of Tailplane [53]

According to Pamadi, the effect of the vertical tail to the directional stability with a fixed rudder can now be formulated as

$$(N_V)_{FIXED} = Y_V l_V = k\bar{q}\eta_V a_V(\beta+\sigma)A_V l_V \tag{145}$$

$$(C_n)_{V,FIXED} = k a_V(\beta+\sigma)\eta_V \overline{V}_V \tag{146}$$

$$(C_{n\beta})_{V,FIXED} = k a_V\left(1+\frac{\partial\sigma}{\partial\beta}\right)\eta_V \overline{V}_V \tag{147}$$

with the Vertical Tail Volume Ratio $\overline{V}_V$ defined as

$$\overline{V}_V = \frac{A_V l_V}{A_W b} \tag{148}$$

Summary Directional Stability

In total, all contribution factors of the directional stability are summed up under the term of the rudder fixed directional stability

$$(C_{n\beta})_{FIXED} = (C_{n\beta})_W + (C_{n\beta})_{B(W)} + (C_{n\beta})_{V,FIXED} + (C_{n\beta})_H \tag{149}$$

6.2.2 Directional Control: The Rudder

The pilot is able to control the aircraft along its vertical axis by using the rudder attached to the vertical stabiliser. Its effectivity is denoted by the value of the yawing-moment coefficient per unit rudder deflection $C_{n\delta r}$, where

$$C_{n\delta r}\begin{cases} <0\text{: Deflection to the right} \rightarrow \text{Positive Side Force} \rightarrow \text{Negative Yawing Moment} \\ >0\text{: Deflection to the left} \rightarrow \text{Negative Side Force} \rightarrow \text{Positive Yawing Moment} \end{cases}$$

Pamadi defines the change of the sideslip angle with respect to the vertical stabiliser per unit deflection of the rudder as

$$\tau_r = \frac{\partial\beta_V}{\partial\delta_r} \tag{150}$$

For this purpose, the change of lift due to the rudder deflection $\Delta\delta_r$ is according to Datcom as follows:

$$\Delta C_L = \Delta C_l\left(\frac{a_V}{a_{0,V}}\right)\left[\frac{(\beta_\delta)C_L}{(\beta_\delta)C_l}\right]K_b \tag{151}$$

The so-called control surface span K_b can be obtained with the help of Figure 6.8(b), with respect to $\eta = \frac{2y}{b_H}$, while the 3D-2D control effectiveness parameter ratio $\frac{(\beta_\delta)_{C_L}}{(\beta_\delta)_{C_l}}$ is given in Figure 6.8(a). By differentating (151) with respect to δ_r, Pamadi suggest that

$$\tau_r = \left(\frac{C_{l\delta}}{a_0}\right)\left[\frac{(\beta_\delta)_{C_L}}{(\beta_\delta)_{C_l}}\right]K_b \tag{152}$$

with $C_{l\delta} = \frac{\partial C_l}{\partial \delta}$ provided in Figure 6.9. Assuming that a positive rudder deflection δ_r^+ is given, the resulting yawing moment is defined as

$$N_r = -k_V \overline{q} \eta_V A_V a_V (\tau_r \delta_r + \sigma) l_V \tag{153}$$

Hence, the coefficient form is written as

$$C_{nr} = \frac{N_r}{\overline{q} A_V b} = -k \eta_V \overline{V}_V a_V (\tau_r \delta_r + \sigma) \tag{154}$$

while its derivative is

$$C_{n\delta r} = \frac{\partial C_{nr}}{\partial \delta_r} = -k \eta_V \overline{V}_V a_v \tau_r \tag{155}$$

The dynamic pressure ratio at the vertical stabiliser η_V, can be evaluated in accordance with (61). Pamadi notes that $\eta_V = \eta_H$. Under these circumstances, the conclusion is made that the amount of rudder deflection required for the generation of a sideslip β is

$$(C_{n\beta})\beta + C_{n\delta r}\delta_r = 0 \tag{156}$$

or in transposed form

$$\delta_r = -\frac{(C_{n\beta})\beta}{C_{n\delta r}} \tag{157}$$

6.2.3 Directional Discussion of the Box Wing Configuration

Directional stability is an important requirement when considering the yawing moment of an aircraft. The yaw moment coefficient, as will be shown later on, can be affected by the rudder, which in return is described by the rudder effectiveness.

Yaw Moment Coefficient

As noted earlier, (149) indicates that directional stability is a combination of effects from the wing, body-to-wing, vertical stabiliser as much as horizontal stabiliser. While the latter may be ignored for cantilever wing configurations with a relatively small horizontal stabiliser, this was not the case for the box wing configuration. Hence, the horizontal tailplane was treated as an additional wing. To calculate the wing effect on the yaw moment coefficient, it was first of all necessary to analyse the wing dihedral and wing sweep as noted by (105) and reminded to the reader here again:

$$(C_{n\beta})_W = (C_{n\beta})_{\Gamma,W} + (C_{n\beta})_{\Lambda,W} \tag{158}$$

where

$$(C_{n\beta})_{\Gamma,W} = -0.075\Gamma_W C_L \frac{1}{rad^2} = -0.075\Gamma_W a_W \alpha \frac{1}{rad^2} \tag{159}$$

Although the abovementioned formula, its derivation as much as the angle are often to referred as dihedral, it shall be noted that the Extra EA 400-500 has no wing dihedral but wing anhedral. This term refers to a negative dihedral, hence a wing with a downward angle towards the ground. For consistence reasons however, the term wing dihedral will be used throughout the following. The Extra EA 400-500 has a wing dihedral of $\Gamma_W = -0.36°$ measured from the half-wing thickness-line extended to the aircraft's centreline. With a_W for the wing calculated earlier, see (82), the following expression was determined:

$$(C_{n\beta})_{\Gamma,W} = -0.075 \cdot (-6.28 \cdot 10^{-3})rad \cdot 5.66\frac{1}{rad} \cdot \alpha\frac{1}{rad^2} = 2.67 \cdot 10^{-3}\alpha\frac{1}{rad^2} \tag{160}$$

In the same manner, the wing sweep was calculated with the help of (138) and $\overline{x}_{a,W} = 0.42m$, thus

$$\begin{aligned}(C_{n\beta})_{\Lambda,W} =&(a_W \cdot \alpha)^2\Bigg[\frac{1}{4\pi AR_W} - \frac{tan(\Lambda_{\frac{c}{4},W})}{\pi AR_W(AR_W + 4cos(\Lambda_{\frac{c}{4},W}))} \\ &\cdot \left(cos(\Lambda_{\frac{c}{4},W}) - \frac{AR_W}{2} - \frac{AR_W^2}{8cos(\Lambda_{\frac{c}{4},W})} - 6\overline{x}_a\frac{sin(\Lambda_{\frac{c}{4},W})}{AR_W}\right)\Bigg]\end{aligned} \tag{161}$$

Afterwards, with all values already at hand, the following expression was derived:

$$\begin{aligned}(C_{n\beta})_{\Lambda,W} = &(5.66\frac{1}{rad} \cdot \alpha)^2\Bigg[\frac{1}{4\pi \cdot 8.96} - \frac{tan(6.6°)}{\pi 8.96(8.96 + 4cos(6.6°))} \\ &\cdot \left(cos(6.6°) - \frac{8.96}{2} - \frac{8.96^2}{8cos(6.6°)} - 6 \cdot 0.42m \cdot \frac{sin(6.6°)}{8.96}\right)\Bigg]\frac{1}{rad}\end{aligned} \tag{162}$$

which simplified led to

$$(C_{n\beta})_{\Lambda,W} = (5.66\frac{1}{rad} \cdot \alpha)^2 \cdot 0.01321 = 0.423\alpha^2\frac{1}{rad^3} \tag{163}$$

In conclusion, the wing effect on the yaw moment coefficient could be described as

$$(C_{n\beta})_W = 0.423\alpha^2\frac{1}{rad^3} + 2.67 \cdot 10^{-3}\alpha\frac{1}{rad^2} \tag{164}$$

Following the same steps, the effect of the horizontal stabiliser on the yaw moment coefficient caused by a dihedral angle of $\Gamma_H = -0.58°$ could be calculated to be

$$(C_{n\beta})_{\Gamma,H} = -0.075 \cdot (-0.010)rad \cdot 6.00\frac{1}{rad} \cdot \alpha\frac{1}{rad^2} = 4.50 \cdot 10^{-3}\alpha\frac{1}{rad^2} \tag{165}$$

The wing sweep effect was calculated with the help of values already known to the reader from previous chapters as much as $\Lambda_{c/4,H} = -19.84°$ and $\overline{x}_{a,H} = 4.10m$, so that

$$(C_{n\beta})_{\Lambda,H} = (6.00\frac{1}{rad} \cdot \alpha)^2 \cdot (-8.74 \cdot 10^{-3}) = -0.314\alpha^2\frac{1}{rad^3} \tag{166}$$

Therefore, the overall effect of the horizontal stabiliser was defined as

$$(C_{n\beta})_H = -0.314\alpha^2\frac{1}{rad^3} + 4.50 \cdot 10^{-3}\alpha\frac{1}{rad^2} \tag{167}$$

In a next step, the fuselage effect needed to be calculated. This was possible by utilising (139). For this purpose, the following values were extracted from CATIA: $A_{B,S} = 9.13m^2$, $l_f = 8.85m$, $h = 1.66m$, $h_1 = 1.40m$, $h_2 = 0.787m$, $\overline{x}_m = 3.63m$ and $b_{f,max} = 1.42m$. The fuselage Reynolds numbers with respect to l_f was calculated to be $Re_{lf} = 5.87 \cdot 10^7$. Utilising Figure 6.16, the Wing-Body Interference Factor was found to be $K_N = 0.0015$, while with the help of Figure 6.17, the Fuselage Reynolds Number Factor was evaluated to be $K_{Rl} = 1.83$. With these values, it was possible to calculate the effect of the body-wing-combination:

$$(C_{n\beta})_{B(W)} = -0.0016 \cdot 1.83 \cdot \frac{9.13m^2}{13.5m^2} \cdot \frac{8.85m}{11.0m} = -1.57 \cdot 10^{-3}\frac{1}{deg} = -0.09\frac{1}{rad} \tag{168}$$

In addition, the tail section was a contributor to the yaw moment coefficient. The calculation was based on empirical data of Datcom, such as the combined value of the sidewash angle σ with respect to β and the vertical stabiliser dynamic pressure ratio η_V, as shown in (143). For this equation, the following values were extracted: $z_W = -0.66m$, $d_{f,max} = 1.66m$ and $A_V = 2.80m^2$. Hence,

$$\left(1 + \frac{\partial\sigma}{\partial\beta}\right)\eta_V = 0.724 + \frac{3.06 \cdot \frac{2.80m^2}{13.5m^2}}{1 + \cos(6.6°)} + \frac{0.4 \cdot (-0.66m)}{1.66m} + 0.009 \cdot 8.96 = 0.964 \qquad (169)$$

Figure 6.18 showed that for $b_V = 2.03m$ and $r_1 = 0.183m$, it could be found that k=1. Eventually, in order to find a_V, see (51), the vertical tail $AR_{V,eff}$ needed to be calculated with the help of (144) as much as Figure 6.19 and Figure 6.20. The vertical tail taper ratio was $\lambda_V = 0.34$. Therefore, $K_H = 1.2$ and $\frac{AR_{V(B)}}{AR_V} = 1.05$. Furthermore, for Figure 6.20, the height from the aircraft centreline to the horizontal tail AC was $-z_H = 1.47m$, $c_V = 0.88m$ and the horizontal tail AC was located at a distance of $\overline{x}_V = 0.72m$ from the leading edge. These values led to $\frac{AR_{V(HB)}}{AR_{V(B)}} = 1.04$, so that the isolated vertical tail aspect ratio was expressed as

$$AR_{V,eff} = 1.05 \cdot \frac{(2.03m)^2}{2.80m^2}\left[1 + 1.2 \cdot (1.04 - 1)\right] = 1.62 \qquad (170)$$

Eventually, it was possible to find the vertical tail lift-curve slope based on the fact that, $\Phi'_{TE,V} = 19.52°$, $(t/c)_V = 0.146$ and $(\Lambda_{c/2})_V = 38.12°$. By using Figure 6.6, it was found that $\left(\frac{a_0}{(a_0)_{theory}}\right)_V = 0.85$ and $(a_0)_{theory,V} = 6.95\frac{1}{rad}$. Hence

$$a_{0,V} = \frac{1.05}{\sqrt{1 - 0.28^2}} \cdot 0.85 \cdot 6.95\frac{1}{rad} = 6.46\frac{1}{rad} \qquad (171)$$

so that $k_V = \frac{a_0}{2\pi} = 1.028\frac{1}{rad}$ and therefore

$$a_V = \frac{2\pi \cdot 1.62}{2 + \sqrt{\frac{1.62^2 \cdot 0.96^2}{(1.028\frac{1}{rad})^2}\left(1 + \frac{tan^2(38.12°)}{0.96^2}\right) + 4}} = 2.12\frac{1}{rad} \qquad (172)$$

This allowed the formulation of the effect of the vertical stabiliser on the yaw moment with the help of $l_V = 4.30m$ measured from the aircraft's CG to the AC of the vertical stabiliser. Or in other words:

$$(C_{n\beta})_V = 1 \cdot 2.12\frac{1}{rad} \cdot 0.964 \cdot \frac{2.80m^2 \cdot 4.30m}{13.5m^2 \cdot 11.0m} = 0.166\frac{1}{rad} \qquad (173)$$

Thus,

$$
\begin{aligned}
(C_{n\beta}) &= (C_{n\beta})_W + (C_{n\beta})_{B(W)} + (C_{n\beta})_V + (C_{n\beta})_H \\
&= 0.423\alpha^2 \frac{1}{rad^3} + 2.67 \cdot 10^{-3}\alpha \frac{1}{rad^2} - 0.09\frac{1}{rad} + 0.166\frac{1}{rad} \\
&- 0.314\alpha^2 \frac{1}{rad^3} + 4.50 \cdot 10^{-3}\alpha \frac{1}{rad^2} \\
&= 0.109\alpha^2 \frac{1}{rad^3} + 7.17 \cdot 10^{-3}\alpha \frac{1}{rad^2} + 0.076\frac{1}{rad}
\end{aligned}
\tag{174}
$$

Table 6.4 below shows the results of the yaw rolling moment coefficient with regard to the angle of attack. Furthermore, a more comprehensive graph of the coefficient is shown in Figure 6.21. The results showed that the Extra EA 400-500 equipped with box wings could be seen as stable regarding longitudinal movement, since $C_{n\beta} > 0$ for all AOAs.

Table 6.4: $C_{n\beta}$ Values for the Box Wing Configuration

α	$-5°$	$-2°$	$0°$	$2°$	$5°$	$7°$	$10°$	$12°$	$15°$
$C_{n\beta}[\frac{1}{rad}]$	0.0762	0.0759	0.0760	0.0764	0.0775	0.0785	0.0806	0.0823	0.0853

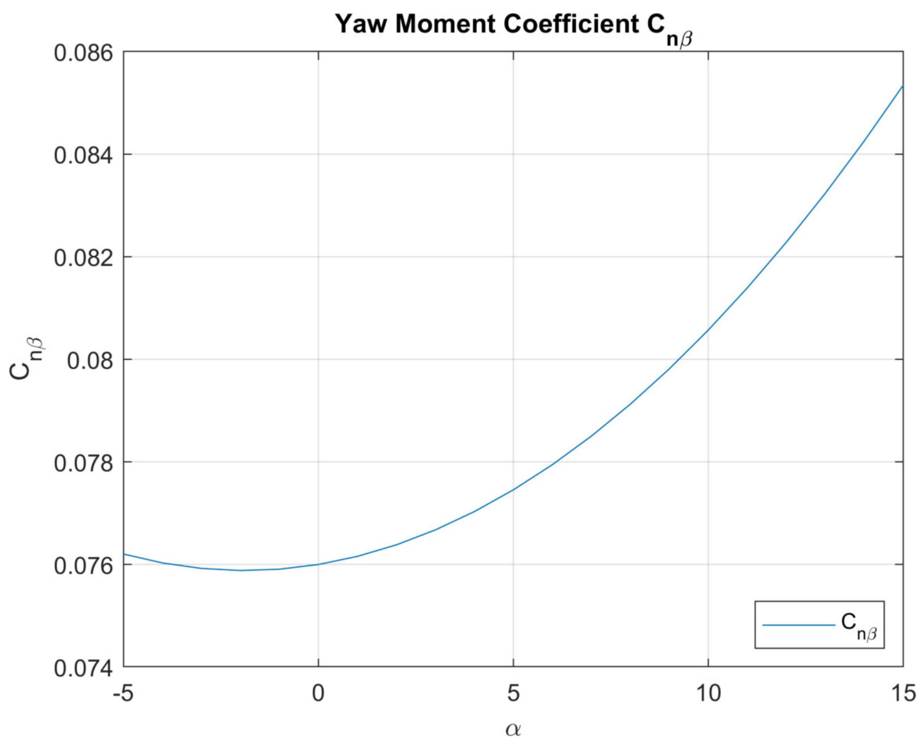

Figure 6.21: $C_{n\beta}$ Values for the Box Wing Configuration

Directional Control

Eventually, the rudder effectiveness was calculated with the help of Figure 6.8(b):

$$K_{b,V} = K_b(\eta_o) - K_b(\eta_i) = K_b(1.36) - K_b(0.087) = 1.0 - 0.12 = 0.88 \tag{175}$$

Furthermore, it was evaluated that $C_{l\delta,V} = 0.354\frac{1}{rad}$, $\left(\frac{(\beta_\delta)_{C_L}}{(\beta_\delta)_{C_l}}\right)_V = 1.08$, so that

$$\tau_r = \left(\frac{C_{l\delta}}{a_{0,V}}\right)\left[\frac{(\beta_\delta)_{C_L}}{(\beta_\delta)_{C_l}}\right]K_{b,V} = \left(\frac{0.354\frac{1}{rad}}{6.46\frac{1}{rad}}\right)\cdot 1.08 \cdot 0.88 = 5.20 \cdot 10^{-2} \tag{176}$$

and

$$C_{n\delta r} = -1.0 \cdot 0.95 \cdot \frac{2.80m^2 \cdot 4.30m}{13.50m^2 \cdot 11.0m} \cdot 2.12\frac{1}{rad} \cdot 5.20 \cdot 10^{-2} = -8.49 \cdot 10^{-3}\frac{1}{rad} \tag{177}$$

The dynamic pressure ratio at the vertical stabiliser η_V, was evaluated in accordance with (61). Additionally, Pamadi notes that $\eta_V = \eta_T$. Under these circumstances, the conclusion was made that the amount of rudder deflection required for the generation of a sideslip β or counteracting force was

$$(C_{n\beta})\beta + C_{n\delta r}\delta_r = 0 \tag{178}$$

or in transposed form

$$\delta_r = -\frac{(C_{n\beta})\beta}{C_{n\delta r}} \tag{179}$$

so that

$$\delta_r = -\frac{(0.109\alpha^2\frac{1}{rad^3} + 7.17 \cdot 10^{-3}\alpha\frac{1}{rad^2} + 0.076\frac{1}{rad}) \cdot \beta}{-8.49 \cdot 10^{-3}\frac{1}{rad}} \tag{180}$$

Figure 6.22 and Table 6.5 show the results of said rudder deflection. It can be seen that the rudder has enough power to compensate a sideslip of approximately $\beta = \pm 25°$

Table 6.5: Required Rudder Deflection δ_r Due to Sideslip β

β	$-11°$	$-7°$	$-5°$	$-2°$	$0°$	$2°$	$5°$	$7°$	$11°$
$\delta_{r,\alpha=-5°}$	$-22°$	$-13°$	$-9°$	$-4°$	$0°$	$4°$	$9°$	$13°$	$22°$
$\delta_{r,\alpha=15°}$	$-25°$	$-15°$	$-10°$	$-5°$	$0°$	$5°$	$10°$	$15°$	$25°$

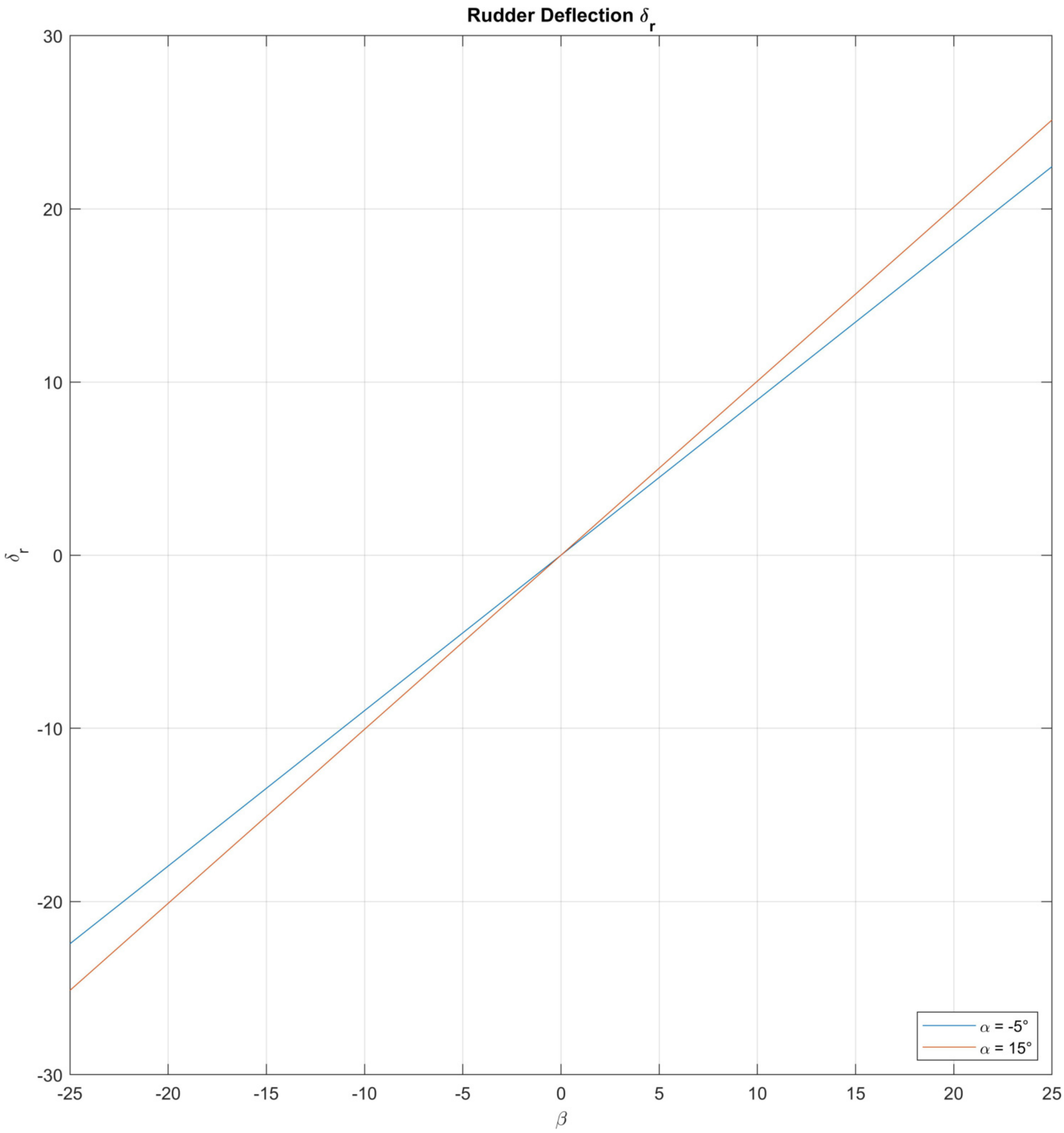

Figure 6.22: Required Rudder Deflection δ_r Due to Sideslip β

The graphs show, that in case of a positive sideslip, hence a sideslip to the starboard side, a positive deflection of the rudder is required. As defined earlier, a positive rudder deflection is achieved when the pilot pushes the left rudder pedal in order for the rudder to deflect to the left. This leads to a negative side force, which eventually results in a positive yawing moment. In this way, directional stability is ensured.

6.2.4 Comparison to the Cantilever Wing Configuration

As shown earlier, the yaw moment coefficient depended on multiple components such as the wing, the fuselage, as much as the horizontal and vertical stabiliser. The biggest contribution, however, when considering the box wing configuration shown in (174), were the wing and horizontal stabiliser. When comparing the yaw moment coefficient of the cantilever wing, see Figure 6.23(a), with the box wing configuration, see Figure 6.23(b), a significant difference was observed.

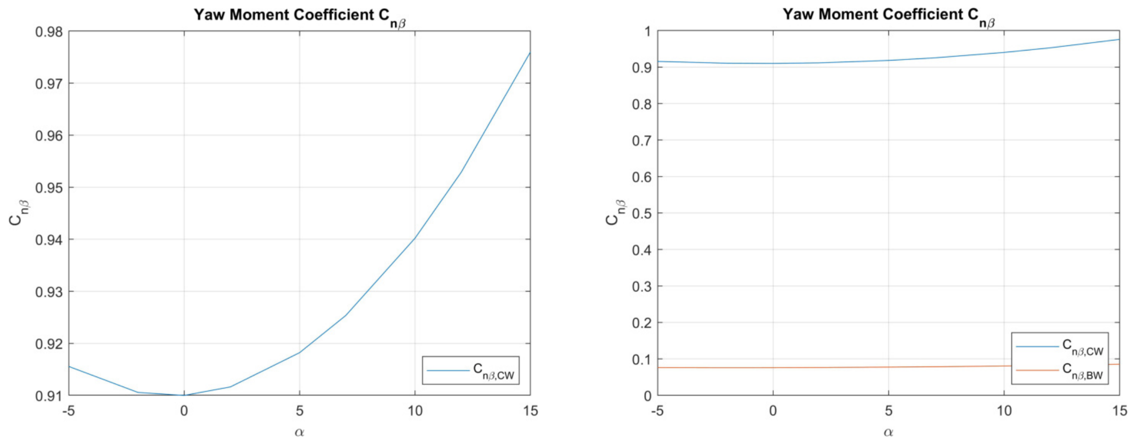

(a) $C_{n\beta}$ for the Cantilever Wing

(b) $C_{n\beta,CW}$ and $C_{n\beta,BW}$

Figure 6.23: Comparison of $C_{n\beta}$ for the Box and Cantilever Wing Configuration

Under normal circumstances, the yaw moment coefficient is often calculated by only considering the wing and even by mostly ignoring the horizontal tailplane. For this study, all main contributors were calculated and it was seen, that the large horizontal stabiliser does indeed had a great effect on the yaw moment coefficient by a reduction of a factor greater ten, as can be seen in Table 6.6. However, further analysis on this matter might be required when considering box wing configurations. For both configuration, it was observed that $C_{n\beta} > 0$.

Table 6.6: Comparison of $C_{n\beta}$ for the Box and Cantilever Wing Configuration

α	$-5°$	$-2°$	$0°$	$2°$	$5°$	$7°$	$10°$	$12°$	$15°$
$C_{n\beta,CW}[\frac{1}{rad}]$	0.916	0.910	0.910	0.912	0.918	0.925	0.940	0.953	0.976
$C_{n\beta,BW}[\frac{1}{rad}]$	0.0762	0.0759	0.0760	0.0764	0.0775	0.0785	0.0806	0.0823	0.0853
$\lvert\Delta C_{n\beta}\rvert[\frac{1}{rad}]$	0.840	0.834	0.834	0.836	0.841	0.847	0.860	0.871	0.891

Furthermore, the box wing and cantilever wing configuration were analysed regarding their directional control effectiveness. During the study, it was seen that the rudder deflection changed only slightly due to the fact the rudder remained the same and the change of $C_{n\beta}$ and $C_{n\delta r}$ maintained an equilibrium, as shown in Table 6.7.

Table 6.7: Directional Control Values for the Box Wing and Cantilever Configuration

Parameter	Cantilever	Boxwing
τ_r	$5.2 \cdot 10^{-2}$	$5.2 \cdot 10^{-2}$
$C_{n\delta r}$	$-9.38 \cdot 10^{-3} \frac{1}{rad}$	$-8.49 \cdot 10^{-3} \frac{1}{rad}$

6.3 Lateral Motion

An aircraft's possibility to roll along its longitudinal axis is called lateral motion, or banking, and is required in order to adjust the heading while flying. While maintaining level flight, thus flying with no bank angle, no lateral motion exists until either deliberately enforced by the pilot or due to a disturbance such as a sudden wind change or gusts. In this case, every aircraft shall develop a sideslip of equal direction to the rolling moment which in return must result in a counteracting rolling moment. This effect, shown in Figure 6.24, is called the dihedral effect – not to be confused with the dihedral angle of a wing Γ – and leads to lateral stability. Vice versa, a development of an enhancing rolling moment would be called lateral instability, while an aircraft's ability to maintain a constant bank angle and sideslip would result in neutral stability. This study focuses on a box wing configured aircraft with lateral stability.

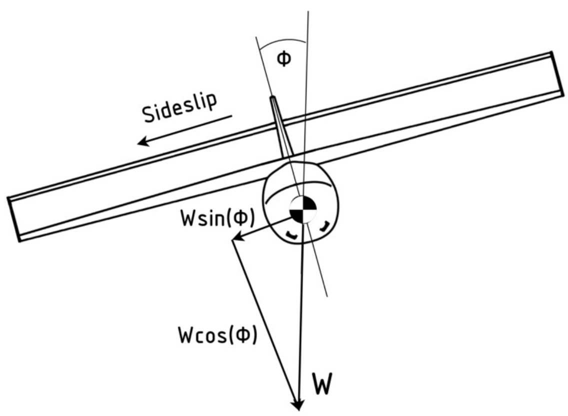

Figure 6.24: Sideslip Due to Bank Angle

6.3.1 Lateral Stability

An analysis of the lateral stability is only possible by defining several boundary conditions. In this case, it is necessary to define that i) a restoring rolling moment is negative if due to a positive sideslip, and ii) a restoring moment is positive if due to a negative sideslip. Overall, it can be said that for lateral stability the rolling moment L – not to be confused with the Lift L – must be

$$L_\beta < 0 \tag{181}$$

and

$$C_{l\beta} < 0 \tag{182}$$

For this, it is defined that

$$L_\beta = \frac{\partial L}{\partial \beta} \tag{183}$$

$$C_l = \frac{L}{\bar{q} A_W b} \tag{184}$$

$$C_{l\beta} = \frac{\partial C_l}{\partial \beta} \tag{185}$$

In total, $C_{l\beta}$ is mainly affected by the fuselage and the wing. Nevertheless, the fuselage alone has only little to no effect on the lateral stability and is therefore ignored [64]. However, the fuselage does have an effect on the wing, which is next to the wing dihedral angle and leading edge sweep one of the main focus areas for this part of the analysis.

Wing-Fuselage Contribution

Depending on the location of the wing, the interference can either be helpful or not. For example, a high wing is producing a stable contribution to the lateral stability, while a low wing configuration is rather considered unstable or in other words: has a destabilising contribution [64]. The reason for this becomes obvious when considering a positive sideslip: the right wing inboard area of a low-wing configured aircraft experiences a downwash which results in a decrease in AOA locally, while the left wing inboard area is affected by an upwash and thus an increase in AOA. This difference in lift results in a further destabilising induced rolling moment. The exact opposite is the case for a high-wing configured aircraft. Here, an upwash would be experienced on the right wing, while the left wing would see a decrease in AOA. Eventually, a counteracting rolling moment is created and the aircraft is stabilised. This effect is shown in Figure 6.25. For completion, it shall be noted that a mid-wing configuration, following the same argumentation, only affects stability little due to a small induced rolling moment.

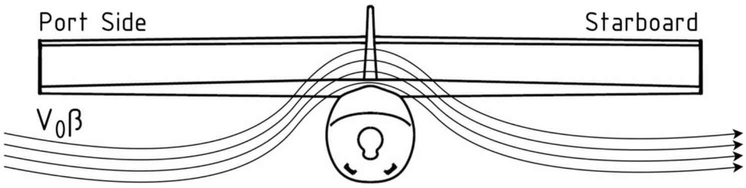

Figure 6.25: High-Wing Configuration During Sideslip

Wing Dihedral Angle Effect

The dihedral of an aircraft, thus $\Gamma_W > 0$, has a stabilising contribution to the overall lateral stability. This can be seen when considering the case of a wing with the dihedral angle Γ_W at α, with sideslip β, and exposed to a forward velocity V_0. Here, the rolling moment L, when applying the strip theory, for an element RT is defined as

$$dL = -\frac{1}{2}\rho V_0^2 c(y) a_{0,W}(y)(\alpha + \beta\Gamma_W) y dy \tag{186}$$

Hence, the rolling moments caused by the starboard (SB) and port side (PS) wing are respectively:

$$L_{SB} = \frac{1}{2}\rho V_0^2 \int_0^{\frac{b}{2}} c(y) a_{0,W}(y)(\alpha - \beta\Gamma_W) y dy \tag{187}$$

$$L_{PS} = -\frac{1}{2}\rho V_0^2 \int_0^{\frac{b}{2}} c(y) a_{0,W}(y)(\alpha + \beta\Gamma_W) y dy \tag{188}$$

Combined, the overall rolling moment is summed up to

$$L = -\rho V_0^2 \beta \Gamma_W \int_0^{\frac{b}{2}} c(y) a_{0,W}(y) y dy \tag{189}$$

with its coefficient form given in

$$(C_l)_{\Gamma,W} = -\frac{2\beta\Gamma_W}{A_W b} \int_0^{\frac{b}{2}} c(y) a_{0,W}(y) y dy \tag{190}$$

as much as

$$(C_{l\beta})_{\Gamma,W} = -\frac{2\Gamma_W}{A_W b} \int_0^{\frac{b}{2}} c(y) a_{0,W}(y) y dy \tag{191}$$

As shown in the last equation, a positive wing dihedral, hence $\Gamma > 0$ is helpful when developing an aircraft with high lateral stability. Pamadi notes that a too large dihedral angle, however, leads to a too sensitive aircraft along its rolling axis when exposed to disturbances, causing discomfort to the passenger. Additionally, crosswind take-offs and landings as much as flights with asymmetric power would be more complicated due to a high dihedral angle.

Wing Sweep Effect

The wing sweep is defined as the backward or forward angle of a wing. For the former, the result is an increase in stability, while the latter has a destabilising effect on the aircraft. This statement is shown to be correct, when considering an aircraft with dihedral angle $\Gamma = 0$, flying at α, with sideslip β^+ and a velocity of V_0. When considering only small angles, the sectional AOA α_{loc} and local dynamic pressure $\overline{q}_{loc}$ can be written as

$$\alpha_{loc} = \begin{cases} \text{Starboard Wing: } \frac{\alpha}{(1+\beta\tan(\Lambda_W))\cos(\Lambda_W)} \\ \text{Port Side Wing: } \frac{\alpha}{(1-\beta\tan(\Lambda_W))\cos(\Lambda_W)} \end{cases} \tag{192}$$

and

$$\overline{q}_{loc} = \begin{cases} \text{Starboard Wing: } \frac{1}{2}\rho V_0^2\cos^2(\Lambda_W^2)(1+\beta\tan(\Lambda_W))^2 \\ \text{Port Side Wing: } \frac{1}{2}\rho V_0^2\cos^2(\Lambda_W^2)(1-\beta\tan(\Lambda_W))^2 \end{cases} \tag{193}$$

Again, the strip theory is used to understand the effect of the wing sweep on lateral stability. For this reason, the lift on a wing strip RT is defined as

$$\begin{aligned} dLift =& \overline{q}_{loc} c(y_h) dy_h a_{0,W} \alpha_{loc} \\ =& \frac{1}{2}\rho V_0^2\cos^2(\Lambda_W)(1+\beta\tan(\Lambda_W))^2 a_{0,W}\left[\frac{\alpha}{(1+\beta\tan(\Lambda_W))\cos(\Lambda_W)}\right]c(y_h)dy_h \\ =& \frac{1}{2}\rho V_0^2\cos(\Lambda_W)(1+\beta\tan(\Lambda_W))a_{0,W}\alpha c(y_h)dy_h \end{aligned} \tag{194}$$

whereas the rolling moment due to RT is

$$dL = \frac{1}{2}\rho V_0^2\cos(\Lambda_W)(1+\beta\tan(\Lambda_W))a_{0,W}\alpha c(y_h)y_h\cos(\Lambda_W)dy_h \tag{195}$$

When considering the whole wing, it can be seen that the rolling moment caused by the left wing and right wing, respectively, are

$$L_{SB} = -\frac{1}{2}\rho V_0^2\cos^2(\Lambda_W)(1+\beta\tan(\Lambda_W))\alpha\int_0^{\frac{b}{2}sec(\Lambda)} a_{0,W}c(y_h)y_h dy_h \tag{196}$$

$$L_{PS} = \frac{1}{2}\rho V_0^2 \cos^2(\Lambda_W)(1 - \beta \tan(\Lambda_W))\alpha \int_0^{\frac{b}{2}sec(\Lambda_W)} a_{0,W} c(y_h) y_h dy_h \tag{197}$$

Thus, the two rolling moments sum up to

$$L = \rho V_0^2 \alpha \beta cos^2(\Lambda_W) tan(\Lambda_W) \int_0^{\frac{b}{2}sec(\Lambda)} a_{0,W} c(y_h) y_h dy_h \tag{198}$$

In coefficient form, it is formulated that

$$C_l = -\left(\frac{2\alpha\beta cos(\Lambda_W) sin(\Lambda_W)}{A_W b}\right) \int_0^{\frac{b}{2}sec(\Lambda_W)} a_{0,W} c(y_h) y_h dy_h \tag{199}$$

and

$$C_{l\beta} = -\left(\frac{2\alpha cos(\Lambda_W) sin(\Lambda_W)}{A_W b}\right) \int_0^{\frac{b}{2}sec(\Lambda_W)} a_{0,W} c(y_h) y_h dy_h \tag{200}$$

According to Pamadi, when an aircraft with swept wing maintains level flight with no sideslip, the lift is generated by

$$Lift = \rho V_0^2 cos^2(\Lambda_W) \int_0^{\frac{b}{2}sec(\Lambda_W)} a_{0,W} \alpha sec(\Lambda_W) c(y_h) dy_h \tag{201}$$

with

$$C_L = \frac{Lift}{\frac{1}{2}\rho V_0^2 A_W} \tag{202}$$

Therefore,

$$C_L = \frac{2cos^2(\Lambda_W)}{A_W} \int_0^{\frac{b}{2}sec(\Lambda_W)} a_{0,W} \alpha sec(\Lambda_W) c(y_h) dy_h \tag{203}$$

This term is simplified under the boundary condition that $a_{0,W}$ is constant, so that

$$C_L = a_{0,W} \alpha cos(\Lambda_W) \tag{204}$$

Hence, the fact that a backward wing sweep improves lateral stability can my seen by

$$C_{l\beta} = -\left(\frac{2\alpha sin(\Lambda_W) C_L}{A_W b}\right) \int_0^{\frac{b}{2}sec(\Lambda_W)} c(y_h) y_h dy_h \tag{205}$$

Datcom considers that the overall geometry of the wing and the effects caused due to the wing-fuselage interference with regard to lateral stability can be empirically expressed as

$$(C_{l\beta})_{W(B)} = C_L \left[\left(\frac{C_{l\beta}}{C_L} \right)_{\Lambda_{\frac{c}{2}},W} K_{M\Lambda,W} K_f + \left(\frac{C_{l\beta}}{C_L} \right)_A \right] + \Gamma_W \left[\frac{C_{l\beta}}{\Gamma_W} K_{M\Gamma,W} + \frac{\Delta C_{l\beta}}{\Gamma_W} \right] + (\Delta C_{l\beta})_{zW} \tag{206}$$

It shall be noted that the dihedral angle Γ_W must be entered in degree, so that the overall equation (206) is per degree. Additionally, the following terms are expressed as

$$\frac{\Delta C_{l\beta}}{\Gamma_W} = -0.0005\sqrt{AR_W}\left(\frac{d_W}{b}\right)^2 \tag{207}$$

and

$$(\Delta C_{l\beta})_{z_w} = \frac{1.2\sqrt{AR_W}}{57.3}\left(\frac{z_w}{b}\right)\left(\frac{2d}{b}\right) \tag{208}$$

where: d_W = Average fuselage diametre at wing root

b = Wing Span

z_w = Distance between fuselage centerline and wing root

For the parameters $(C_{l\beta}/C_L)_{\Lambda_{c/2}}$, $(C_{l\beta}/\Gamma)$, K_f, $(C_{l\beta}/C_L)_A$, $K_{M\Lambda}$, and $K_{M\Gamma}$ one shall refer to Figure 6.26, Figure 6.27, Figure 6.28, Figure 6.29 and Figure 6.30, respectively.

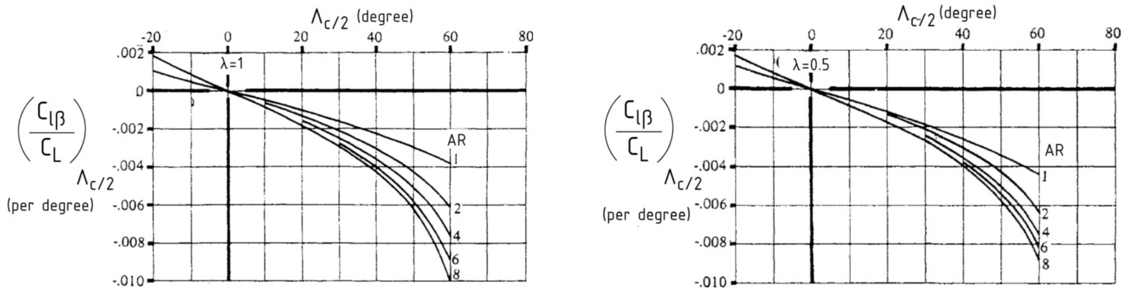

(a) $\lambda = 1$ (b) $\lambda = 0.5$

Figure 6.26: $(C_{l\beta}/C_L)_{\Lambda_{c/2}}$ Factor for Roll Moment Calculation [53]

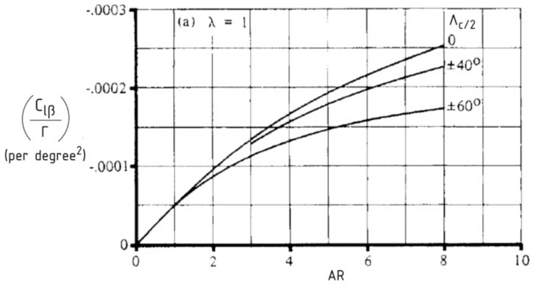

(a) $\lambda = 1$

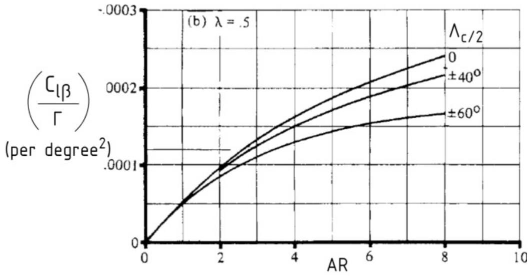

(b) $\lambda = 0.5$

Figure 6.27: $(C_{l\beta}/\Gamma)$ Factor for Roll Moment Calculation [53]

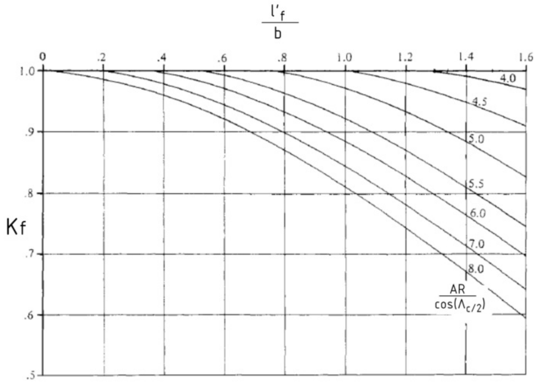

(a) K_f

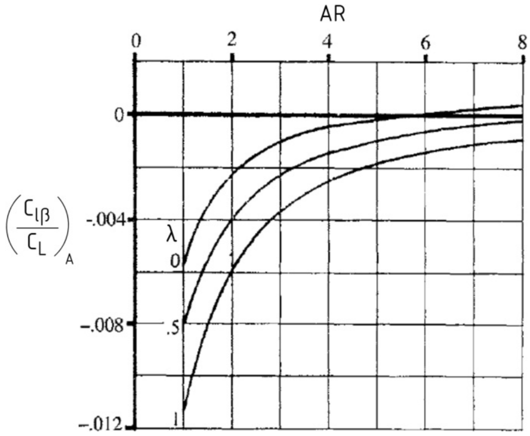

(b) $(C_{l\beta}/C_L)_A$

Figure 6.28: K_f and $(C_{l\beta}/C_L)_A$ Factors for Roll Calculation [53]

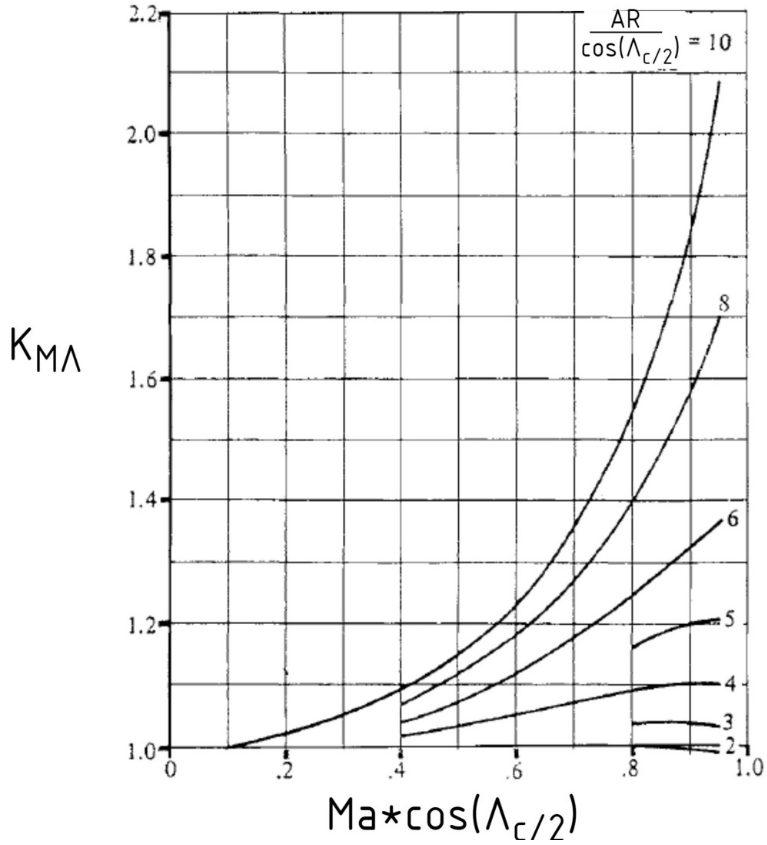

Figure 6.29: $K_{M\Lambda}$ Factor for Roll Calculation [53]

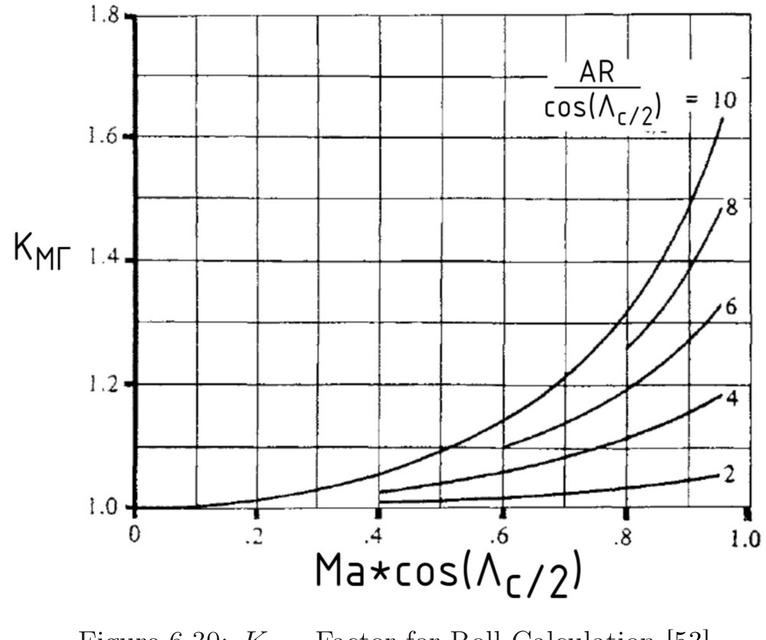

Figure 6.30: $K_{M\Gamma}$ Factor for Roll Calculation [53]

Tail Section

As mentioned earlier, the tail section holds virtually zero contribution to the lateral stability under normal circumstances. However, when considering large horizontal tail sections such as for box wing configurations, this statement becomes redundant so that the horizontal stabiliser shall be seen as a wing with its respective dihedral and wing sweep. Hence, a thorough analysis of the stabiliser was conducted. Additionally, the tail section must be analysed regarding the vertical stabiliser's effect on the lateral stability. For this, Pamadi suggest that

$$(C_{l\beta})_V = C_{Y\beta,V}\left(\frac{z}{b}\right) = C_{Y\beta,V}\left(\frac{z_v cos(\alpha) - l_V sin(\alpha)}{b}\right) \tag{209}$$

where: z = Moment Arm of rolling moment

l_V = Longitudinal distance between CG and AC of horizontal stabiliser

z_V = Distance between the aircraft's reference line and AC of vertical stabiliser

The factor $C_{Y\beta,V}$ has been evaluated earlier, see (142), so that the final coefficient can be summed up to

$$(C_{l\beta})_V = -ka_V\left(1 + \frac{\partial\sigma}{\partial\beta}\right)\eta_V\left(\frac{A_V}{A_W}\right)\left(\frac{z_V cos(\alpha) - l_V sin(\alpha)}{b}\right) \tag{210}$$

For most cases, it can be noted that $(C_{l\beta})_V < 0$ due to $z_V cos(\alpha) > l_V sin(\alpha)$ so that a stabilising effect can be expected from the vertical stabiliser with regard to lateral stability [64].

Summary Lateral Stability

For the purpose of analysing the lateral stability of a box wing configured conceptual design, it is therefore required that

$$(C_{l\beta}) = (C_{l\beta})_{W(B)} + (C_{l\beta})_H + (C_{l\beta})_V < 0 \tag{211}$$

6.3.2 Lateral Control: The Ailerons

Not only to compensate any disturbances while flying, but also in order to change the heading, aircraft are equipped with so-called ailerons. Those components are in general located at the outer portion of each wing and can be deflected upward δ_a^+ or downward δ_a^- in order to produce a rolling moment C_l by increasing the lift on one wing, while decreasing on the other. With this convention, a rolling aircraft always generates a negative moment L, so that $C_{l\delta a} < 0$, where

$$C_l = \frac{L}{\overline{q} A_W b} \tag{212}$$

as much as

$$C_{l\delta a} = \frac{\partial C_l}{\partial \delta_a} \tag{213}$$

In order to calculate the coefficient for the rolling moment (RM) per unit deflection $C_{l\delta a}$, the strip theory is utilised in which the rolling moment for a differential deflection δ_a can be described as

$$\Delta L_{RM} = -2\Delta L y = -2\overline{q} c_a(y) dy \Delta C_l y = -2\overline{q} c_a(y) dy a_W \tau_a \delta_a y \tag{214}$$

In this case, $c_a(y)$ is the expression for the local wing chord including the aileron and τ_a the change of the wing AOA for a unit aileron deflection. For the calculation of τ_a, the reader shall be referred to (68). Following the strip theory, the rolling moment L_{RM} caused by ailerons with measurements from y_i to y_o can be expressed as

$$L_{RM} = -2\overline{q} \int_{y_i}^{y_o} a_W \tau_a c_a(y) y dy \tag{215}$$

and its coefficient form as

$$C_{l\delta a} = -\frac{2 a_W \tau_a}{A_W b} \int_{y_i}^{y_o} c_a(y) y dy \tag{216}$$

6.3.3 Lateral Discussion of the Box Wing Configuration

In the following, the lateral stability of the Extra EA 400-500 will be analysed by taking the wing-body and the tailplane contribution into account.

Rolling Moment Coefficient

As mentioned earlier, Datcom suggests calculating the wing-body-contribution to lateral stability instead of the isolated wing. For this purpose, several factors needed to be taken into account. In a first step, the lift coefficient with respect to the angle of attack and the wing sweep was calculated:

$$C_{L,W} = a_{0,W} \alpha cos(\Lambda_{c/4,W}) = 7.06 \frac{1}{rad} \cdot \alpha \cdot \cos(6.6°) = 7.01 \alpha \frac{1}{rad} \tag{217}$$

In a next step, see (207), with the help of Datcom it was found that

$$\frac{\Delta C_{l\beta}}{\Gamma_W} = -0.0005\sqrt{AR_W}\left(\frac{d_W}{b}\right)^2 = -0.0005\sqrt{8.96}\left(\frac{1.59m}{11.0m}\right)^2 = -3.13\cdot 10^{-5}\frac{1}{deg^2} \tag{218}$$

where the average fuselage diametre at wing root was $d_W = 1.59m$. Furthermore, the distance height difference between the fuselage centreline and wing root was determined from CATIA to be $z_W = -0.66m$. Therefore,

$$(\Delta C_{l\beta})_{z_W} = \frac{1.2\sqrt{8.96}}{57.3}\left(\frac{-0.66m}{11.0m}\right)\left(\frac{2\cdot 1.59m}{11.0m}\right) = -1.09\cdot 10^{-3}\frac{1}{deg} \tag{219}$$

Afterwards, several factors needed to be estimated. First, with the help of Figure 6.26(b), it was found that $(C_{l\beta}/C_L)_{\Lambda_{c/2,W}} = -0.0005\frac{1}{deg}$. Figure 6.27(b) showed that with the same values, $(C_{l\beta}/\Gamma)_W = -0.00025\frac{1}{deg^2}$. With the help of the length from the aircraft nose to the half wing sweep line $l'_{f,W} = 3.78m$ and Figure 6.28(a), it was evaluated that $K_{f,W} = 0.97$. Figure 6.28(b) showed that $(C_{l\beta}/C_L)_{A,W} = -0.0001\frac{1}{deg}$ and by using Figure 6.29 it was found that $K_{M\Lambda,W} = 1.08$. In a last step, it was approximated from Figure 6.30 that $K_{M\Gamma,W} = 1.02$. With these values, the effect of the wing-body contribution to lateral stability was found to be

$$\begin{aligned}(C_{l\beta})_{W(B)} &= 7.01\alpha\frac{1}{rad}\left[-0.0005\frac{1}{deg}\cdot 1.08\cdot 0.97 - 0.0001\frac{1}{deg}\right]\\ &- 0.36^\circ\left[-0.00025\frac{1}{deg^2}\cdot 1.02 - 3.13\cdot 10^{-5}\frac{1}{deg^2}\right] - 1.09\cdot 10^{-3}\frac{1}{deg}\\ &= -0.251\alpha\frac{1}{rad^2} - 0.057\frac{1}{rad}\end{aligned} \tag{220}$$

The same steps had to be conducted again for the horizontal stabiliser. It was found that

$$C_{L,H} = a_{0,H}\alpha cos(\Lambda_{c/4,H}) = 7.14\frac{1}{rad}\cdot\alpha\cdot\cos(-19.84^\circ) = 6.72\alpha\frac{1}{rad} \tag{221}$$

and, with the help of $d_H = 0.36m$,

$$\frac{\Delta C_{l\beta}}{\Gamma_H} = -0.0005\sqrt{13.75}\left(\frac{0.36m}{11.0m}\right)^2 = -1.99\cdot 10^{-6}\frac{1}{deg^2} \tag{222}$$

Furthermore, with $z_H = -1.47m$:

$$(\Delta C_{l\beta})_{z_H} = \frac{1.2\sqrt{13.75}}{57.3}\left(\frac{-1.47m}{11.0m}\right)\left(\frac{2\cdot 0.36m}{11.0m}\right) = 6.80\cdot 10^{-4}\frac{1}{deg} \tag{223}$$

Additionally, with all values already known to the reader and $l'_{f,H} = 6.88m$, it was found that: $(C_{l\beta}/C_L)_{\Lambda_{c/2,H}} = 0.002\frac{1}{deg}$, $(C_{l\beta}/\Gamma)_H = -0.00028\frac{1}{deg^2}$, $K_{f,H} = 0.8$, $(C_{l\beta}/C_L)_{A,H} = -0.001\frac{1}{deg}$, $K_{M\Lambda,H} = 1.08$ and $K_{M\Gamma,H} = 1.02$. Thus,

$$
\begin{aligned}
(C_{l\beta})_{H(B)} &= 6.72\alpha\frac{1}{rad}\left[0.002\frac{1}{deg}\cdot 1.08\cdot 0.80 - 0.001\frac{1}{deg}\right] \\
&- 0.58^\circ\left[-0.00028\frac{1}{deg^2}\cdot 1.02 - 1.99\cdot 10^{-6}\frac{1}{deg^2}\right] - 6.80\cdot 10^{-4}\frac{1}{deg} \\
&= 0.28\alpha\frac{1}{rad^2} - 0.03\frac{1}{rad}
\end{aligned}
\tag{224}
$$

Eventually, the contribution of the vertical tail had to be evaluated. For this purpose, the normal distance between the aircraft's reference line and AC of the vertical tail was found to be $z_V = 0.83m$ and the distance from CG to the AC of the vertical tail to be $l_V = 4.3m$. Therefore

$$
\begin{aligned}
(C_{l\beta})_V &= -1\cdot 2.12\frac{1}{rad}\cdot 0.964\left(\frac{2.80m^2}{13.5m^2}\right)\left(\frac{0.83m\cdot cos(\alpha) - 4.3m\cdot sin(\alpha)}{11.0m}\right) \\
&= -0.0385(0.83m\cdot cos(\alpha) - 4.3m\cdot sin(\alpha))\frac{1}{rad}
\end{aligned}
\tag{225}
$$

In summary, the lateral stability coefficient for the rolling moment had to be calculated with:

$$
\begin{aligned}
C_{l\beta} &= (C_{l\beta})_{W(B)} + (C_{l\beta})_H + (C_{l\beta})_V \\
&= 0.029\alpha\frac{1}{rad^2} - 0.087\frac{1}{rad} - 0.0385(0.83m\cdot cos(\alpha) - 4.3m\cdot sin(\alpha))\frac{1}{rad}
\end{aligned}
\tag{226}
$$

Special attention needed to be paid to the fact that values of α within the trigonometric function were in degree, while the remaining angles were in radians. With this fact, the rolling moment coefficient was found. The results are shown in Figure 6.31 and Table 6.8. In this way, it was proven that the box wing configuration was lateral stable since $C_{l\beta} < 0$.

Table 6.8: $C_{l\beta}$ Values for the Box Wing Configuration

α	-5°	-2°	0°	2°	5°	7°	10°	12°	15°
$C_{l\beta}[\frac{1}{rad}]$	-0.136	-0.126	-0.120	-0.112	-0.102	-0.095	-0.0085	-0.078	-0.067

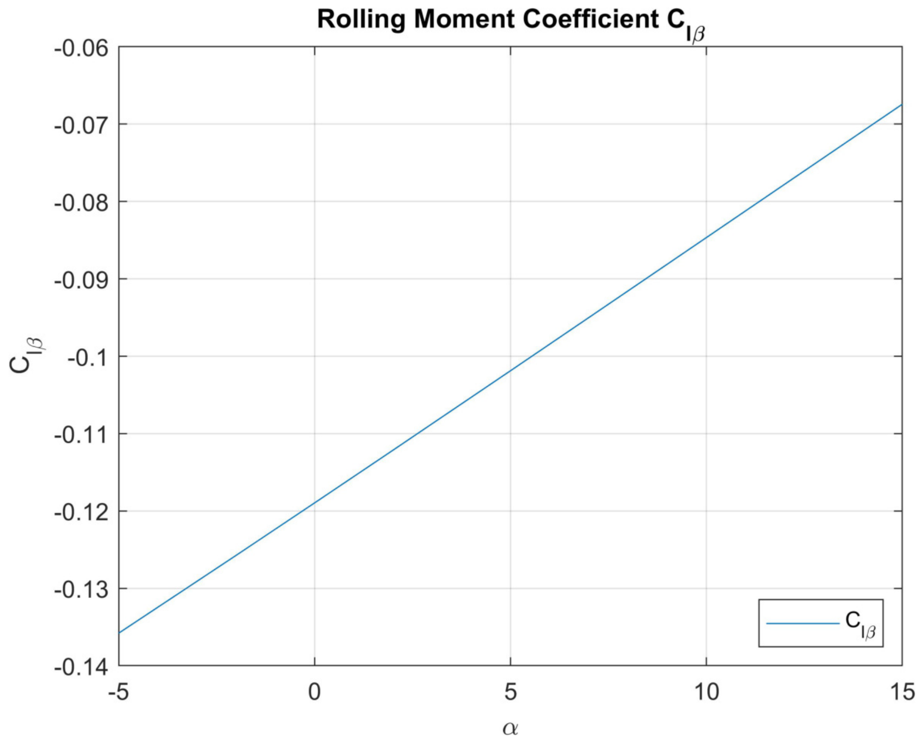

Figure 6.31: $C_{l\beta}$ Values for the Box Wing Configuration

Lateral Control

In order to calculate the aileron effectiveness of the Extra EA 400-500 with box wings, and as suggested by Datcom, the same approach as shown during the calculation of the elevators was chosen. Hence, Figure 6.8 and Figure 6.9, were used to extract the required values to find the respective change of wing AOA per aileron deflection unit τ_a. Since the box wing configured Extra EA 400-500 received a second set of ailerons on the horizontal stabiliser, two calculations needed to be conducted. In a first step, it was found that $\left(\frac{c_f}{\bar{c}}\right)_{H,a} = 0.45$. With this information, the following values were extracted from abovementioned figures: $(\beta\delta)_{C_l,H,a} = -0.78\frac{1}{rad}$ so that $\left(\frac{(\beta\delta)_{C_L}}{(\beta\delta)_{C_l}}\right)_{H,a} = 1.05$. Furthermore, $(c_{l\delta})_{theory,H,a} = 0.56\frac{1}{rad}$ and $\left(\frac{c_{l\delta}}{(c_{l\delta})_{theory}}\right)_{H,a} = 0.88$. With these numbers, it was calculated that $c_{l\delta,H,a} = 0.493\frac{1}{rad}$. Eventually, the factor $K_{b,H,a}$ was determined to be

$$K_{b,H,a} = K_b(\eta_o) - K_b(\eta_i) = K_b(0.88) - K_b(0.63) = 0.93 - 0.77 = 0.16 \tag{227}$$

This led to a horizontal tail value $\tau_{a,H}$ of

$$\tau_{a,H} = \frac{0.493\frac{1}{rad}}{7.14\frac{1}{rad}} \cdot 1.05 \cdot 0.16 = 0.0116 \tag{228}$$

For the horizontal tail, it was found that $c_{a,H}(y) = -0.0344y + 0.88m$ described the chord length with respect to the position on the wing. It was followed that

$$\begin{aligned} C_{l\delta a,H} &= -\frac{2a_H\tau_{a,H}}{A_H b}\int_{3.45m}^{4.86m}(-0.0344y^2 + 0.88y)dy \\ &= -\frac{6.0\frac{1}{rad}\cdot 0.0116}{8.8m^2\cdot 11.0m}\cdot 4.3m^3 = -0.0031\frac{1}{rad} \end{aligned} \tag{229}$$

In the same manner, the wing aileron effectiveness was to be calculated. In summary, the values were found to be: $\left(\frac{c_f}{\bar{c}}\right)_{W,a} = 0.29$, $(\beta_\delta)_{C_l,W,a} = -0.65\frac{1}{rad}$ and $\left(\frac{(\beta_\delta)_{C_L}}{(\beta_\delta)_{C_l}}\right)_{W,a} = 1.05$. Additionally, $(c_{l\delta})_{theory,W,a} = 0.48\frac{1}{rad}$ and $\left(\frac{c_{l\delta}}{(c_{l\delta})_{theory}}\right)_{W,a} = 0.82$. This led to $c_{l\delta,W,a} = 0.39\frac{1}{rad}$. In a last step, $K_{b,W,a}$ was found:

$$K_{b,W,a} = K_b(\eta_o) - K_b(\eta_i) = K_b(0.96) - K_b(0.76) = 0.98 - 0.88 = 0.10 \tag{230}$$

In total, this allowed the formulation of the change of wing AOA per aileron deflection unit:

$$\tau_{a,W} = \frac{0.39\frac{1}{rad}}{7.06\frac{1}{rad}}\cdot 1.05\cdot 0.10 = 0.0058 \tag{231}$$

For the wing, it was found that $c_{a,W}(y) = -0.0854y + 1.32m$ described the chord length, so that

$$\begin{aligned} C_{l\delta a,W} &= -\frac{2a_W\tau_{a,W}}{A_W b}\int_{4.2m}^{5.3m}(-0.0854y^2 + 1.32y)dy \\ &= -\frac{5.66\frac{1}{rad}\cdot 0.0058}{13.5m^2\cdot 11.0m}\cdot 4.8m^3 = -0.0011\frac{1}{rad} \end{aligned} \tag{232}$$

Summed up, the total aileron effectiveness value was expressed as

$$C_{l\delta a} = C_{l\delta a,H} + C_{l\delta a,W} = -0.0042\frac{1}{rad} \tag{233}$$

The second pair of ailerons provided to the pilot on the horizontal stabiliser offered two main advantages. Mainly, more aileron authority was available during turns, which was deemed necessary due to the large area of the horizontal stabiliser. In this way, turns could be coordinated more precise when compared to a box wing configuration without a second pair of ailerons. More importantly, however, was the location of the ailerons on the horizontal tail. Wings with a positive sweep, thus towards the nose of the aircraft, are known to provide intrinsic stall characteristics: the wing stalls at the wing root first. In this way, in case of a stall at the main wing, the horizontal tail, which was seen as a second pair of wings throughout this study, would still provide lift at the wing tips and in such a case may be a help to recover the aircraft from an upset.

6.3.4 Comparison to the Cantilever Wing Configuration

During evaluation of the results between the cantilever and box wing configuration, a significant difference was observed. As seen in Figure 6.32, the stability criteria for lateral stability, thus $C_{l\beta} < 0$, was given for both configuration. However, while the box wing configuration had a positive inclination, the cantilever wing had a negative inclination. This difference occurred due to the horizontal stabiliser, whose contribution to the overall rolling moment coefficient was negative. The results are shown in Table 6.9.

Table 6.9: Comparison of $C_{l\beta}$ for the Box and Cantilever Wing Configuration

α	$-5°$	$-2°$	$0°$	$2°$	$5°$	$7°$	$10°$	$12°$	$15°$
$C_{l\beta,CW}[\frac{1}{rad}]$	-0.070	-0.089	-0.101	-0.113	-0.131	-0.144	-0.162	-0.173	-0.192
$C_{l\beta,BW}[\frac{1}{rad}]$	-0.136	-0.126	-0.120	-0.112	-0.102	-0.095	-0.085	-0.078	-0.067
$\lvert\Delta C_{l\beta}\rvert[\frac{1}{rad}]$	0.066	0.037	0.019	0.001	0.029	0.049	0.077	0.095	0.125

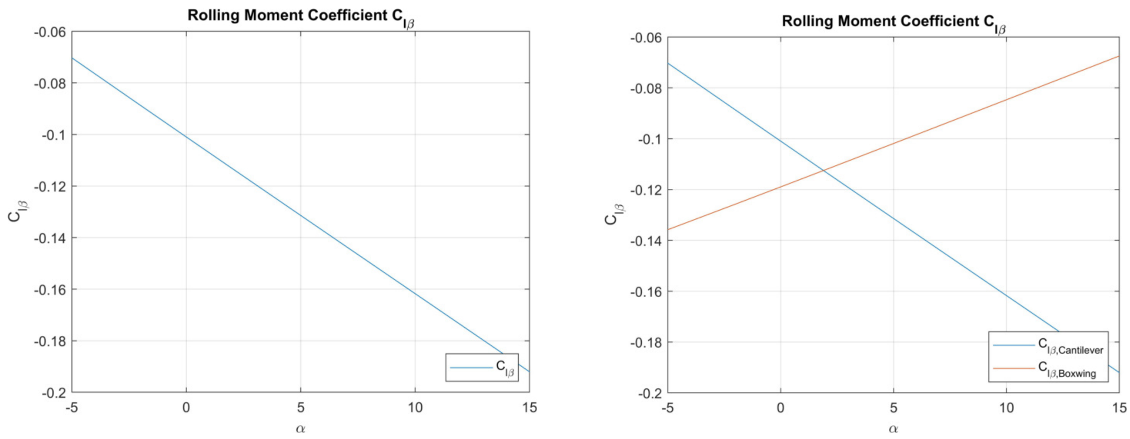

(a) $C_{l\beta}$ for the Cantilever Wing

(b) $C_{l\beta,CW}$ and $C_{l\beta,BW}$

Figure 6.32: Comparison of $C_{l\beta}$ for the Box and Cantilever Wing Configuration

Furthermore, the aileron effectiveness was analysed. Due to the fact that the box wing configured Extra EA 400-500 received a second set of ailerons, it could be observed that the total aileron effectiveness for the box wing configuration was higher than compared to the cantilever wing design. In order to see whether the second pair of ailerons was really required, a third parameter was calculated, which showed the aileron effectiveness for a box wing configuration without a second pair of ailerons. In this case, marked with an asterisk, it was assumed that the overall wing area would be equal to the sum of the area of the wing and horizontal stabiliser of the box wing minus the horizontal stabiliser area of the cantilever wing design. It was found that the aileron effectiveness would have dropped significantly, as can be seen in Table 6.10. Therefore, it could be concluded that a second pair of ailerons was indeed useful for a box wing configuration.

Table 6.10: Lateral Control Values for the Box Wing and Cantilever Configuration

Parameter	Cantilever	Boxwing
$\tau_{a,W}$	0.0058	0.0058
$\tau_{a,H}$	-/-	0.0116
$C_{l\delta a}$	$-0.0011\frac{1}{rad}$	$-0.0042\frac{1}{rad}$
$C^*_{l\delta a}$	$-0.00073\frac{1}{rad}$	-/-

CHAPTER 7

WING WEIGHT ESTIMATION

The cantilever wing is known for reducing the induced drag and hypothetically increasing the lift due to its larger horizontal tail. However, because of the addition of two vertical structures as much as the greater tail area, it became obvious that the weight of the aircraft in this study had to increase as well. This was mainly due to the fact that it was decided that the main wing was not to be changed significantly. If this had not been the case, the wing were to be considered as statically indeterminate, which could have reduced the wing weight [71]. Therefore, to find by which extend the aircraft weight changed, a wing weight estimation was conducted.

7.1 The Torenbeek-Raymer Approach

Torenbeek of the TU Delft [72], who was part of the development team of the Extra EA 400-500, developed an empirical approach for weight estimation of wing designs in early stages. Tested on a total of 46 aircraft wings of different sizes, it was found to produce an error of approximately 9.64% [73]. For the purpose of this study and a comparison of two wing designs, this approach was evaluated to be sufficient. As shown in (234), Torenbeck suggests that the wing group weight consists of a basic wing weight $W_{W,basic}$, which is the wing weight without additions such as high-lift devices or spoilers. These are added in the W_{hld} term for high-lift devices (hld) and W_{sp} term for the spoilers. Since the Extra EA 400-500 does not have spoilers, the formula was further simplified to:

$$W_W = W_{W,basic} + 1.2 \cdot (W_{hld} + W_{sp}) = W_{W,basic} + 1.2 \cdot W_{hld} \tag{234}$$

where

$$W_{W,basic} = k_{cor} k_{no} k_{\lambda} k_e k_{uc} k_{st} \left[k_b n_{ult} (W_{des} - 0.8 W_W) \right]^{0.55} b^{1.675} \left(\frac{t}{c} \right)_W^{-0.45} (cos(\Lambda_{\frac{c}{2}}))^{-1.325} \tag{235}$$

and

$$W_{hld} = W_{tef} \tag{236}$$

with all parameters introduced and explained in the following subchapter. Furthermore, the horizontal tail weight was to be calculated by a formula presented by Raymer [74]. This approach is especially designed for general aviation aircraft and takes not only the load factor, but also the dynamic pressure into account. Raymer writes that:

$$W_H = 0.016 \cdot (n_{ult} W_{dg})^{0.414} \cdot \overline{q}^{0.168} \cdot A_H^{0.896} \cdot \left(\frac{100 \cdot (t/c)_W}{cos(\Lambda_W)}\right)^{-0.12} \cdot \left(\frac{AR_W}{cos^2(\Lambda_H)}\right)^{0.043} \cdot \lambda_H^{-0.02} \tag{237}$$

However, Raymer uses British units and the result is in pounds. Thus, a conversion was required for the calculation, as will be shown in the next subchapter. The reader may be refered to Table 1 for conversion rates.

7.1.1 Wing Weight Discussion of the Box Wing Configuration

As shown above, the wing weight is estimated by dividing between the main wing and accessories such as high-lift devices.

Basic Wing Structure Weight

In a first step, the weight of the basic wing was calculated. Torenbeek formulates that

$$W_{W,basic} = k_{cor} k_{no} k_\lambda k_e k_{uc} k_{st} \left[k_b n_{ult}(W_{des} - 0.8W_W^*)\right]^{0.55} b^{1.675} \left(\frac{t}{c}\right)_W^{-0.45} (cos(\Lambda_{\frac{c}{2}}))^{-1.325} \tag{238}$$

The constant correction factor k_{cor} is defined by Torenbeek to be $k_{cor} = 4.58 \cdot 10^{-3}$. Furthermore, the non-optimum weight factor k_{no}, which represents weight penalties due to joints or non-tapered skins, was found by

$$k_{no} = 1 + \sqrt{\frac{1.905m \cdot \cos(\Lambda_{\frac{c}{2},W})}{b}} = 1 + \sqrt{\frac{1.905m \cdot \cos(4.4°)}{11.0m}} = 1.42 \tag{239}$$

The wing taper ratio correction factor was defined by

$$k_\lambda = (1 + \lambda_W)^{0.4} = (1 + 0.53)^{0.4} = 1.19 \tag{240}$$

Furthermore, the so-called bending moment relief factor based on the engine location was set to $k_e = 1$ for aircraft with non wing-mounted engines. The undercarriage suspension factor was $k_{uc} = 0.95$ for aircraft with landing gears not mounted to the wing. The interested reader may be referred to [73] for other values of k_e and k_{uc}. In a next step, Torenbeek defines that extra weight is required for stiffness against flutter for high-subsonic jet aircraft. However, since the Extra EA 400-500 flies at rather low-subsonic speeds, the stiffness correction factor was evaluated to be $k_{st} = 1$. Additionally, the braced wing factor was $k_b = 1$ since the Extra EA 400-500 wing is not braced. In another step, the ultimate load factor n_{ult} was to be found. As suggested by Torenbeek, the value is equal to 1.5 times the limit load factor. As written in the Type Certificate of the Extra EA 400-500, the maximum limit load factor with retracted flaps is $LL = +3.8g$, so that $n_{ult} = 5.7$. Eventually, the wing group weight in accordance with AN 9103-D, see [72, p. 279], was found to be equal to the Cessna C-310 due to the similar maximum take-off weight, so that $W_W^* = 206kg$. Torenbeek proposes that W_{des}, the design all-up weight of the aircraft, equals the zero fuel weight of the aircraft, thus 1945 kg. With the rest of the values already known, the wing weight was estimated to be

$$\begin{aligned} W_{W,basic} &= 4.58 \cdot 10^{-3} \cdot 1.42 \cdot 1.19 \cdot 1 \cdot 0.95 \cdot 1 \cdot \left[1 \cdot 5.7 \cdot (1954kg - 0.8 \cdot 206kg)\right]^{0.55} \\ &\cdot (11.0m)^{1.675} \cdot (0.2)^{-0.45} \cdot (cos(4.4°))^{-1.325} \\ &= 135.4kg \pm 13kg \end{aligned} \tag{241}$$

High Lift Devices

Torenbeek defines that the weight of high-lift devices is the sum of trailing-edge flaps (tef) and leading-edge high-lift devices. As the Extra EA 400-500 is not equipped with the latter, the formula was simplified to only include single-slotted flaps:

$$W_{hld} = W_{tef} \tag{242}$$

and

$$W_{tef} = A_{fl} k_{cor,fl} k_{fl} (A_{fl} b_{fl})^{3/16} \left[\left(\frac{v_{lf}}{100} \right)^2 \frac{\sin(\delta_{fl}) \cos(\Lambda_{fl})}{(t/c)_{fl}} \right]^{3/4} \tag{243}$$

The area of the slotted flaps was found to be $A_{fl} = 1.07m^2$, while the flap correction factor was $k_{cor,fl} = 2.706$, according to Torebeck. The flaps factor k_{fl} was set to 1.0 for single slotted flaps with a flaps span of $b_{fl} = 3.83m$ for one wing. The EA 400-500 has a maximum flap speed with Flaps 30° of $v_{lf} = 109kts = 56\frac{m}{s}$, which defines that $\delta_{fl} = 30°$. Furthermore $\Lambda_{fl} = 1.24°$ and $(t/c)_{fl} = 0.11$, each extracted from CATIA. It was therefore found that

$$\begin{aligned} W_{tef,1} &= 1.07m^2 \cdot 2.706 \cdot 1.0 \cdot (1.07m^2 \cdot 3.83m^2)^{3/16} \left[\left(\frac{56 \frac{m}{s}}{100} \right)^2 \frac{\sin(30°)\cos(1.24°)}{0.11} \right]^{3/4} \\ &= 4.9kg \end{aligned} \tag{244}$$

Therefore, the flaps for both wings added up to a total of $W_{tef} = 9.8kg$. Those values allowed to calculate the weight of the wing. It was decided that a conservative weight was to be chosen, hence the weight summed up to:

$$W_W = 135.4kg + 13kg + 1.2 \cdot 9.8kg = 160.2kg \tag{245}$$

This result was in accordance with findings of Thurston [75, p. 113], who analysed that the wing weight of an aircraft with a design gross weight of $W_{dg} = 1,360kg$ $(3,000lb)$ is in general close to 160kg.

Horizontal Tail

With all values already known to the reader, it was possible to calculate the weight of the horizontal tail by considering that the dynamic pressure at $V_{NO} = 97m/s$ and ISA conditions at sea level was $\overline{q} = 5,763 \frac{kg}{ms^2}$ $(120.4 \frac{lb}{ft^2})$. Hence,

$$\begin{aligned} W_H &= 0.016 \cdot \left(5.7 \cdot 3,000lb\right)^{0.414} \cdot \left(120.4 \frac{lb}{ft^2}\right)^{0.168} \cdot \left(94.7ft^2\right)^{0.896} \\ &\cdot \left(\frac{100 \cdot 0.2}{\cos(6.6°)}\right)^{-0.12} \cdot \left(\frac{8.96}{\cos^2(-19.84°)}\right)^{0.043} \cdot 0.78^{-0.02} \\ &= 92.44lb \end{aligned} \tag{246}$$

Converting the result to SI units, the weight of the horizontal stabiliser was found to be $W_H = 42kg$. In comparison, Thurston suggest that a T-tail, hence the vertical and horizontal stabiliser together, weights approximately 30 kg in total for a given design gross weight of $W_{dg} = 1,360kg$.

Vertical Connecting Structures

No method was found to evaluate the weight of the vertical connecting structures between the main wing and the horizontal stabiliser. However, since the dimensions of the structure were comparable to the high-lift devices of the Extra EA 400-500, it was assumed to assign the same weight to the vertical structures. Hence, the total weight of both structures was determined to equal

$$W_{VS} = 1.2 \cdot 9.8kg = 11.76kg \tag{247}$$

Total Wing Weight

In summary, the total wing weight consisted of the basic wing weight to which the high lift devices, horizontal stabiliser and vertical structures weight was added. Therefore:

$$W_{TWW,BW} = 160.2kg + 42kg + 11.76kg = 213.96kg \tag{248}$$

7.1.2 Wing Weight Discussion of the Cantilever Wing Configuration

To compare both aircraft designs, only the horizontal tail needed to be calculated again. With a smaller horizontal tail area, a backward sweep as much as a different taper ratio, the following weight for the horizontal tail was found:

$$\begin{aligned} W_{H,CW} &= 0.016 \cdot \left(5.7 \cdot 3,000lb\right)^{0.414} \cdot \left(120.4\frac{lb}{ft^2}\right)^{0.168} \cdot \left(30.1ft^2\right)^{0.896} \\ &\cdot \left(\frac{100 \cdot 0.2}{\cos(6.6°)}\right)^{-0.12} \cdot \left(\frac{9.3}{\cos^2(8.31°)}\right)^{0.043} \cdot 0.60^{-0.02} \\ &= 33.18lb \end{aligned} \tag{249}$$

With this calculation, it was found that the horizontal tail of the cantilever wing configured Extra EA 400-500 weighted approximately 15 kg, so that the overall total wing weight was about:

$$W_{TWW,CW} = 160.2kg + 15kg = 175.2kg \tag{250}$$

7.2 Results of the Wing Weight Estimation

In conclusion, the box wing configuration was estimated to be 38.76 kg heavier than the cantilever wing configuration. This result could be interpreted in various ways. In general, it could be said that the aircraft could travel less, due to the fact that the additional weight could be counteracted by reducing the usable fuel from 652 litres to 603.5 litres by utilising the fact that one kilogram of jet fuel equals 1.25 litres [76]. Together with the fact, that the Extra EA 400-500 has a best power fuel consumption of 128 l/h (92%/FL120) and a best economy fuel consumption of 61 l/h (40%/FL250), this would mean that the flight time would be reduced by about 7.5%. On the other hand, it could be said, as mentioned earlier, that the wing system may be seen as statically indeterminate, thus allowing the wings to be lighter in general. Especially the main wing weight could be reduced further and therefore allow carrying more fuel. To compensate for the additional weight of 38.76 kg however, the main wing weight would need to be reduced by 24%. As another solution, it might be viable to include fuel tanks within the horizontal stabiliser. This would typically increase the weight further due to the fuel system structures and especially the fuel tank. Nevertheless, the increase of fuel capacity might justify the effort.

CHAPTER 8 CONCLUSION

During the course of this study, a box wing configured Extra EA 400-500 was developed based on the Datcom methodology and subjected to a CFD analysis. Eventually, it was possible to compare the two aircraft and find the advantages and disadvantages of a box wing configuration when compared to a standard cantilever wing configured aircraft.

8.1 Comparative Overview of the Cantilever and Box Wing

As provided to the reader in an earlier chapter, it was seen that the Extra EA 400-500 with box wings had a slightly higher lift coefficient than the cantilever wing. This difference is once again shown in the comparison of Figure 8.1, where a marginally larger difference is seen at medium-to-high AOAs. This difference is however neglectable small when considering the lift coefficient. Overall, the mean difference between the cantilever wing and the box wing lift coefficient was found to be approximately 3.78%. This value is very much attributed to the second pair of wings on the horizontal stabiliser but most probably limited due to the fact that NACA 0012 was chosen as the aerofoil of said stabiliser. Although the aerofoil is common in horizontal stabilisers, it did not find many main wing applications when in unchanged configuration. It may therefore be of advantage to consider a different aerofoil more beneficial for aircraft wings for the horizontal tail. In this case, an aerofoil specifically used in forward-swept wings may be viewed upon. Since this design configuration has however only seem limited usage in general aviation aircraft, the author might suggest the aerofoil of the HFB 320 Hansa, which consisted of a modified NACA 65A at the wing root and NACA 63A at the wing tip [16]. Another example would be the Honda MH02, which was built with a Somers S203 aerofoil. In this way the lift coefficient might be improved further, however, the stability requirements would have to be revisited in such a situation. Apart from the aerofoil, the increased weight of the aircraft had to be taken into consideration. Due to the fact, that the wing system of the box wing configuration weighted 38.76 kg more than the cantilever wing aircraft, the effect of the lift coefficient improvement might be limited, so that further studies on the matter shall be required.

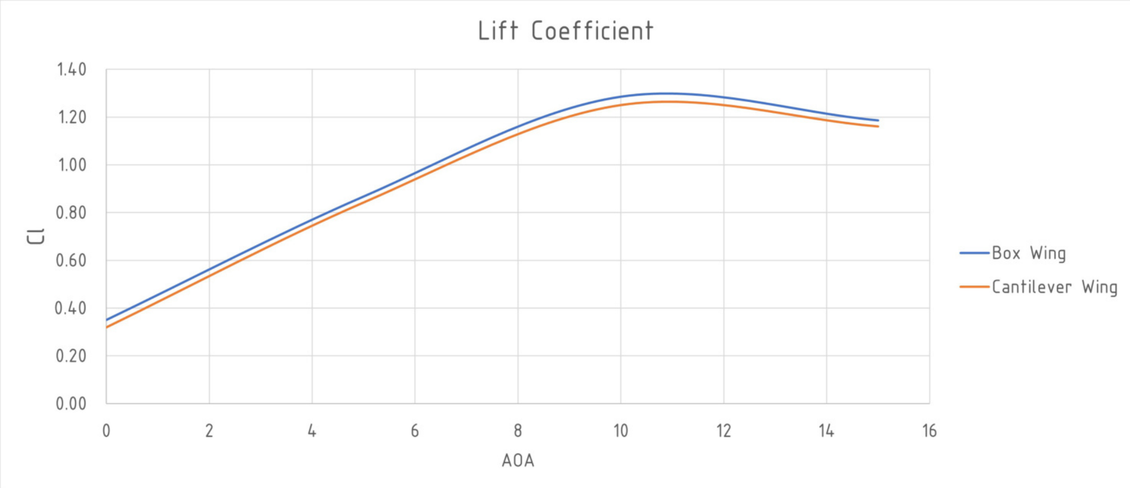

Figure 8.1: Comparison of C_L for the Box and Cantilever Wing Configuration

During the study, it was also seen that the box wing configuration had a lower drag coefficient throughout all AOAs. This decrease was mainly attributed to the characteristics of the box wing configuration as proofed by Prandtl and summarised to the reader in an earlier chapter. The total drag itself, a combination of parasitic drag and the lift-induced drag, as shown in Figure 8.2, could be reduced with a mean value of 14.83%. Since the parasitic drag must have increased due to the fact that two vertical connecting structures were added and the relatively short original horizontal stabiliser extended to wing length, the reduction must have occurred within the induced drag. This observation is in accordance with Prandtl's theory, in which the box wing configuration is supposed to reduce the induced drag when compared to an aircraft of same wing span.

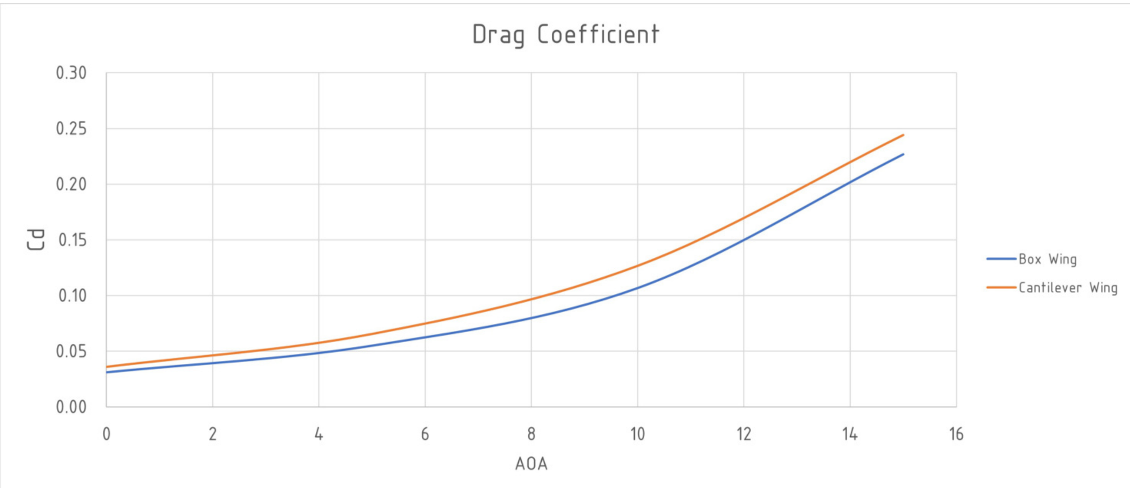

Figure 8.2: Comparison of C_D for the Box and Cantilever Wing Configuration

Eventually, the two values for C_L and C_D could be compared in a so-called Lift-to-Drag ratio (L/D). In general, it can be said that the L/D ratio is an indicator for the aircraft's aerodynamic efficiency [77]. This idea is mainly based on the fact that a high L/D ratio is due to high lift capabilities while maintaining a low total drag profile. Since an aircraft with low drag would require less thrust, the fuel consumption could be lowered. In return, this would increase the flight time or distance, depending on the chosen speed. Overall, an aircraft with higher L/D ratio can therefore fly greater payload over longer distances and for an extended time. The maximum L/D ratio of the box wing configuration with ISA flight conditions at sea level was found to be nearly 16, while the cantilever wing had a maximum L/D ratio of approximately 13. Figure 8.3, which visualises said ratio, shows that the L/D ratio stays nearly parallel for most AOA. However, after reaching the maximum value, the two aircrafts L/D ratios are seen to converge. With a value of around 16, the box wing configuration has a L/D ratio equal to aircraft such as the Dornier D328 or Cessna C177 Cardinal [78][79].

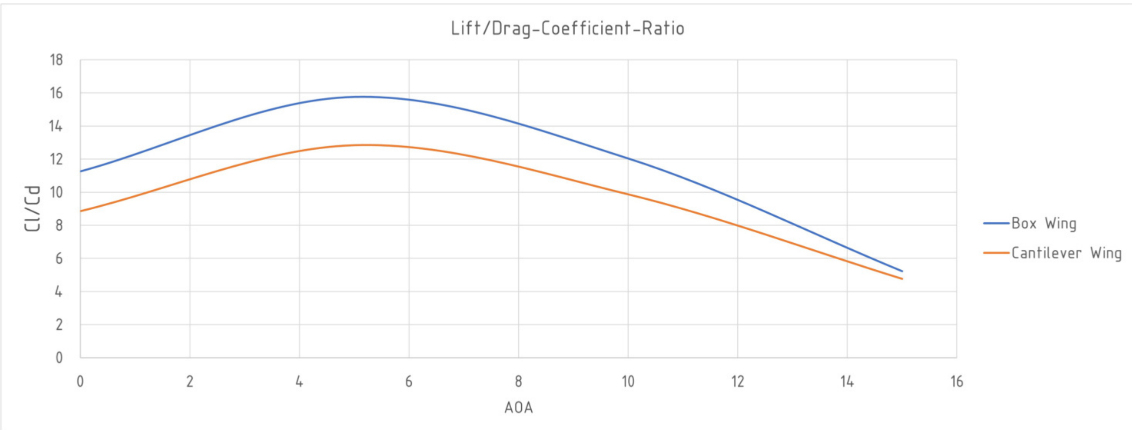

Figure 8.3: Comparison of C_L/C_D for the Box and Cantilever Wing Configuration

In summary, it was found that next to fulfilling all stability requirements available during the early conceptual stage, the box wing configured Extra EA 400-500 proved to have an increase of lift, decrease of drag and therefore an overall increase of the L/D ratio. This meant, from an aerodynamical point of view, that the box wing configuration allowed to create a more fuel efficient aircraft when compared to its original state.

8.2 Outlook for Applications in the Aviation Industry

The box wing configuration developed during the course of this study showed aerodynamical advantages when compared to an aircraft of same dimensions. Not only was it possible to increase lift and decrease drag, but with the design of a box wing configuration came other interesting advantages. Namely of great interest was the fact that a forward-swept horizontal tail was required. By equipping the tail with a second pair of ailerons, and applying aerodynamical advantages of a forward sweep, it was possible to create an aircraft which still kept aileron effectiveness high even after the main wing stalled. In addition, it might become a viable solution to insert fuel tanks within the extended horizontal stabiliser in order to counteract the weight increase of the wing system and thus limit the decrease or even reverse the effect on flight range and endurance. It was therefore proven, that the box wing configuration is a viable solution for the design of aircraft in the category of general aviation. This fact was enhanced by the idea that the whole wing as much as fuselage could be developed from materials such as carbon-fibre-reinforced-polymers, which allow to design complex structures with little to no weight penalties. Structures such as the vertical connecting structure or the extended horizontal tail could therefore be built more effectively and with less design restrictions.

With all aspects in mind, the conclusion can be made that the box wing configuration is an innovation worth exploring in more detail – An innovation which shall be part of a sustainable strategy in the aviation industry of creating a long-term value in the matters of the global ecology.

BIBLIOGRAPHY

[1] International Civil Aviation Organization, "Annex 5 - units of measurement to be used in the air and ground services," 2010. [Online]. Available: https://store.icao.int/en/annex-5-units-of-measurement-to-be-used-in-the-air-and-ground-services

[2] M. de Vries and D. Taalfax, "Nine pioneers' stories: 75 years aerospace engineering tu delft," Delft, December 2015. [Online]. Available: https://d1rkab7tlqy5f1.cloudfront.net/LR/Organisatie/Negen%20pioneersverhalen_ENG_web.pdf

[3] Aerospace Technology, "Extra ea-500 light utility aircraft - aerospace technology," 15.10.2021. [Online]. Available: https://www.aerospace-technology.com/projects/extra-ea-500-light-utility-aircraft/

[4] P. Jackson, Ed., *Jane's All The World's Aircraft*, ninety-fifth year of issue ed., ser. 2004-2005, 2004.

[5] K. Büttner, J. Dorner-Müller, G. Blau, F. Kühne, H. Peters, and V. Rybowiak, "Untersuchungsbericht 3x329-0/98, juni 1999," Braunschweig. [Online]. Available: https://www.bfu-web.de/DE/Publikationen/Untersuchungsberichte/1998/Bericht_3X329-0.98.pdf?__blob=publicationFile

[6] European Aviation Safety Agency, "Easa type-certificate data sheet easa.a.011 ea 400," 14 December 2015. [Online]. Available: https://www.easa.europa.eu/sites/default/files/dfu/TCDS_SST-EA500_A.011_Issue-06_MM1.pdf

[7] "Successful change from type rating to class rating for extra ea400 and ea500 - sst flugtechnik," Memmingen, 15.10.2021. [Online]. Available: https://www.sst-flugtechnik.com/news/successful-change-from-type-rating-to-class-rating-for-extra-ea400-and-ea500.html

[8] SST Flugtechnik, "Continuing airworthiness - sst flugtechnik," 15.10.2021. [Online]. Available: http://www.sst-flugtechnik.com/continuing-airworthiness.html

[9] P. Berg, “Pilot report: Extra ea 500: Extra-klasse,” *Fliegermagazin*, vol. 2008, no. February, pp. 6–12. [Online]. Available: https://www.extraaircraft.com/allegati/pressrelease/5/06-12_Extra_500_Musterseite.pdf

[10] Extra Flugzeugproduktions- und Vertriebs GmbH, “Maintenance manual extra 500: Doc.-no. ea-0b702,” Hünxe. [Online]. Available: https://www.extraaircraft.com/docs/tech-manuals/MM500/0B702_Maintenance%20Manual_20120330.pdf

[11] “Rolls-royce signs long-term contract with jiangsu a-star of china | aero-news network,” 16.10.2021. [Online]. Available: http://www.aero-news.net/index.cfm?do=main.textpost&id=b79cf42f-843d-4354-a65a-c60b97fa1a4e

[12] B. A. Elliott, *Blériot: Herald of an age.* Stroud: Tempus, 2000.

[13] L. E. Opdycke, *French Aeroplanes Before the Great War*, 1st ed. Schiffer Publishing, 2004.

[14] “Nova | a daring flight | too much imagination | pbs,” December 2004. [Online]. Available: https://www.pbs.org/wgbh/nova/bleriot/imag-nf.html

[15] R. Guttman, “Custer’s channel wing,” *HistoryNet*, 30.3.2018. [Online]. Available: https://www.historynet.com/custers-channel-wing.htm

[16] D. Lednicer, “The incomplete guide to airfoil usage,” 2010. [Online]. Available: https://m-selig.ae.illinois.edu/ads/aircraft.html

[17] L. Bridgman, Ed., *Jane’s All the World’s Aircraft 1956-57.* Mcgraw-Hill Book Company, 1957.

[18] “Aerospaceweb.org | ask us - channel wing,” 18.10.2021. [Online]. Available: http://www.aerospaceweb.org/question/aerodynamics/q0022b.shtml

[19] S. Vanderbauwede, “Custer ccw-5 channel wing 1/4 scale model,” 2017. [Online]. Available: https://conference.ep.liu.se/index.php/TMAL02/article/download/673/590/

[20] “Narushevich ring wing ow-1,” 18.10.2021. [Online]. Available: http://airwar.ru/enc/xplane/kolceplan.html

[21] “Project idintos,” 18.10.2021. [Online]. Available: http://www.idintos.eu/eng/?page_id=4

[22] A. Frediani, V. Cipolla, and F. Oliviero, "Idintos: the first prototype of an amphibious prandtlplane-shaped aircraft," *Aerotecnica Missili & Spazio*, vol. 94, no. 3, pp. 195–209, 2015.

[23] European Commission, "Reducing emissions from aviation," 18.10.2021. [Online]. Available: https://ec.europa.eu/clima/eu-action/transport-emissions/reducing-emissions-aviation_en

[24] International Civil Aviation Organization, "Trends in emissions that affect climate change," 18.10.2021. [Online]. Available: https://www.icao.int/environmental-protection/Pages/ClimateChange_Trends.aspx

[25] The European Commission, "The european green deal: Com(20199) 640 final," 11 December 2019. [Online]. Available: https://eur-lex.europa.eu/resource.html?uri=cellar:b828d165-1c22-11ea-8c1f-01aa75ed71a1.0002.02/DOC_1&format=PDF

[26] W. Schneider, "The importance of aerodynamics in the development of commercially successful transport aircraft," in *Aerodynamic Drag Reduction Technologies*, ser. Springer eBook Collection, P. Thiede, Ed. Berlin and Heidelberg: Springer, 2001, pp. 9–16.

[27] S. Jacklin, J. Schumann, P. Gupta, M. Lowry, J. Bosworth, E. Zavala, K. Hayhurst, C. Belcastro, and C. Belcastro, "Verification, validation, and certification challenges for adaptive flight-critical control system software," in *AIAA Guidance, Navigation, and Control Conference and Exhibit*. Reston, Virigina: American Institute of Aeronautics and Astronautics, 08162004.

[28] L.M.M. Boermans, "Information about the nlf-mod22 of the extra ea 400-500: E-mail," 30.10.2021.

[29] D. M. Somers, "Design and experimental results for a natural-laminar-flow airfoil for general aviation applications: Technical publication (tp): Nasa-tp-1861 / l-14117," 1 June 1981. [Online]. Available: https://ntrs.nasa.gov/api/citations/19810015487/downloads/19810015487.pdf

[30] Ir. L.M.M. Boermans, "Lecture notes college lr4-16: Vliegtuigaero ii – airfoil for general aviation aircraft part two: The real case: [internal lecture notes]," 1998.

[31] L. Boermans and P. Rutten, "Two-dimensional aerodynamic characteristics of airfoil nlf-mod22 with fowler flap: Internal report lsw 95-3."

[32] "The naca airfoil series: Aa220 course material," 2004. [Online]. Available: https://web.stanford.edu/~cantwell/AA200_Course_Material/The%20NACA%20airfoil%20series.pdf

[33] I. H. Abbott, *Theory of wing sections: Including a summary of airfoil data.* Mineola: Dover Publications, 1999.

[34] N. Gregory and C. O'Reilly, "Low-speed aerodynamic characteristics of naca 0012 aerofoil section, including the effects of upper-surface roughness simulating hoar frost," no. N7111016, 1970.

[35] C. Ladson, "Effects of independent variation of mach and reynolds numbers on the low-speed aerodynamic characteristics of the naca 0012 airfoil section," 1988. [Online]. Available: https://ntrs.nasa.gov/archive/nasa/casi.ntrs.nasa.gov/19880019495.pdf

[36] NASA - Langley Research Center, "2d naca 0012 airfoil validation: Turbulence modeling resource," 2014. [Online]. Available: https://turbmodels.larc.nasa.gov/naca0012_val.html

[37] A. Grima, C. Theodore, O. Garrow, B. Lawrence, and L. Persson, "Aerodynamic analysis of the elytron 2s experimental tiltwing aircraft," in *SAE Technical Paper Series*, ser. SAE Technical Paper Series. SAE International400 Commonwealth Drive, Warrendale, PA, United States, 2016.

[38] H. Gagnon and D. W. Zingg, "Aerodynamic optimization trade study of a box-wing aircraft configuration," *Journal of Aircraft*, vol. 53, no. 4, pp. 971–981, 2016.

[39] National Research Council, *Uninhabited Air Vehicles: Enabling Science for Military Systems: Publication NMAB-495.* Washington: National Academies Press, 2000. [Online]. Available: https://ebookcentral.proquest.com/lib/kxp/detail.action?docID=3375435

[40] Lockheed Martin Aeronautics, "Advanced mobility aircraft: Current status: Archived website: http://www.lmasc.com/ama/status.htm," 2000. [Online]. Available: http://web.archive.org/web/20000929172400/http://www.lmasc.com/ama/status.htm

[41] P. Jansen and R. Perez, "Effect of size and mission requirements on the design optimization of non-planar aircraft configurations," in *13th AIAA/ISSMO Multidisciplinary Analysis Optimization Conference*. Reston, Virigina: American Institute of Aeronautics and Astronautics, 09132010.

[42] J. Wolkovitch, "Joined wing aircraft," Patent US-4 365 773-A, 1982. [Online]. Available: https://patentimages.storage.googleapis.com/88/0a/0b/6fb469f3865df5/US4365773.pdf

[43] L. L. Miranda, "Boxplane wing and aircraft," Patent US-3 834 654-A, 1974. [Online]. Available: https://patentimages.storage.googleapis.com/ea/ab/54/1178cb5ab184af/US3834654.pdf

[44] L. Prandtl, "Der induzierte widerstand von mehrdeckern," in *Ludwig Prandtl Gesammelte Abhandlungen*, F. Riegels, Ed. Springer-Verlag Berlin Heidelberg 1961, 1961.

[45] ——, "Induced drag of multiplanes: Technical note no. 182," 1924. [Online]. Available: https://ntrs.nasa.gov/api/citations/19930080964/downloads/19930080964.pdf

[46] M. Munk, "The minimum induced drag of aerofoils," 1979. [Online]. Available: https://digital.library.unt.edu/ark:/67531/metadc53402/m2/1/high_res_d/19800006779.pdf

[47] E. Larrabee, "Trim drag in the light of munk's stagger theorem," *Proceedings of the NASA, Industry, University, General Aviation Drag Reduction Workshop*, pp. 319–329, 1975. [Online]. Available: https://core.ac.uk/download/pdf/42886364.pdf

[48] H. H. Hurt and H. H. Hurt, *Aerodynamics for naval aviators: NAVWEPS 00-80T-80 ; [wing & airfoil forces, thrust & power, principles of propulsion, airplane performance, transonic & supersonic flight, stability & control, operating limitations & specific problems*, repr. [of the ed. 1965] ed. New York, NY: Skyhorse Publishing, 2012.

[49] K. Pohlhausen, "Zur näherungsweisen integration der differentialgleichung der iaminaren grenzschicht," *ZAMM - Journal of Applied Mathematics and Mechanics / Zeitschrift für Angewandte Mathematik und Mechanik*, vol. 1, no. 4, pp. 252–290, 1921.

[50] S. Srinivasan, Deepa, and G. K. Sanjana, "Investigation of aerodynamic characteristics of a typical t-tail box wing aircraft," in *ADVANCED TRENDS IN MECHANICAL*

AND AEROSPACE ENGINEERING: ATMA-2019, ser. AIP Conference Proceedings. AIP Publishing, 2021, p. 020006.

[51] D. Scholz and D. Schiktanz, "The conflict of aerodynamic efficiency and static longitudinal stability of box wing aircraft," *3rd CEAS Air & Space Conference (CEAS) ; Council of European Aerospace Societies (CEAS) ; Venice, Italy*, pp. 910–921, 2011. [Online]. Available: https://reposit.haw-hamburg.de/handle/20.500.12738/2301

[52] D. Scholz, "Induced drag estimation of box wings for conceptual aircraft design."

[53] R. Finck, *USAF (United States Air Force) Stability and Control DATCOM (Data Compendium): Final rept. Sep 1975-Sep 1977: Accession Number: ADB072483*, 01 April 1978. [Online]. Available: https://apps.dtic.mil/sti/pdfs/ADB072483.pdf

[54] M. Kuntz, "Erste schritte mit dem digital datcom: Theoretische arbeit - flugzeugbau -," Hamburg, 1999. [Online]. Available: https://www.fzt.haw-hamburg.de/pers/Scholz/arbeiten/TextKuntz.pdf

[55] J. C. Puig, P. J. Gamez, and G. Raush, "Openfoam guide for beginners," Barcelona, June 2014. [Online]. Available: https://the-foam-house5.webnode.es/products-/

[56] Extra Flugzeugproduktions- und Vertriebs GmbH, "Pilot's operating handbook (poh) of the extra ea 400-500 (extra 500): Information manual," Hünxe, 22 May 2013. [Online]. Available: https://www.extraaircraft.com/docs/service/POH_500_20130522_CUS.pdf

[57] C. Inac, "Bachelor thesis kick-off," Online Meeting, 04.08.2020.

[58] A. Lintermann, "Computational meshing for cfd simulations," in *Clinical and Biomedical Engineering in the Human Nose*, ser. Biological and Medical Physics, Biomedical Engineering Ser, K. Inthavong, Ed. Singapore: Springer Singapore Pte. Limited, 2021, pp. 85–115.

[59] gestione, "Cfd computational domain," *Idealsimulations*, 07.09.2020. [Online]. Available: https://www.idealsimulations.com/resources/cfd-computational-domain/

[60] "Blockmesh - openfoamwiki," 23.08.2018. [Online]. Available: https://openfoamwiki.net/index.php/BlockMesh

[61] "Snappyhexmesh - openfoamwiki," 08.01.2020. [Online]. Available: https://openfoamwiki.net/index.php/SnappyHexMesh

[62] "Longitudinal stability," 11.12.2019. [Online]. Available: http://avstop.com/ac/flighttrainghandbook/longitudinalstability.html

[63] W. Fichter, "Statische stabilität der längsbewegung: Kurzmanuskript," Stuttgart, 2015. [Online]. Available: https://www.ifr.uni-stuttgart.de/dokumente/SkriptStatischeStabilitaet.pdf

[64] B. N. Pamadi, *Performance, stability, dynamics, and control of airplanes*, 2nd ed., ser. AIAA education series. Reston, Va.: American Institute of Aeronautics and Astronautics, 2004.

[65] M. Müller, "Der schwerpunkt und seine folgen: Theorie und praxis," in *Aufwind*, vol. 2/2017, pp. 32–34. [Online]. Available: http://www.s4a.ch/eflight/docs/aufwind_17_2.pdf

[66] S. Eftekhari and A. S. M. Al-Obaidi, "Investigation of a naca0012 finite wing aerodynamics at low reynold's numbers and 0º to 90º angle of attack," *Journal of Aerospace Technology and Management*, 2019.

[67] D. Scholz, "Empennage sizing with the tail volume complemented with a method for dorsal fin layout," 2021. [Online]. Available: https://www.fzt.haw-hamburg.de/pers/Scholz/Aero/AERO_PUB_INCAS_TailVolume_Vol13No3_2021.pdf

[68] J. R. Wright and J. E. Cooper, *Introduction to aircraft aeroelasticity and loads*, repr ed., ser. Aerospace series. Chichester: Wiley, 2008.

[69] T. Megson, *Aircraft Structures for Engineering Students*. Elsevier, 2022.

[70] S. Edward, *Stability and Control of Airplanes and Helicopters*. Elsevier, 1964.

[71] S. A. Andrews and R. E. Perez, "Comparison of box-wing and conventional aircraft mission performance using multidisciplinary analysis and optimization," *Aerospace Science and Technology*, vol. 79, pp. 336–351, 2018.

[72] E. Torenbeek, *Synthesis of subsonic airplane design: An introduction to the preliminary design of subsonic general aviation and transport aircraft, with emphasis on*

layout, aerodynamic design, propulsion and performance, 1st ed. Dordrecht: Kluwer Academic Publ, 1982.

[73] E. TORENBEEK, "Quick estimation of wing structural weight for preliminary aircraft design," *Aircraft Engineering and Aerospace Technology*, vol. 44, no. 2, pp. 18–19, 1972.

[74] D. P. Raymer, *Aircraft design: A conceptual approach*, 5th ed., ser. AIAA education series. Reston, Va.: AIAA American Inst. of Aeronautics and Astronautics, 2012.

[75] D. B. Thurston, *Design for flying*, New York, 1978.

[76] Aviation: Benefits Beyond Borders, "Sustainable fuel conversions," 28.02.2022. [Online]. Available: https://aviationbenefits.org/environmental-efficiency/climate-action/sustainable-aviation-fuel/conversions-for-saf/

[77] N. Hall, "L/d ratio," 11.03.2022. [Online]. Available: https://www.grc.nasa.gov/www/k-12/airplane/ldrat.html

[78] R. Babikian, *The historical fuel efficiency characteristics of regional aircraft from technological, operational, and cost perspectives*, 2001. [Online]. Available: https://dspace.mit.edu/handle/1721.1/38440

[79] T. Ikeda and B. Cees, "Aerodynamic performance of a blended- wing-body configuration aircraft," *25TH INTERNATIONAL CONGRESS OF THE AERONAUTICAL SCIENCES*, 2006. [Online]. Available: http://www.icas.org/ICAS_ARCHIVE/ICAS2006/PAPERS/304.PDF

APPENDIX A

OVERVIEW OF ALL VALUES

A.1 Geometric and Aerodynamic Data

Table A.1: Geometric and Aerodynamic Data of the Cantilever and Box Wing

Value	Cantilever Wing Configuration	Box Wing Configuration
A_W	$14.3m^2$	$13.5m^2$
A_H	$2.8m^2$	$8.8m^2$
A_V	$2.8m^2$	$2.8m^2$
x_{CG}	$3.57m$ aft RD	$3.95m$ aft RD
x_{AC}	$3.53m$ aft RD	$3.53m$ aft RD
x_{NP}	$3.80m$ aft RD	$4.16m$ aft RD
$x_{NP} - x_{CG}$	$0.23m$	$0.21m$
$\Delta x_{AC \to NP}$	$0.26m$	$0.63m$
$\Delta x_{AC,W \to AC,H}$	$5.6m$	$4.52m$
b	$11.60m$	$11m$
b_H	$3.8m$	$11m$
l_H	$5.6m$	$4.5m^2$
Φ_T	0.85	0.85
Fi	6.7	6.7
$(k_2 - k_1)$	0.88	0.88
$A_{b,max}$	$1.94m^2$	$1.94m^2$
K_N	0.25	0.25
$b_{f,max}$	$1.42m$	$1.42m$
$K_{B(W)}$	1.11	1.11
$K_{W(B)}$	0.18	0.18
χ	0.96	0.96
$\Phi'_{TE,W}$	$15.85°$	$15.85°$
$\tan\left(\frac{\Phi'_{TE,W}}{2}\right)$	0.14	0.14
Re	$8.76 \cdot 10^8$	$8.76 \cdot 10^8$

Continuation of Table A.1		
Value	Cantilever Wing Configuration	Box Wing Configuration
$(t/c)_W$	0.2	0.2
$\overline{c}_W$	$1.32m$	$1.32m$
$\left(\frac{a_0}{a_{0,theory}}\right)_W$	0.89	0.89
$(a_0)_{theory,W}$	$7.25\frac{1}{rad}$	$7.25\frac{1}{rad}$
$\Lambda_{\frac{c}{2},W}$	$4.4°$	$4.4°$
AR_W	9.3	8.96
$a_{0,W}$	$7.06\frac{1}{rad}$	$7.06\frac{1}{rad}$
k_W	$1.12\frac{1}{rad}$	$1.12\frac{1}{rad}$
a_W	$5.56\frac{1}{rad}$	$5.56\frac{1}{rad}$
$c_{root,W}$	$1.61m$	$1.61m$
$c_{tip,W}$	0.85	0.85
λ_W	0.53	0.53
h_H	$0.8m$	$0.8m$
K_{AR}	0.088	0.088
K_λ	1.20	1.20
K_H	0.92	0.99
$\frac{d\epsilon}{d\alpha}$	$0.28\frac{1}{rad}$	$0.29\frac{1}{rad}$
ϵ	0.28α	0.29α
$\Lambda_{0.35c,W}$	$5.7°$	$5.7°$
$c_{f,W}$	0.002	0.002
$R_{LS,W}$	1.1	1.1
$\Lambda_{(\frac{t}{c})_{max}}$	$=\Lambda_{0.35c,W}$	$=\Lambda_{0.35c,W}$
$c_{D0,W}$	$3\cdot10^{-3}$	$3\cdot10^{-3}$
η_T	0.96	0.96
l_{H1}	$4.57m$	$3.53m$
$\Phi'_{TE,H}$	$4.12°$	$4.12°$
$\tan\left(\frac{\Phi'_{TE,H}}{2}\right)$	0.036	0.036
$\left(\frac{a_0}{a_{0,theory}}\right)_H$	0.95	0.95
$(t/c)_H$	0.12	0.12
$(a_0)_{theory,H}$	$6.87\frac{1}{rad}$	$6.87\frac{1}{rad}$
AR_H	5.2	13.75

Continuation of Table A.1		
Value	Cantilever Wing Configuration	Box Wing Configuration
$\Lambda_{\frac{c}{2},H}$	$5.56°$	$-20°$
$a_{0,H}$	$7.14\frac{1}{rad}$	$7.14\frac{1}{rad}$
k_H	$1.14\frac{1}{rad}$	$\frac{1}{rad}$
a_H	$4.78\frac{1}{rad}$	$6.0\frac{1}{rad}$
i_W	$1.9°$	$1.9°$
i_T	$0°$	$0°$
$(\frac{c_f}{c})_H$	0.41	0.54
$(\alpha_\delta)_{c_l,H}$	-0.78	-0.83
$(\frac{\alpha_\delta)_{c_L}}{\alpha_\delta)_{c_l}})_H$	1.08	1.02
λ_H	0.6	0.78
$\eta_{o,H}$	1	0.78
$\eta_{i,H}$	0.07	0.093
$K_b(\eta_{o,H})$	1	0.55
$K_b(\eta_{i,H})$	0.12	0.15
$K_{b,H}$	0.88	0.4
$(c_{l\delta})_{theory,H}$	$0.53\frac{1}{rad}$	$0.59\frac{1}{rad}$
$\left(\frac{c_{l\delta}}{(c_{l\delta})_{theory}}\right)_H$	0.95	0.95
$c_{l\delta,H}$	$0.504\frac{1}{rad}$	$0.551\frac{1}{rad}$
τ_e	0.067	0.0315
$c_{m\delta e}$	$-0.271\frac{1}{rad}$	$-0.40\frac{1}{rad}$
$\frac{d\delta_e}{dc_l}$	-0.85	-0.524
Γ_W	$-0.36°$	$-0.36°$
$(c_{n\beta})_{\Gamma,W}$	$2.67 \cdot 10^{-3}\frac{1}{rad^2}$	$2.67 \cdot 10^{-3}\frac{1}{rad^2}$
$\overline{x}_{a,W}$	$0.04m$	$0.42m$
$\Lambda_{\frac{c}{4},W}$	$6.6°$	$6.6°$
$\Lambda_{\frac{c}{4},H}$	$8.31°$	$-19.84°$
$(c_{n\beta})_{\Lambda,W}$	$0.423\alpha^2\frac{1}{rad^3}$	$0.423\alpha^2\frac{1}{rad^3}$
Γ_H	$-2°$	$-0.58°$
$(c_{n\beta})_{\Gamma,H}$	$1.25 \cdot 10^{-2}\alpha\frac{1}{rad^2}$	$4.5 \cdot 10^{-3}\alpha\frac{1}{rad^2}$
$\overline{x}_{a,H}$	$5.52m$	$4.10m$

Continuation of Table A.1		
Value	Cantilever Wing Configuration	Box Wing Configuration
$(c_{n\beta})_{\Lambda,H}$	$0.482\alpha^2\frac{1}{rad^3}$	$-0.314\alpha^2\frac{1}{rad^3}$
$A_{B,S}$	$9.13m^2$	$9.13m^2$
l_f	$8.85m$	$8.85m$
h	$1.66m$	$1.66m$
h_1	$1.40m$	$1.40m$
h_2	$0.787m$	$0.787m$
$\overline{x}_m$	$3.63m$	$3.63m$
$b_{f,max}$	$1.42m$	$1.42m$
K_{RL}	1.83	1.83
K_N	0.0016	0.0016
z_W	$-0.66m$	$-0.66m$
A_V	$2.80m^2$	$2.80m^2$
$(1+\frac{\partial\sigma}{\partial\beta})\eta_V$	0.964	0.964
b_V	$2.03m$	$2.03m$
r_1	$0.183m$	$0.183m$
k	1	1
λ_V	0.34	0.34
$c_{root,V}$	$2.0m$	$2.0m$
$c_{tip,V}$	$0.68m$	$0.68m$
K_H	0.9	1.2
$\frac{AR_{V(B)}}{AR_V}$	0.5	1.05
z_H	$-1.47m$	$-1.47m$
c_V	$0.925m$	$0.88m$
$\overline{x}_V$	$0.36m$	$0.72m$
$\frac{AR_{V(HB)}}{AR_{V(B)}}$	0.95	1.04
AR_V	1.47	1.47
$AR_{V,eff}$	1.62	1.62
$\Phi'_{TE,V}$	19.52°	19.52°
$(t/c)_V$	0.146	0.146
$(\Lambda_{\frac{c}{2}})_V$	38.12°	38.12°
$(\frac{a_0}{a_{0,theory}})_V$	0.85	0.85

Continuation of Table A.1		
Value	Cantilever Wing Configuration	Box Wing Configuration
$tan(0.5 \cdot \Phi'_{TE,V})$	0172	0.172
$a_{0,theory,V}$	$6.95\frac{1}{rad}$	$6.95\frac{1}{rad}$
$a_{0,V}$	$6.46\frac{1}{rad}$	$6.46\frac{1}{rad}$
k_V	$1.028\frac{1}{rad}$	$1.028\frac{1}{rad}$
a_V	$2.12\frac{1}{rad}$	$2.12\frac{1}{rad}$
l_V	$4.70m$	$4.30m$
$\eta_{o,V}$	1.36	1.36
$\eta_{i,V}$	0.087	0.087
$K_{b,V}(\eta_o)$	1	1
$K_{b,V}(\eta_i)$	0.12	0.12
$K_{b,V}$	0.88	0.88
$(t/c)_V$	0.136	0.136
$(c_f/c)_V$	0.315	0.315
$(\beta_\delta)_{C_l,V}$	-0.68	-0.68
$(\frac{(\beta_\delta)_{C_L}}{(\beta_\delta)_{C_l}})_V$	1.08	1.08
$(\frac{C_{l\delta}}{C_{l\delta,th}})_V$	0.77	0.77
$C_{l\delta,th,V}$	0.46	0.46
$C_{l\delta,V}$	0.354	0.354
τ_r	$5.2 \cdot 10^{-2}$	$5.2 \cdot 10^{-2}$
d_W	$1.59m$	$1.59m$
$\frac{\Delta C_{l\beta}}{\Gamma_W}$	$-3.13 \cdot 10^{-5}\frac{1}{rad}$	$-3.13 \cdot 10^{-5}\frac{1}{rad}$
$(\Delta C_{l\beta})_{zw}$	$-1.09 \cdot 10^{-3}\frac{1}{deg}$	$-1.09 \cdot 10^{-3}\frac{1}{deg}$
$(\frac{C_{l\beta}}{C_l})_{\Lambda_{c/2}}$	$-0.0005\frac{1}{deg}$	$-0.0005\frac{1}{deg}$
$(\frac{C_{l\beta}}{\Gamma})_W$	$-0.0001\frac{1}{deg}$	$-0.0001\frac{1}{deg}$
$l'_{f,W}$	$3.78m$	$3.78m$
$(\frac{C_{l\beta}}{C_l})_{A,W}$	$-0.001\frac{1}{deg}$	$-0.001\frac{1}{deg}$
$K_{f,W}$	0.97	0.97
$K_{M\Lambda,W}$	1.08	1.08
$C_{l,H}$	$7.07\alpha\frac{1}{rad}$	$6.72\alpha\frac{1}{rad}$
$\frac{\Delta C_{l\beta}}{\Gamma_H}$	$-1.22 \cdot 10^{-6}\frac{1}{deg^2}$	$-1.99 \cdot 10^{-6}\frac{1}{deg^2}$
$(\Delta C_{l\beta})_{ZH}$	$-4.17 \cdot 10^{-4}\frac{1}{deg}$	$-6.80 \cdot 10^{-4}\frac{1}{deg}$

Continuation of Table A.1		
Value	Cantilever Wing Configuration	Box Wing Configuration
$l'_{f,H}$	$9.06m$	$6.88m$
$(\frac{C_{l\beta}}{C_l})_{\Lambda_{c/2},H}$	$-0.0005\frac{1}{deg}$	$0.002\frac{1}{deg}$
$(\frac{C_{l\beta}}{\Gamma})_H$	$-0.0001\frac{1}{deg}$	$-0.0001\frac{1}{deg}$
$(\frac{C_{l\beta}}{C_l})_{A,H}$	$-0.00018\frac{1}{deg^2}$	$-0.001\frac{1}{deg^2}$
$K_{f,H}$	0.99	0.8
$K_{M\Lambda,H}$	1.04	1.08
$K_{M\Gamma,H}$	1.01	1.02
$(c_f/c)_{H,a}$	–	0.45
$(\beta\delta)_{C_l,H,a}$	–	$0.78\frac{1}{rad}$
$(\frac{(\beta\delta)_{C_L}}{(\beta\delta)_{C_l}})_{H,a}$	–	1.05
$(\frac{C_{l\delta}}{C_{l\delta,th}})_{H,a}$	–	0.88
$C_{l\delta,th,H,a}$	–	$0.56\frac{1}{rad}$
$C_{l\delta,H,a}$	–	$0.493\frac{1}{rad}$
$\eta_{o,H,a}$	–	0.88
$\eta_{i,H,a}$	–	0.627
$K(\eta_o)_{H,a}$	–	0.93
$K(\eta_i)_{H,a}$	–	0.77
$K_{b,H,a}$	–	0.16
$\tau_{a,H}$	–	0.0116
$(c_f/c)_{W,a}$	0.29	0.29
$(\beta\delta)_{C_l,H,a}$	$0.65\frac{1}{rad}$	$0.65\frac{1}{rad}$
$(\frac{(\beta\delta)_{C_L}}{(\beta\delta)_{C_l}})_{W,a}$	1.05	1.05
$\eta_{o,W,a}$	0.963	0.963
$\eta_{i,W,a}$	0.763	0.763
$K(\eta_o)_{W,a}$	0.98	0.98
$K(\eta_i)_{W,a}$	0.88	0.88
$K_{b,W,a}$	0.10	0.10
$\tau_{a,W}$	0.0058	0.0058
$c_{a,W}(y)$	$-0.0854y^2 + 1.32y$	$-0.0854y^2 + 1.32y$
$C_{l\delta,a,W}$	$-0.0011\frac{1}{rad}$	$-0.0011\frac{1}{rad}$
$C_{l\delta,a}$	$-0.0042\frac{1}{rad}$	$-0.0042\frac{1}{rad}$

Continuation of Table A.1		
Value	Cantilever Wing Configuration	Box Wing Configuration
$C^*_{l\delta,a}$	$-0.00073\frac{1}{rad}$	–
End of Table		

A.2 Coefficient Equations

A.2.1 Box Wing Configuration

$$C_{m,CG} = 0.25 + 7.19\frac{1}{rad} \cdot \alpha - 12.72\frac{1}{rad} \cdot (0.71 \cdot \alpha - 0.033rad)$$

$$C_{n\beta} = 0.109\alpha^2\frac{1}{rad^3} + 7.17 \cdot 10^{-3}\alpha\frac{1}{rad^2} + 0.076\frac{1}{rad}$$

$$C_{l\beta} = 0.029\alpha\frac{1}{rad^2} - 0.087\frac{1}{rad} - 0.0385(0.83m \cdot cos(\alpha) - 4.3m \cdot sin(\alpha))\frac{1}{rad}$$

A.2.2 Cantilever Wing Configuration

$$C_{m,CG} = 0.23 + 5.0\frac{1}{rad} \cdot \alpha - 9.0\frac{1}{rad} \cdot (0.72 \cdot \alpha - 0.033rad)$$

$$C_{n\beta} = 0.905\alpha^2\frac{1}{rad^3} + 1.517 \cdot 10^{-2}\alpha\frac{1}{rad^2} + 0.91\frac{1}{rad}$$

$$C_{l\beta} = -0.531\alpha\frac{1}{rad^2} - 0.069\frac{1}{rad} - 0.0385(0.83m \cdot cos(\alpha) - 4.7m \cdot sin(\alpha))\frac{1}{rad}$$

APPENDIX B

TECHNICAL DRAWING OF THE EXTRA EA 400-500

B.1 Cantilever Wing Configuration

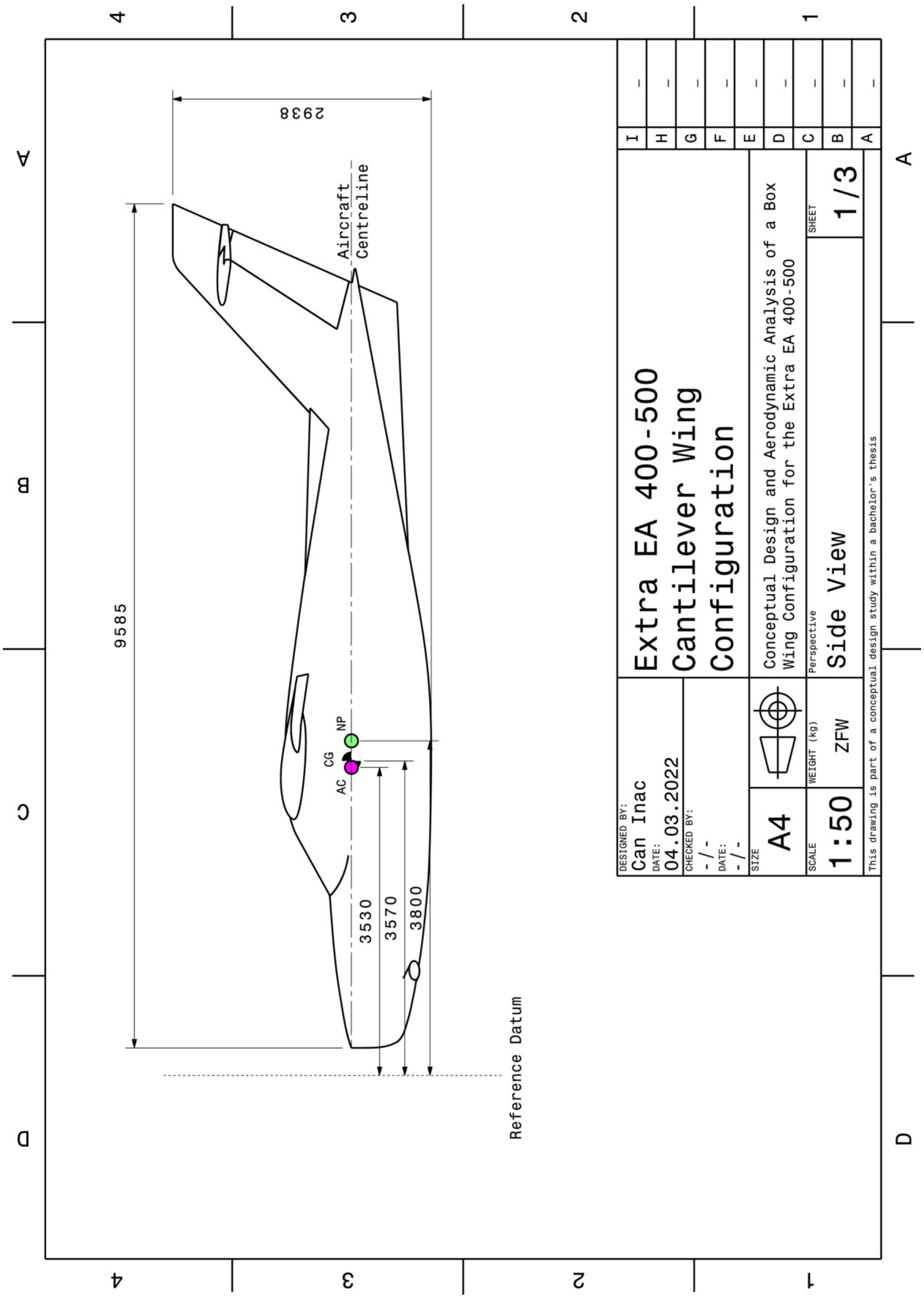

Figure B.1: Side View of the Extra EA 400-500 Cantilever Wing

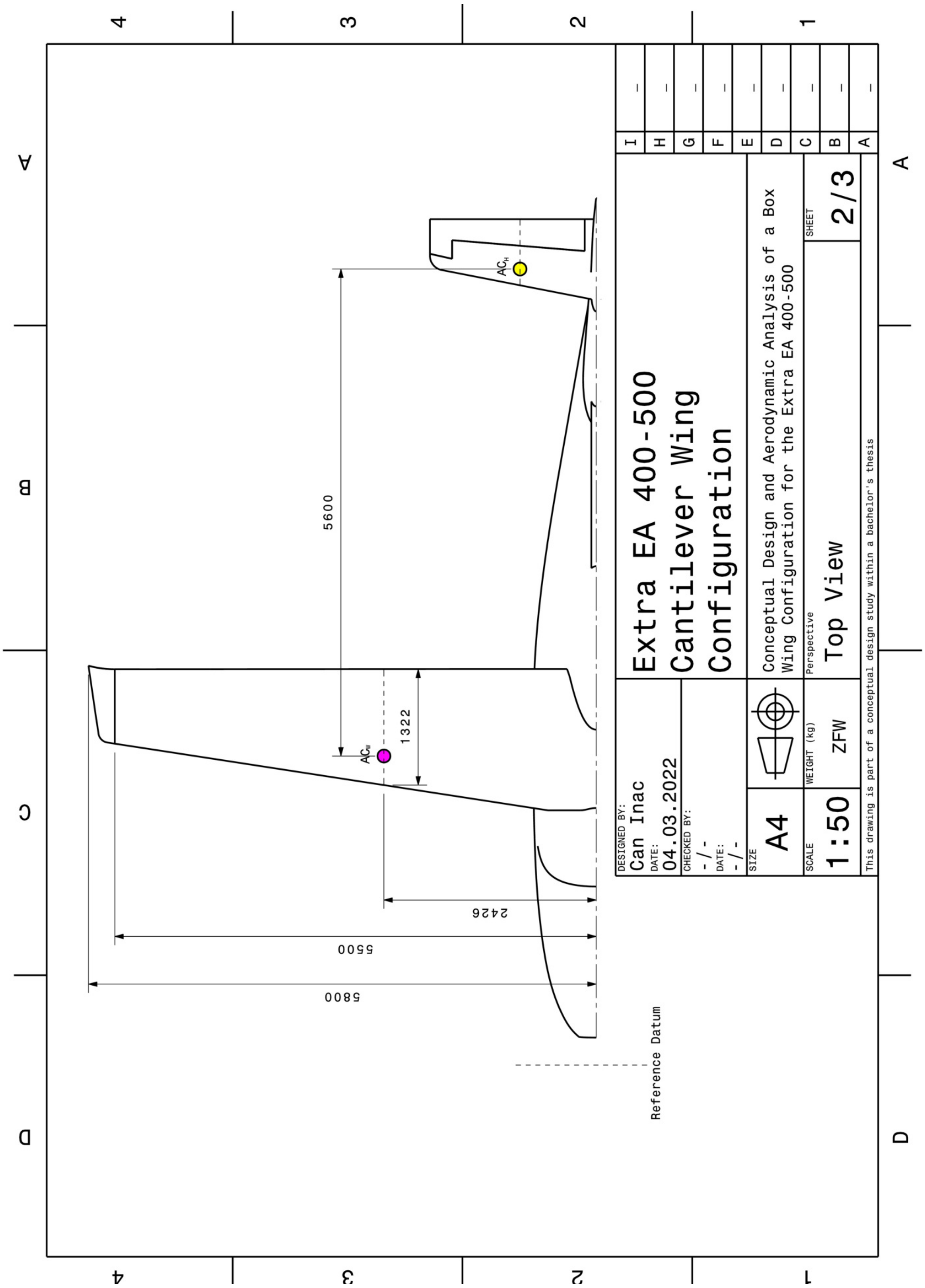

Figure B.2: Top View of the Extra EA 400-500 Cantilever Wing

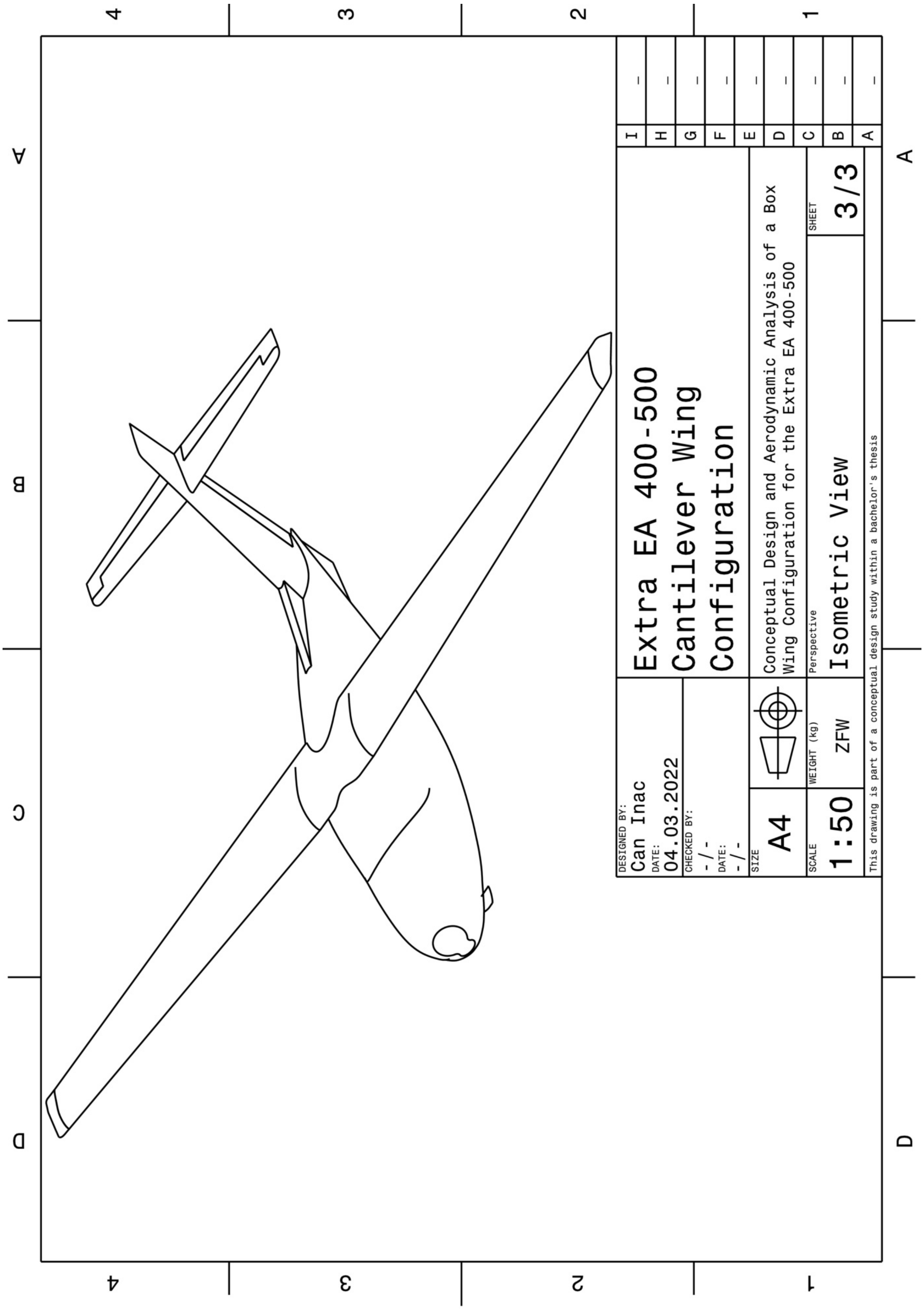

Figure B.3: Isometric View of the Extra EA 400-500 Cantilever Wing

B.2 Box Wing Configuration

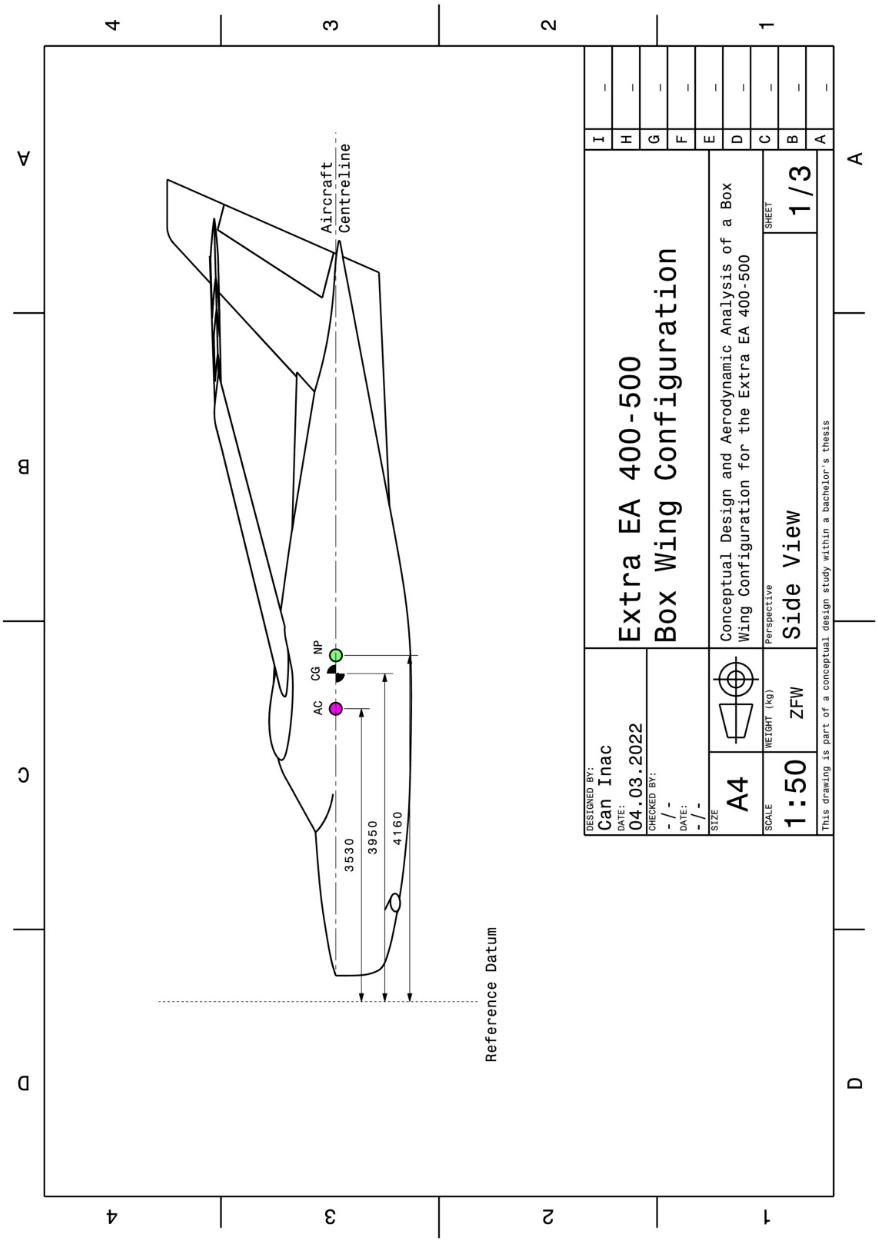

Figure B.4: Side View of the Extra EA 400-500 Box Wing

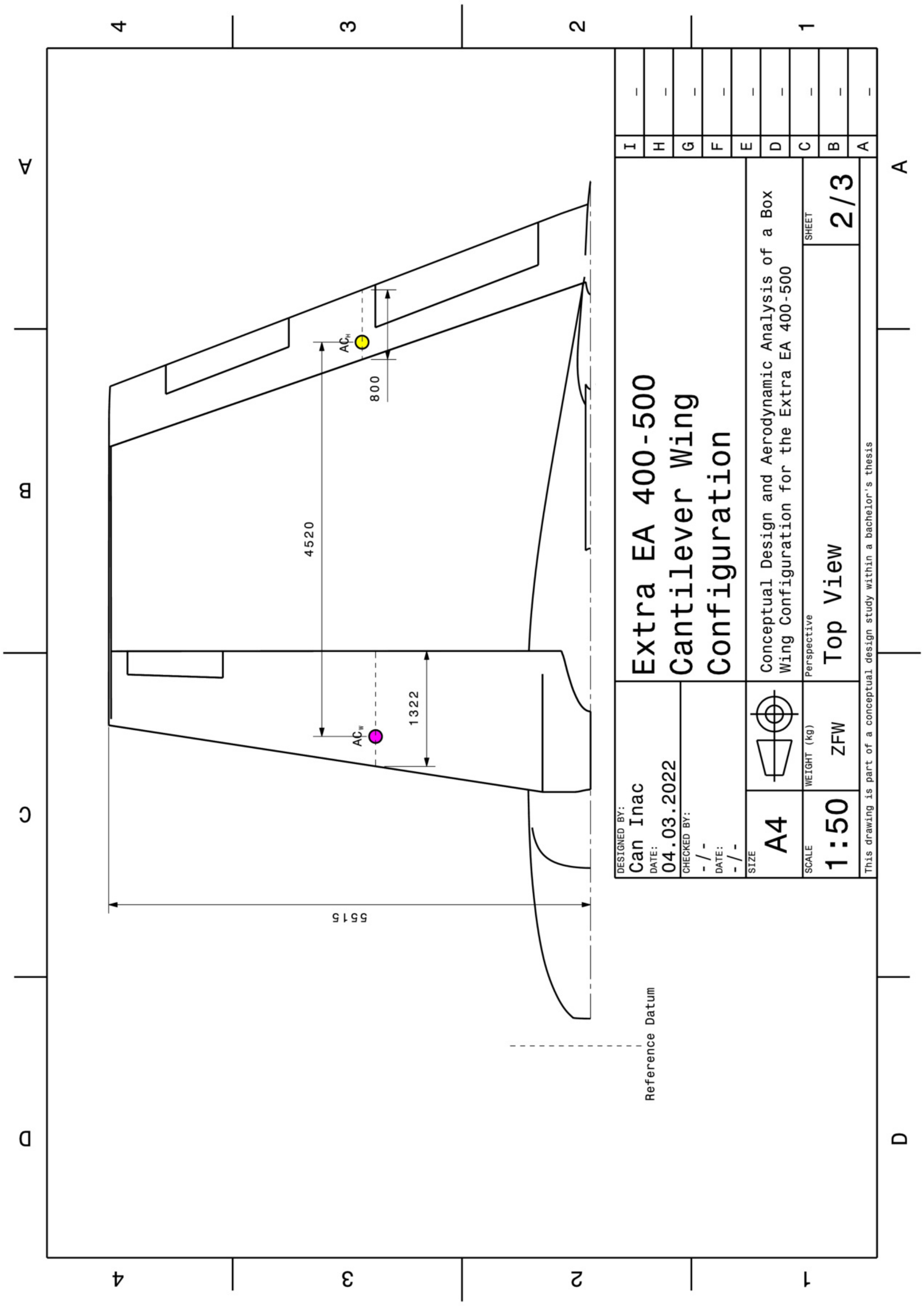

Figure B.5: Top View of the Extra EA 400-500 Box Wing

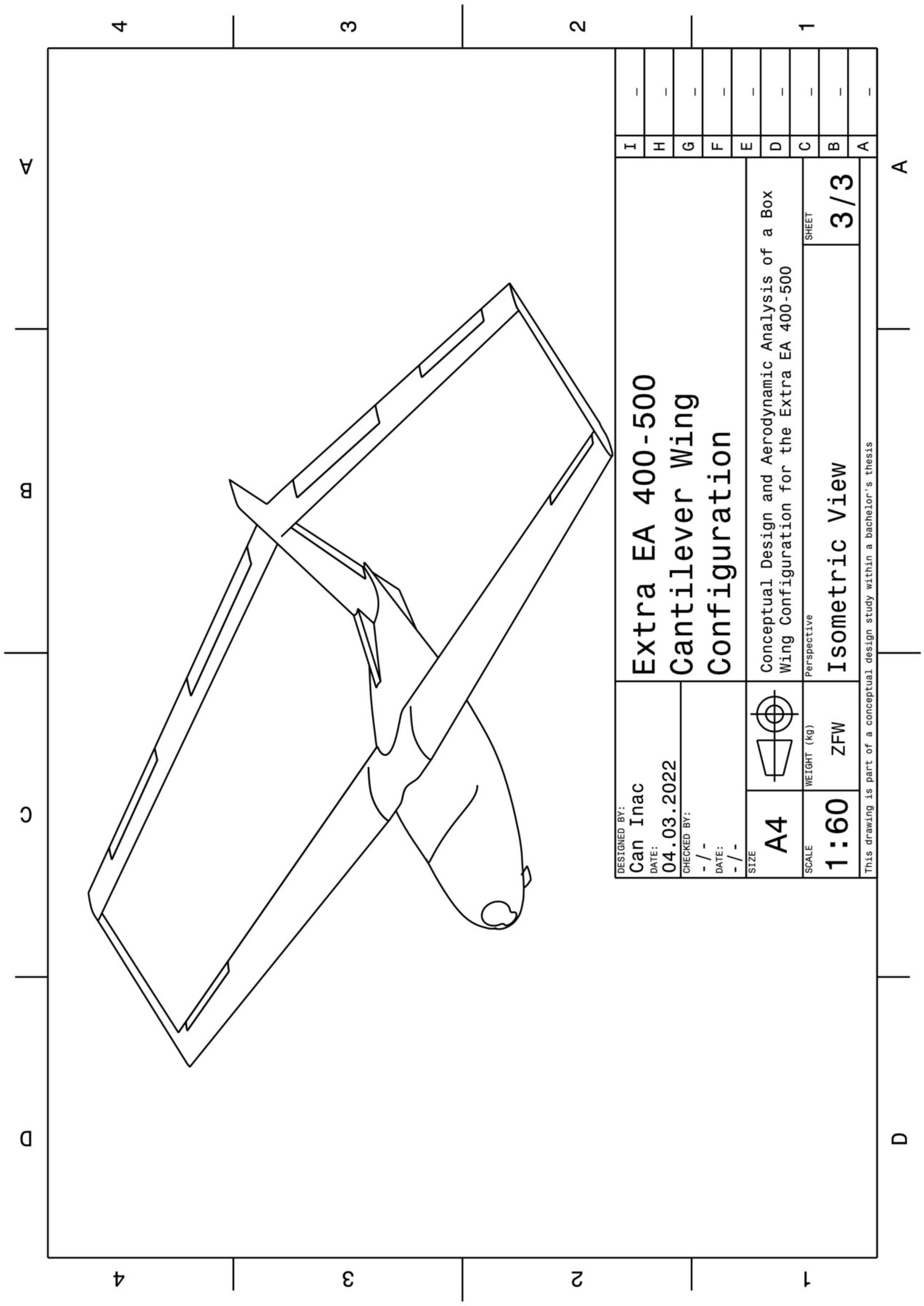

Figure B.6: Isometric View of the Extra EA 400-500 Box Wing